The Dissertation Committee for Steven Jay Hallam Certifies that this is the approved version of the following dissertation:

The introduction of incompatibility between Junin virus Z protein and other viral proteins results in impaired replication and attenuation

Committee:

Slobodan Paessler Ph.D, DVM,
Supervisor or Mentor

Tetsuro Ikegami Ph.D.,

Tomoko Makishima MD, Ph.D.,

Roberto Garofalo MD,

Juan Carlos de la Torre Ph.D.,

The introduction of incompatibility between Junin virus Z protein and other viral proteins results in impaired replication and attenuation

by

Steven Jay Hallam, B.S.

Dissertation

Presented to the Faculty of the Graduate School of

The University of Texas Medical Branch

in Partial Fulfillment

of the Requirements

for the Degree of

Doctor of Philosophy

The University of Texas Medical Branch

July 2019

Dedication

All of my work and accomplishments I dedicate to my wife Jaclyn and our son William. They are the reason I strive to better myself personally and professionally. Everything I have I owe to you two.

Acknowledgements

Dr. Slobodan Paessler, Dr. Tetsuro Ikegami, Dr. Tomoko Makishima, Dr. Juan Carlos de la Torre, Dr. Alan Brasier, Dr. Roberto Galofalo, Dr. Cheng Huang, Dr.Takaaki Koma, Dr. Tyler Manning, Dr. Alexey Seregin, Dr. Junki Maruyama, Dr. Jere McBride, Dr. Hoai Hallam, Elizabeth Mateer, Rachel Sattler, Natalya Bukreyev, and Emma Mantlo

The introduction of incompatibility between Junin virus Z protein and other viral proteins results in impaired replication and attenuation

Publication No._____

Steven Jay Hallam Ph.D.

The University of Texas Medical Branch, 2019

Supervisor: Slobodan Paessler D.V.M., Ph.D.

The genus *Mammarenavirus* with the family *Arenaviridae* contains many species that are pathogenic in human hosts. Among these, Junin virus (JUNV) is a New World mammarenavirus that is the causative agent of Argentine hemorrhagic fever (AHF). AHF resulted in 15-20% case fatality during epidemics until the introduction of a vaccine that drastically reduced the incidence of the disease. This live-attenuated vaccine, Candid#1 (Can), contained many amino acid divergences from wild type JUNV that may contribute to the attenuation profile. Preliminary experiments identified a natural incompatibility between the Can Z protein and wild type Romero (Rom) strain LP that was not seen in Can Z and Can LP. Characterization of this incompatibility demonstrated reduced growth and replication in rJUNV harboring Can Z and Rom LP. When characterized in the *in vivo* guinea pig model, the CanZ/RomLP mismatch resulted in attenuation of the virus and a pathology profile similar to rCan. In addition, it was narrowed down to a single mutation (V64G) within the Z that conferred the attenuation when paired with Rom LP. The LP is comprised of four domains. We generated chimeric LPs representing permutations of Can and Rom to determine which Rom domain exhibited an incompatibility with Can Z. The *in vitro* characterization results of these chimeric proteins indicated that both domains I and III likely contribute to incompatibility with Can Z. These studies characterize a novel attenuation method for JUNV utilizing the Z protein in addition to elucidating further mechanisms caused by Z incompatibility.

TABLE OF CONTENTS

List of Abbreviations

SLEV	St. Louis encephalitis virus
NHP	Non-human primate
LCVM	Lymphocytic Choriomeningitis virus
JUNV	Junin virus
LASV	Lassa virus
AHF	Argentine hemorrhagic fever
ICTV	International Committee on the Taxonomy of Viruses
ORF	Open reading frame
OW	Old World
NW	New World
LUJV	Lujo virus
PICV	Pichinde virus
TACV	Tacaribe virus
MACV	Machupo virus
GTOV	Guanarito virus
SABV	Sabia virus
BHF	Bolivian hemorrhagic fever
VHF	Venezuelan hemorrhagic fever
BzHF	Brazilian hemorrhagic fever
LATV	Latino virus
WWAV	White-water Arroyo virus
L	Large
S	Small
NP	Nucleoprotein
GPC	Glycoprotein precursor protein
IGR	Intergenic region
LP	L protein
RdRp	RNA-dependent RNA polymerase
Kb	Kilobase
PRR	Pattern recognition receptor
IRF-3	Interferon regulatory factor 3
TBK1	TANK Binding Kinase 1
IKKe	I-kappa-B kinase epsilon
DNA	Deoxyribonucleic acid
RNA	Ribonucleic acid
SSP	Stable signal peptide
GP1	glycoprotein I
GP2	glycoprotein II
kDa	Kilodalton
ER	Endoplasmic reticulum
SPase	Signal peptidase
SKI-1	Subtilisin kexin isozyme-1

S1P	Site 1 protease
RBD	Receptor binding domain
RING	Really Interesting New Gene
ESCRT	Endosomal sorting complex required for transport
Tsg101	Tumor suppressant gene 101
NRP2	Neuropilin-2
TIM	Transmembrane immunoglobulin and mucin domain
LAMP1	Lysosomal-associated membrane protein 1
mRNA	Messenger RNA
gRNA	Genomic RNA
agRNA	Anti-genomic RNA
TLR	Toll-like receptor
RIG-I	Retinoic acid-inducible gene I
Mda-5	Melanoma differentiation-associated protein 5
TRAF3	TNF receptor-associated factor 3
NFκB	Nuclear factor kappa-light-chain-enhancer of activated B cells
eIF2α	Eukaryotic translation initiation factor 2α
dsRNA	Double stranded RNA
IFN	Interferon
MAVS	Mitochondrial antiviral signaling protein
MOPV	Mopeia virus
PKR	Protein Kinase R
TRIM2	Tripartite Motif Containing 2
FDA	Food and Drug Administration
WHO	World Health Organization
VSV	Vesicular stomatitis virus
TCS	Tissue culture supernatant
BSL-4	Biosafety level 4
UTMB	The University of Texas Medical Branch at Galveston
DMEM	Dublecco’s modified Eagle’s medium
FBS	Fetal bovine serum
P/S	Penicillin/streptomycin
MEM	Modified Eagle’s medium
fLuc	Firefly luciferase
GFP	Green fluorescent protein
MOI	Multiplicity of infection
VLP	Virus like particles
HBSS	Hank’s balanced salt solution
SDS	Sodium dodecyl sulfate
PBS	Phosphate buffered saline
cDNA	Complementary DNA
PCR	Polymerase chain reaction
qPCR	Quantitative PCR
IACUC	Institutional Animal Care and Use Committee
NIH	National Institutes of Health
PFU	Plaque forming unit

i.p.	Intraperitoneal
EDTA	Ethylenediaminetetraacetic acid
PBMC	Peripheral blood mononuclear cell
H&E	Hematoxylin and eosin
PRNT	Plaque reduction neutralization test
ANOVA	Analysis of variance
HGP	Hartley guinea pig
WBC	White blood cell
PLT	Platelet
ALT	Alanine transferase
AMY	Amylase
BUN	Blood urea nitrogen
LAV	Live attenuated virus

Chapter 1 Introduction

ARENAVIRUS DISCOVERY

In the summer of 1933, an epidemic of *encephalitis lethargica* began to be described in St. Louis, Missouri USA. Soon after, reported cases began to spread and instances of the disease were being reported in neighboring Kansas City and multiple other surrounding population centers. In total, 1315 cases would be reported in St. Louis and the surrounding areas from this Missouri outbreak (1). Epidemiological investigation would conclude that the agent responsible for the majority of these cases was the mosquito-borne St. Louis encephalitis virus (SLEV), a member of the family *Flaviviridae*. During the course of the investigation, however, many clinical samples were collected and passaged through non-human primate (NHP) hosts in order to characterize and identify the infectious agent contained therein. One such sample was obtained from a 42-year-old woman, designated C.G. This patient presented with severe headache, nausea, fever and delirium during the course of disease. During NHP infection, it became clear that this was not SLEV, but a previously uncharacterized virus causing fever and encephalitis. This new virus, characterized by Dr. Charles Armstrong in 1933, was designated as Lymphocytic Choriomeningitis virus (LCMV) and later began a new family of viruses: *Arenaviridae* (2). Electron microscope imaging of the isolated viruses revealed a grainy, or sandy interior to the viral particles. These grains were later identified as host ribosomes, incorporated into the budding virions. This gave rise to the name arenavirus, *arena* meaning sand in Latin. Since then, dozens of additional arenaviruses have been isolated and characterized comprising several genera. Chief among these was the characterization of Junin virus (JUNV) in 1958 (3), and Lassa virus (LASV) in 1969 (4). JUNV was isolated from human patients during an outbreak of Argentine hemorrhagic fever (AHF) in the town of Junin, Argentina. LASV, conversely was isolated on the African continent in the town of Lassa,

Nigeria, during a hemorrhagic fever outbreak. Recently, multiple species have been isolated from the Asian continent (5), giving the *Arenaviridae* family a large geographic distribution.

ARENAVIRUS PHYLOGENY

According to the latest report of the International Committee on the Taxonomy of Viruses (ICTV), the family *Arenaviridae* is classified in the phylum *Negarnaviricota,* subphylum *Polyploviricotina*, class *Ellioviricetes*, order *Bunyavirales* (6). Like other members of the *Bunyavirales* order, arenaviruses contain a negative sense, segmented RNA genome. In addition, arenaviruses are enveloped viruses containing an outer enveloped purloined from the host plasma membrane. The virions can vary greatly in size from 40 to 200 nm in diameter. This genome is comprised of two segments, encoding four viral open reading frames (ORF). These ORFs are encoded in an ambi-sense strategy, resulting in viral transcription from both genomic and anti-genome viral RNA. Phylogenetic analysis of the arenavirus genome has yielded 4 presently recognized genera within the family: *Hartmanivirus, Mammarenavirus, Reptarenavirus,* and *Antennavirus*. Together, the family contains 41 recognized species with 1, 35, 5, and 2 species represented in *Hartmanivirus, Mammarenavirus*, *Reptarenavirus,* and *Antennavirus* respectively. The mammarenaviruses include all of the known human pathogens found within the family. Within this genus, there are two major phylogenetic groups: Old World (OW) and New World (NW) viruses. This phylogeny is demonstrated in Figure 1 (7). The newly

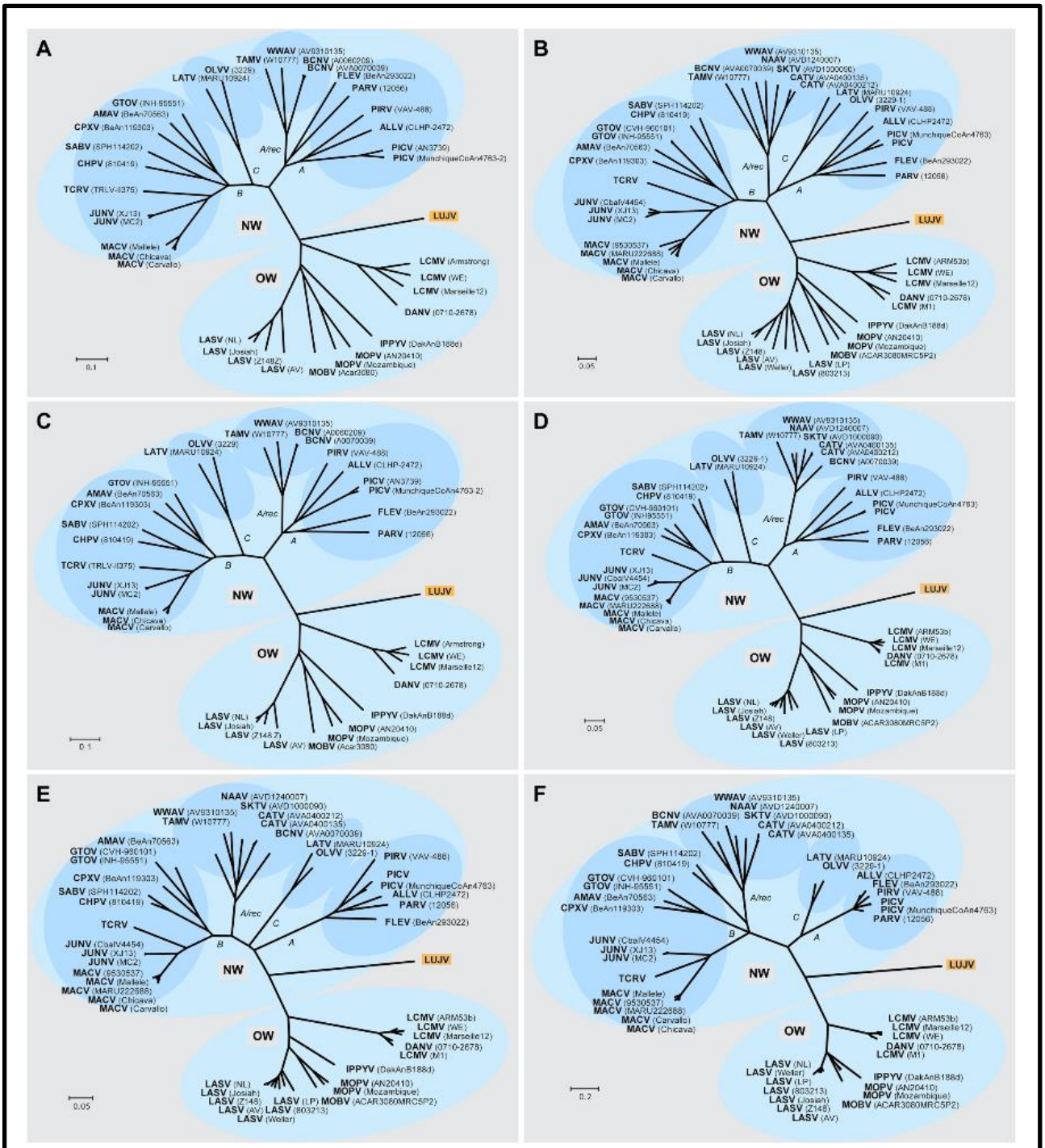

Figure 1. Mammarenavirus Phylogeny. Phylogeny was based on full L (A) and S segment nucleotide sequence (B), as well as on deduced amino acid sequences of L (C), NP (D), Signal/G2 (E) and G1 (F) ORF's. Adapted from Briese 2009

characterized Asian viruses were not included in the latest graphical phylogenetic trees. Recent phylogeny, however, indicates that they are phylogenetically related to the OW

mammarenaviruses and cluster accordingly with that group.

The OW viruses are classically restricted to the African continent, with the exception of LCMV, which enjoys a world-wide distribution, and newly characterized Asian viruses. This group includes the well characterized LASV, as well as emerging viruses Lujo virus (LUJV) and Wenzhou virus. The ICTV does not officially recognize LUJV as either a mammarenavirus or OW virus, but phylogenetic studies predict its place in those groups. The LASV species are further divided into 5 lineages, representing widely divergent genome sequence within a single species. Between lineages, LASV species can demonstrate as little as 85% amino acid identity in the NP (8). The NW viruses are geographically located in North and South America and are divided into 4 clades: Clade A, Clade B, Clade C, and Clade A/Rec (Clade D). Clade A contains non-pathogenic viruses and is represented by the prototypic Pichinde virus (PICV). PICV is commonly used as a surrogate for LASV infection, as it mimics many features of LASV pathology *in vivo* (9). Clade B, or the Tacaribe serocomplex (named after prototype member Tacaribe virus (TACV)), contains all NW human pathogens including JUNV, Machupo virus (MACV), Guanarito virus (GTOV), Sabia virus (SABV), and Chapare virus. JUNV, MACV, GTOV, and SABV are the causative agents of Argentine hemorrhagic fever (AHF), Bolivian hemorrhagic fever (BHF), Venezuelan hemorrhagic fever (VHF), and Brazilian hemorrhagic fever (BzHF) respectively. Clade C contains viruses that differ from other NW viruses in their host receptor usage and is represented by the Latino virus (LATV). Finally Clade A/Rec (Clade D) represents likely recombination events between Clades A and C (10–12). This clade is represented by the White-water Arroyo virus (WWAV) and has a current geographic range on the North American continent (13). The *Reptarenavirus* genus is comprised of viruses isolated from snakes and other reptiles. These are not currently hypothesized to be current or future human pathogens. The genus *Hartmanivirus* is the latest edition to the family *Arenaviridae* and contains only one recently characterized virus: Haartman virus. This novel arenavirus was isolated from a snake host and is the only

known arenavirus to not contain a detectable ORF for the Z protein (14). Current hypotheses postulate that this virus is always found in the presence of other reptarenaviruses and utilizes heterologous Z proteins for virion formation and budding.

ARENAVIRUS GENOME

As stated earlier, the arenavirus genome is comprised of two negative sense RNA segments that encode four ORFs as shown in Figure 2, with the exception of the genus *Antennavirus* that exhibits genomes comprised of three segments (15). These two segments are designated as the Large (L) and Small (S) segments. The L segment is approximately 7.2 kb long and contains the ORFs for the L protein (LP) and the small Z protein. The S segment is approximately 3.3 kb long and contains the ORFs for the nucleoprotein (NP) and the glycoprotein precursor protein (GPC). The 5' and 3' terminal ends of each genome segment contain conserved sequences that form panhandle structures critical for transcription and replication. These have been shown to be highly conserved across related arenaviruses with the 17 of 19 terminal nucleotides being identical in many (16). Finally, located between the two ORFs on each segment is an intergenic region (IGR). These

arenavirus IGRs are predicted to form single or double hairpin secondary structures that are necessary for transcriptional termination.

L protein

The LP ORF is located on the L segment of the arenavirus genome. It comprises the largest ORF (6.6 kb) and the largest protein produced by the virus. Given its orientation on the L segment, LP is an early gene product during the viral life cycle. The LP functions as the RNA-dependent RNA polymerase (RdRp) for the virus and is responsible for both transcription and replication during the viral life cycle. Characterization has shown that the

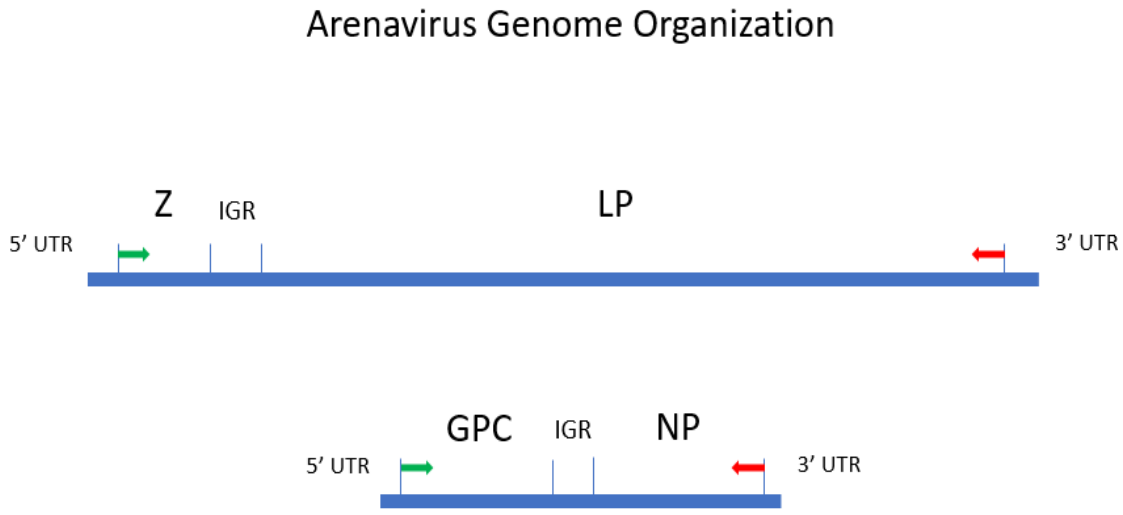

Figure 2. Arenavirus Genome Organization. Gene elements indicated above the genome. Green and red arrows represent promoters on either the agRNA and gRNA respectively.

LP is comprised of four relatively conserved domains connected by three less conserved linker regions (17). Enzymatic studies demonstrate that Domain I of the LP exhibits endonuclease activity (18). In addition, this domains shares structural similarity to orthomyxovirus endonucleases, supporting confirmation of its endonuclease role (19). However, this activity has not been confirmed in the context of virus replication, only in

expression studies. This activity is necessary for the cleavage of 5' mRNA caps from host mRNA. These re-appropriated caps are used by the virus to initiate transcription of the viral ORFs. Domain III of the LP exhibits strongly conserved sequences indicative of an RdRp (20). This function has been confirmed by biochemical assays to localize polymerase activity to this domain (19, 21). Polymerase function is, however, dependent on the presence of NP. Together NP, LP and RNA form the replicative complex necessary for polymerase activity. Expression studies performed with the LASV LP demonstrated that Domains I and II could be expressed separately from the remainder of the protein and still assemble into functional polymerases (17). This indicates an independent nature to these domains that are linked together into a single polyprotein. To date, no enzymatic or allosteric activity has been ascribed to either Domains II or IV of the LP. Given the fact that the LP is hypothesized to form a multimer of itself during polymerase activity(22), these domains could contain regions critical for oligomerization or they could possibly contain novel proof-reading functions. Future research is necessary to determine what, if any role, these domains play in the progression or regulation of the viral life cycle.

Nucleoprotein

The arenavirus NP is located on the S segment of the viral genome. It is oriented as an early gene product (along with the LP on the L segment) and is the most abundantly produced protein by the virus. The NP ORF is approximately 1.6 kb long and is translated into a 65 kDa protein. Like most arenavirus proteins, the NP is multifunctional and contains domains responsible for different tasks. The N terminal domain of NP contains an exonuclease domain. Enzymatic activity for this domain has been confirmed via biochemical assays. While the exact function of this activity is debated, it is currently shown that this activity is necessary for degradation of viral RNA (23). This degradation is hypothesized to allow the virus to evade recognition by host pattern recognition receptions (PRRs) within the cell. Recent studies have indicated that this activity might be

ablated in NW mammarenaviruses, perhaps accounting for their induction of interferon responses by the host(24, 25). OW LASV has been shown to retain this activity and exhibits little interferon induction following infection (25). Aside from its exonuclease activity, the NP is also involved in antagonizing the host immune response at other points in the signal cascade. NP has been shown to inhibit interferon induction through interaction with interferon regulatory factor 3 (IRF-3)(26). This signaling molecule is a critical link in the signaling of PRRs to the nucleus. IRF-3 is phosphorylated by TANK binding kinase 1 (TBK1) and then translocates into the nucleus to enhance transcription of interferon β. In addition, the NP of LCMV has been shown to bind and interfere with I-kappa-B kinase epsilon (IKKe), another important interferon signaling molecule (26).

In addition to its role in immune evasion, the canonical role of viral NPs is to bind to the viral genomic RNA. Arenavirus NPs have been shown to bind viral genomic RNA and interact with the viral LP. These interactions facilitate the transcription and replication of the RNA by LP (16). As stated previously, the genome is coded in an ambi-sense strategy separated by IGRs. Accumulation of the NP is necessary for read-through of the IGR and production of full length anti-genomic RNA (16).

Glycoprotein Precursor

The glycoprotein precursor (GPC) is a viral polyprotein destined to be cleaved by the host during maturation. It is encoded as a late gene product on the S segment and is transcribed from the anti-genomic RNA. The polyprotein is destined to become 3 separate but associated proteins: the stable signal peptide (SSP), glycoprotein I (GP1), and glycoprotein II (GP2). The original translated protein is about 55 kDa, produced from a 1.4 kb ORF. One of the hallmarks of a viral glycoprotein is the host glycosylation of the protein following translation. This glycosylation results in multiple sugar/carbohydrate groups being covalently bound to the protein via either available oxygen (O-linked) or nitrogen (N-linked) atoms in the side chain of asparagine or serine/threonine, respectively.

Following translation, the mammarenavirus glycoprotein is predicted to undergo multiple N-glycosylation events in the rough endoplasmic reticulum (ER) covering the regions of GP1 and GP2. Pathogenic NW mammarenaviruses contain as many as 8 to 11 proposed N-linked glycosylation sites. It is currently proposed that glycosylation is critical for proper protein folding in the rough ER. Lack of essential glycosylation motifs, such as those found in the JUNV vaccine strain Candid#1, result in upregulation of the unfolded protein response, ER stress, and degradation of the protein (27). This results in less glycoprotein being found on the cell surface compared to viruses which have these glycosylation motifs intact. Following translation, the SSP is cleaved from the remaining protein by the host signal peptidase (SPase) in the rough ER (28). This signal peptide is crucial for trafficking of the protein through the Golgi apparatus to the cell surface. Unlike many signal peptides, SSP remains associated with the other components of the glycoprotein on the cell surface and is not degraded prior to membrane localization (29, 30). Following SSP cleavage, the glycosylated protein is then transported from the rough ER to the Golgi body. Here the remaining bulk of the protein is cleaved into GP1 and GP2 by the host subtilisin kexin isozyme-1 (SKI-1)/site 1 protease (S1P) (31, 32). GP1 comprises the most distal region of the glycoprotein and contains the receptor binding domain (RBD). This region confers specificity to each arenavirus for the cellular receptor utilized for binding and entry into the target cell. GP2 forms the classic “spike” portion of the glycoprotein and contains extracellular, transmembrane, and cytosolic domains. The cytosolic tail of GP2 is critical for interaction with the Z protein prior to budding while the extracellular end will remain associated with GP1. After this cleavage, the protein is finally trafficked to the cell membrane as an associated SSP-GP1-GP2 unit. These assembled glycoproteins form tripartite structures as they await replicative complexes to reach the cell surface in preparation for virion formation. Studies have shown that the glycoprotein is the major protective antigen in the virus and that attenuation of the glycoprotein is sufficient to confer attenuation to the virus (33).

Z Protein

The final protein encoded in the arenavirus genome is the small multifunctional Z protein. The Z is approximately 11 kDa and is produced from a 284 nt ORF on the L segment. The Z is encoded as a late gene product and is transcribed from the anti-genomic L segment. The canonical role of the Z protein is as a viral matrix protein. These proteins act as a structural protein to coordinate the LP and NP proteins of the replication complex with the GP found in the envelope. The Z protein accomplishes multiple tasks during the virus life cycle and therefore contains several functional domains. The number of functions accomplished, paired with the proteins small size make it a true example of efficiency on the part of the virus. The protein is currently recognized to contain 3 domains: An N-terminal domain, a Really Interesting New Gene (RING) domain, and a C-terminal domain (late domain). The N-terminal domain contains a conserved N-terminal myristoylation site. This motif allows for the addition of a myristoyl group to the protein. This long fatty acid allows the Z protein to localize and embed itself into the plasma membrane of the host. This function is critical for the later budding of the virus (34). In addition, the N-terminal domain is necessary for interaction with the cytosolic tail of GP2 on the cell surface (35, 36). The center region of the protein contains the RING domain. This region contains conserved sequences to chelate two positively charged zinc ions. The chelation of these ions is necessary for correct function of the RING domain. This domain has been shown to interact with both the LP and NP proteins of the virus (37–40). Interaction of Z with LP locks the polymerase onto the RNA template and ends transcription and replication (41). The accumulation of Z as a late product signals sufficient production of protein by the virus. Therefore, inhibition of the LP allows for locked LP/NP/RNA/Z complexes that are necessary for inclusion into nascent virions. In addition, it has been shown that an ablation of the LP/Z interaction can result in rapid degradation of the Z protein (42). The final domain, the C-terminal domain, is crucial for the final steps of the virus life cycle leading

up to budding (43). Z has been shown to be the minimum budding factor and is able to exhibit self-budding activity (44). The C-terminal domain contains conserved late domains. OW viruses usually contain domains containing PTAP and PPPY late domains while the NW viruses contain PT/SAP domains (45). These domains interact with the host endosomal sorting complex required for transport (ESCRT) system. Specifically the late domains interact with tumor suppressant gene 101 (Tsg101) to move the replicative complex from the cytoplasm to the cell membrane (38). Additionally, the late domain of LCMV Z has been shown to drive the production of interfering particles, possibly playing a role in immune suppression (46).

ARENAVIRUS LIFECYCLE

Attachment and Entry

The arenavirus lifecycle begins when the virion finds and attaches to its host receptor protein. This attachment is mediated by the viral GP1 protein. While many host proteins have been shown to be involved in receptor binding, it is generally agreed that α-dystroglycan and transferrin-1 receptor are the canonical receptors for OW and NW viruses respectively, with some notable exceptions (47–49). LASV and LCMV demonstrate use of α-dystroglycan, a ubiquitous glycan found in the extracellular matrix. Additional evidence is available to suggest that the active cycling patterns of a-dystroglycan assist LASV entry in conjunction with cellular kinases (50). Recent studies implicate Tyro3, Axl, and Mer (TAM) family proteins and C-type lectins as potential candidate receptors for these viruses, although further studies are necessary to determine these proteins' role in viral entry (51–53). LUJV has been recently characterized to use neuropilin-2 (NRP2) as its cellular receptor, separating it from the receptors used by both OW and NW viruses (54). NW Clade B viruses utilize the transferrin-1 receptor, whereas Clade C viruses utilize α-dystroglycan in a similar fashion to OW viruses (55). The interaction site of the transferrin-

1 receptor and MACV GP1 has been shown to be on the apical surface of the receptor (56). Transmembrane immunoglobulin and mucin domain (TIM) family proteins have demonstrated an ability to enhance NW mammarenavirus infectivity (57).

Following attachment, the virus enters the cell through divergent pathways. NW viruses, including JUNV, enter the cell through a clatherin-dependent fashion (58). OW viruses instead pursue a clatherin-independent strategy that utilizes the ESCRT system for successful entry (59). In addition, there is evidence that the micropinocytosis pathways play a role in OW mammarenavirus entry (60). Once endocytosed, acidification of the endosome leads to fusion of the viral envelope with the endosome that is mediated by GP2, a class I fusion protein (61). Cyro-EM studies of the GP2 unit indicate that the protein is able to form specific fusion configurations that enhance cell entry more efficiently than other class I fusion proteins (62). In LASV, acidification leads to an altered GP1 conformation that changes its binding specificity. The protein gains a specificity for lysosomal-associated membrane protein 1 (LAMP1) and aids in fusion and escape from the endosome (63). LUJV, in a similar manner, utilizes CD63 inside the endosome to facilitate escape (64). At this time, it is unknown if NW mammarenaviruses utilize a secondary GP1 receptor to enhance fusion and escape to the cytoplasm.

Replication

Once released into the cytoplasm of the cell, the replicative complex of the virus is then able to begin transcription. The LP and NP of the virus use the packaged RNA genome as a template for production of the early gene products. These are the LP and NP ORFs on the L and S segments respectively. To initiate transcription, Domain I of the LP cleaves the 5'm^7G cap from host mRNAs. These caps serve to stabilize the nascent viral mRNA and assist in translation. Structural analysis of NP indicates that the N terminal domain of the protein can accommodate the stolen host cap (22). Polymerization of the transcripts is

facilitated by Domain III of the LP in conjunction with the NP. Initiation of transcription and replication is facilitated by the 5' and 3' ends of the genome forming a panhandle structure. Once aligned, the 5' end has been shown to separate from the 3' end and form a hook structure due to the first seven nucleotides forming base pairs(65). This hook-like structure helps to initiate the polymerase and subsequent transcription and replication. Transcripts are terminated by hairpin formation of RNA bases localized within the IGR. It is currently hypothesized that build up NP in the cell binds to genomic RNA in the IGR and facilitates read-through of the polymerase past these terminating hairpins (16). This results in anti-genomic copies of both the L and S segment and triggers the switch from early to late gene production during the replicative cycle. LP and NP are then able to produce Z and GPC mRNA from the anti-genomic L and S segments respectively. The GPC mRNA is translated into the rough ER. During translation, the protein is concurrently glycosylated at N-linked motifs. In addition, the SSP is cleaved from the remainder of the protein by the SPase in the rough ER (28). The SSP continues to associate with the remainder of the glycoprotein all the way to the plasma membrane and into nascent virions. Following proper folding of GP1/GP2, the protein complex is trafficked from the rough ER and into the trans-Golgi network. In the Golgi body, GP1 is cleaved from GP2 buy the host SKI-1/S1P (31, 32). This cleavage event by SKI-1/S1P is highly unusual for type-1 fusion proteins that are canonically cleaved by host furin-like proteases (66). Finally, the SSP/GP1/GP2 complex is trafficked to the plasma membrane where they await future budding with the remainder of the viral proteins and RNA. When the Z protein is in high abundance it is able to interact with the LP and lock the polymerase onto the template (41). The exact location on LP that Z bind to is still unknown, however, computational studies have indicated that Z can bind LP in both Domain I and Domain III of TACV (38). It is unknown whether these sites represent the maximum binding positions or whether one, both or neither site is actually used during viral infection. Additionally, Z is able to bind to NP, resulting in multiple anchor points on the replicative complex.

Assembly and Budding

After Z has bound to the complex, it facilitates transport to the cell membrane via the host ESCRT system. Specifically, the PTAP, PPPY, or PT/SAP late domains directly interact with Tsg101 of the ESCRT system (45). Recent studies suggest that the late domain of LCMV is able to drive defective interfering particle production during the late stages of the viral life cycle (46). This results in trafficking of the complex to the plasma membrane where the Z is able to anchor itself into the lipid bilayer utilizing its N terminal myristoyl group (34). At the same time Z localizes the complex to the waiting glycoproteins by interaction of the N terminal domain of Z with the cytoplasmic tail of GP2. Oligomerization of Z forms the matrix of the budding virion at the plasma membrane. Together with GPC and NP/LP/RNA, the nascent virion is able to pinch and bud from the host cell and be released to pursue subsequent infection.

An overview of the arenavirus life cycle is shown in Figure 3.

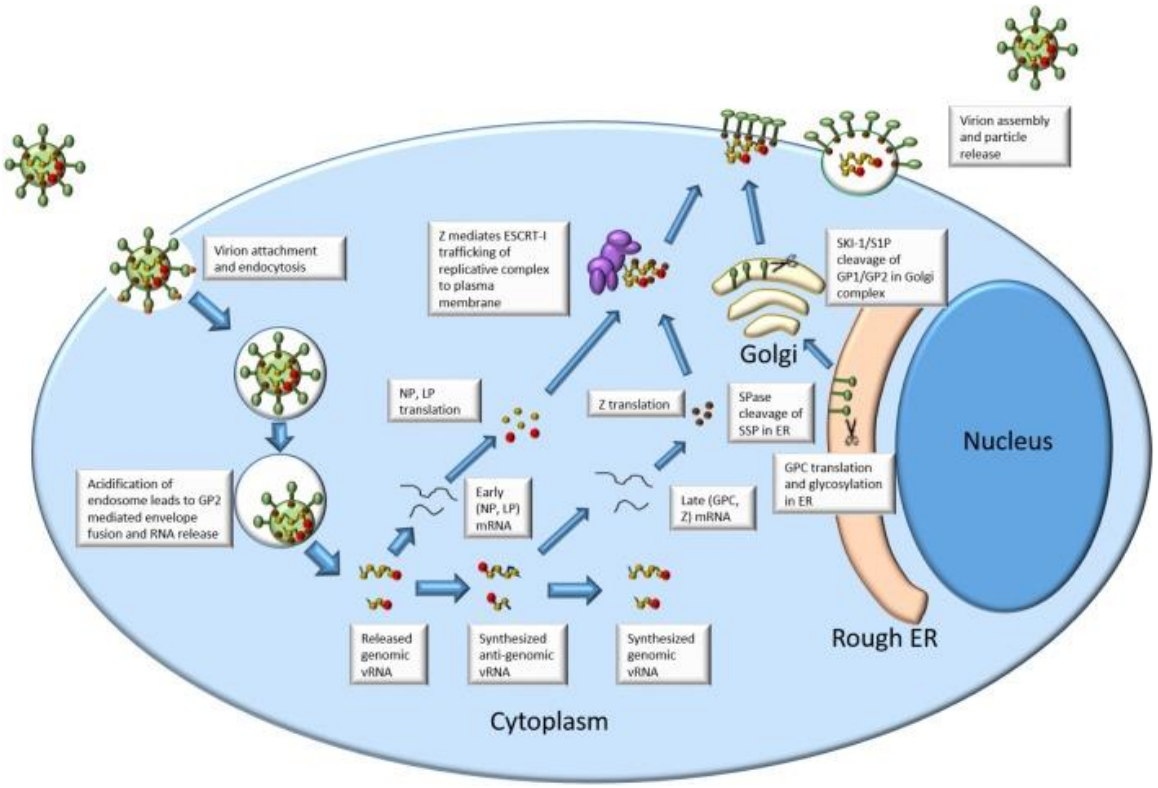

Figure 3. Mammarenavirus Lifecycle. Adapted from Hallam 2018

IMMUNE EVASION

Mammarenaviruses have developed multiple mechanisms to modulate or evade the host immune system in an effort to maximize replication and infectious virus production. The first mechanism to be characterized is the activity localized to the viral NP protein. NP has been shown to inhibit immune signaling through interaction with IRF-3 (67, 68). IRF-3 is a component of an innate immune signaling pathway, which can begin with detection of viral RNA by cell surface Toll-like receptors (TLRs) or intracellular dsRNA sensors retinoic acid-inducible gene I (RIG-I) and melanoma differentiation-associated protein 5 (Mda-5) (69). Both RIG-I and Mda-5 are RNA helicases and are therefore able to sense dsRNA produced during the viral life cycle. Activation of these pathogen recognition

receptors (PRRs) will eventually result in signaling through TNF receptor-associated factor 3 (TRAF3) and TBK1. Finally, IRF-3 becomes phosphorylated and translocates to the nucleus where it acts as an enhancer of IFN-β mRNA transcription. By inhibiting IRF-3 signaling, NP has been shown to be effective in reducing IFN-β production, although some viruses such as TACV do not demonstrate this capability. Other methods of antagonizing the IFN-β induction pathway is through the inhibition of IKKe and NFκB. Mammarenavirus NP has been shown to interfere with both of these proteins to evade immune activation (26, 70). Another cytoplasmic PRR found in the host cell is the dsRNA activated protein kinase (PKR). Activation of PKR leads to phosphorylation of and sequestration of eukaryotic translation initiation factor 2α (eIF2α). Unavailability of this translational initiation factor leads to a halt of translation, both host and viral. Various studies indicate that perhaps JUNV can inhibit activation of PKR or allow activation but still continue prolific viral translation (25, 71). LASV does not activate PKR, effectively nullifying the immune response through evasion of detection. Regardless, in the presence of activated PKR, JUNV and MACV are still able to replicate efficiently, indicating an alternative translation initiation method divergent from the currently identified canonical pathways. Another way in which NP evades innate immune activation is through the degradation of dsRNA. The C-terminal domain of NP demonstrates exonuclease activity that is able to degrade dsRNA, the ligand for RIG-I and Mda-5 (23). Recent studies have shown that this results in a decrease of dsRNA in cells infected with OW LASV, but not those infected with NW JUNV and MACV (Mateer unpublished). This support reports that the NW NP may be defective in exonuclease activity, leading to the high type-I IFN production measured in AHF and BHF, respectively.

In addition to activity by the NP, NW mammarenaviruses have been shown to exert immune suppression through the Z protein. Studies have shown that the Z binds to RIG-I and prevents downstream signaling to produce IFN-β (72). This physical binding prevents activation of the next protein in the cascade, mitochondrial antiviral signaling protein

(MAVS). This represents an impairment of IFN-β production upstream of NP interference with IRF-3. However, since clinical cases of AHF and BHF demonstrate high IFN level it is unknown what effect the Z/RIG-I interference has on IFN production *in vivo.* Together with NP, these proteins allow the virus to replicate effectively while avoiding most detrimental effects of the innate immune system.

Another way in which the Z protein can assist in immune evasion and cellular survival is through the inhibition of autophagy. Screening experiments with OW LASV and Mopeia virus (MOPV) Z proteins uncovered multiple cellular binding partners, including autophagy mediators (73). Infections indicate that the LASV Z is able to inhibit autophagy while MOPV Z is less effective. The inhibition of cellular autophagy allows for an increased production of viral particles, and consequently a likely more robust infection. In this way, the early innate immune activation is avoided or reduced, allowing the virus to be more pathogenic. In a marked difference between OW and NW viruses, JUNV appears to promote an opposite effect. Studies have shown that JUNV infection results in increased autophagy (74, 75). Not only is autophagy enhanced, it is also shown to promote JUNV growth and infection. This is in stark contradiction to the replicative strategy of OW LASV and MOPV. This difference may also help to contribute to the differential interferon production between LASV and JUNV/MACV.

EPIDEMIOLOGY AND CLINICAL MANIFESTATION

LASV was first isolated in 1969 from a missionary nurse working in Nigeria (4). Since that time, LASV has been shown to be endemic to Sierra Leon, Guinea, and Liberia (76–82). In addition, serological evidence suggests that this range is likely far larger and includes the Ivory Coast, Mali, and the Central African Republic (83, 84). LASV is currently predicted to cause between 100,000-500,000 infections each year and approximately 5,000 deaths (85). This results in a fatality rate of approximately 1-5%. The *Mastymos natalensis* rat is thought to be the primary reservoir and vector for LASV,

although other rodents including *R. rattus* and *M. musculus* have been shown to be infected with the virus (86). It is currently thought that these infections are temporary, and that these rodents are not likely reservoirs of the virus. Human infections primarily occur from inhalation of infected rodent feces or urine, or through the consumption of infected rodent tissue (87).

LUJV was first isolated from a nosocomial outbreak of hemorrhagic fever in Johannesburg, South Africa (7, 88, 89). Since that time LUJV has not caused future outbreaks and is thought to be located primarily in southern Africa. The natural reservoir of LUJV is currently unknown. LCMV is the only arenavirus to enjoy a world-wide distribution due to its animal reservoir, the *Mus musculus* mouse. Non-reservoir rodents, such as hamsters, may become infected with the virus when in near proximity to infected mice but do not serve as natural hosts (90). Due to the mild nature of most LCMV infections, under-reporting of the disease is likely. Serological studies of urban cities around the world demonstrate that 2-5% of the population has been exposed to the virus (90).

Among the NW mammarenavirus, the major human pathogens are represented by JUNV, MACV, GTOV, SABV, and Chapare virus. JUNV, MACV, GTOV, and SABV are the causative agents of AHF, BHF, VHF, and BzHF respectively. According to the most recent reports, AHF, BHF, and VHF produce a case fatality rate of 15-20%, 35%, and 33% respectively (91–93). JUNV and MACV utilize *Calomys* spp. mice as their natural reservoir. GTOV, on the other hand, has been found in *Zygodontomys brevicauda* mice. Chapare virus has only been isolated from human cases, and as of present, no known reservoir has been identified for SABV (6). Like LASV and LCMV, these NW mammarenaviruses are primarily transmitted to humans through the inhalation of infected rodent feces or urine. Sharing the Clade B complex with these viruses, TACV has been shown to not use a rodent reservoir at all. In fact, the reservoir for TACV has been shown to be the *Artibeus* spp. of bats, representing a marked departure from closely related

mammarenaviruses. In addition, TACV has also been isolated a single time from *Amblyomma americanum* ticks, opening the possibility for arthropod adaptation (94). Information on pathogenic and nonpathogenic arenaviruses and their reservoirs can be found in Table 1 (95, 96).

Table 1: Mammarenavirus Disease and Reservoir

Virus	**Disease**	**Natural Reservoir**
Lassa virus	Lassa Fever	*Mastymos* spp
LCMV	Lymphocytic choriomeningitis	*Mus musculus*
Lujo virus	Unknown	Unknown
Junin virus	Argentine hemorrhagic fever	*Calomys* spp
Machupo virus	Bolivian hemorrhagic fever	*Calomys* spp
Guanarito virus	Venezuelan hemorrhagic fever	*Zygodontomys brevicauda*
Sabia virus	Brazilian hemorrhagic fever	Unknown
Chapare virus	Unknown	Unknown
Tacaribe virus	None	*Artibeus* spp

Adapted from *Arenaviridae*, ICTV 9th Report
https://talk.ictvonline.org/ictv-reports/ictv_9th_report/negative-sense-rna-viruses-2011/w/negrna_viruses/203/arenaviridae

Mammarenavirus infections in humans are thought to be largely asymptomatic, with severe cases progressing to hemorrhagic fever. OW LASV is the causative agent of Lassa fever, a severe hemorrhagic diseases endemic to West Africa. Lassa fever initially presents as a flu-like illness after an initial incubation period of 7-21 days (97, 98). These

initial symptoms include fever, weakness, malaise, and headache (99). In addition, patients may exhibit gastrointestinal symptoms including nausea, vomiting, and diarrhea. The majority of patients will begin to recover from Lassa fever within 8-10 days following the onset of symptoms. Those that progress into more severe disease begin to show neurological symptoms, and potentially develop pulmonary edema and respiratory distress. Many patients exhibit bleeding from mucosal regions. In both late stage patients and survivors, unilateral or bilateral hearing loss has been observed (98–100).

NW JUNV, being the prototypic of human infection for the Clade B viruses, also results in hemorrhagic manifestations following human infection. JUNV is the causative agent of AHF, which presents as flu-like symptoms following an incubation period of 6-14 days (91). Initial flu-like symptoms include fever, chills, myalgia, malaise, headache, and anorexia (103). This can be followed by flushing of the face and upper chest, edema and petechial bleeding, conjunctival and periorbital congestions, and occasionally backache, epigastric pain, nausea, and vomiting. This initial phase of disease is usually characterized by a petechial skin rash. Accompanying these symptoms, patients also exhibit thrombocytopenia, hemoconcentration, leukopenia, and proteinuria. AHF patients were shown to exhibit demonstrably reduced CD4 and CD8 T cell levels (104). This phase can also present with neurological symptoms including disorientation, lethargy, ataxia, tremors, irritability, and decreased muscle reflexes. Following the first week, 70-80% of patients will begin to recover, with the remaining 20-30% progressing into hemorrhagic and neurological symptoms and shock. Pathological examination of patients who succumbed to AHF indicated a marked depletion of white pulp in the spleen (105). This correlates with the leukocytopenia seen in AHF patients. In addition to the manifestations of AHF, laboratory experiments were able to demonstrate that JUNV has the ability to infect osteoblast cells (OBCs) and promote differentiation (106). It is unknown what effect the viral-induced differentiation might have on the infected host.

Mammarenavirus infection can be recognized by several PRRs in the cell. RIG-I, Mda5, and PKR can recognize dsRNA produced during the viral lifecycle. This recognition leads to IFN-β production and the establishment of an immune response. Studies have also shown that Toll-like receptor 2 (TLR2) is able to recognize the JUNV glycoprotein and initiate immune signaling as well (107, 108). The IFN-inducible protein, Tripartite Motif Containing 2 (TRIM2), has exhibited antiviral activity, and strong expression of this protein reduces JUNV infectivity (109). In addition, LCMV has been shown to induce TLR7 immune signaling during infection (110, 111). LCMV has also been shown to increase TLR3 and TLR9 induced signaling, representing a varied network where mammarenaviruses can induce an interferon response (112).

JUNV was identified as a potential biowarfare agent and is therefore classified as a Select Agent in the USA. To prepare for the potential weaponization of JUNV or natural outbreaks, the United States Army, in collaboration with the Argentine government, developed a live attenuated vaccine, designated Candidate #1 or Candid#1 (113). This vaccine was produced by serial passage of pathogenic JUNV human isolate XJ. The virus was submitted to 2 passages in guinea pig, 43 passages in mouse brain, and a final 16 passages in fetal rhesus lung cell culture. The resulting vaccine was demonstrated to be attenuated in guinea pig and mouse models, as well as in human clinical trials. The vaccine became available for use in 1990 in Argentina and has resulted in a dramatic decrease in the incidence of AHF. In addition to the original human trials, an additional clinical study of Argentine and American volunteers (946) demonstrated 95.5% seroconversion upon immunization with no severe adverse effects (114). These results characterize Candid#1 as a highly safe and effective vaccine against a highly pathogenic, hemorrhagic virus. While vaccine development for other mammarenaviruses is ongoing, there are currently no FDA licensed vaccines for arenaviruses, or any other arenavirus vaccines distributed besides Candid#1.

Within OW mammarenaviruses, LASV represents the agent in most need of a vaccine. Given the high incidence, large vulnerable population, and severe disease associated with Lassa Fever, it stands to reason why this pathogen would become a WHO Blueprint priority pathogen (115). At this time, vaccine candidates have been based on a vast variety of vaccine systems including adenovirus vectors, poxvirus vectors, chimeric live attenuated OW mammarenavirus platforms, DNA vaccines, alphavirus replicons, flavivirus vectors, VSV vectors, Salmonella vectors, inactivated viruses, and nanocarrier antigen systems (116). One of the major obstacles to the development of a LASV vaccine is the divergence in viral sequences between LASV strains. When comparing prototypic viruses from the five proposed lineages of LASV, amino acid divergence in the GPC and NP proteins of 8.4% and 10.7% is reported. Therefore, the need to drive immunity against conserved epitopes, or the inclusion of several viral strains is necessary for proposed protection. Following successful clinical trials, it is my hope that a safe and effective vaccine against LASV will be available for distribution in endemic west Africa.

Both OW (LASV, LCMV) and NW (JUNV, MACV, GTOV) viruses are used in various infection models to study pathogenesis and/or to test vaccines (117–120). These models include mouse, guinea pig, and NHP systems that are able to recapitulate various aspects of human disease (108). The majority of the mouse models are based on immunocompromised mice that while recapitulating disease, are not appropriate for the study of immune responses and vaccination. Guinea pig and NHP models both allow for infections in immune competent hosts. In lethal challenges, both of these models exhibit the hallmark attributes of mammarenavirus hemorrhagic fevers including fever, hemorrhaging, leukopenia, and thrombocytopenia (121). Due to the cost and facility requirements for NHPs, guinea pigs are frequently used as the model of choice, with NHPs being required for pre-clinical testing of vaccine candidates.

TREATMENT OF JUNV INFECTIONS

The treatment, and success of treatment, of mammarenavirus infections varies both on the species and the length of infection. For JUNV infection, very effective treatment can be given using the immune plasma from convalescent AHF patients. Administration of this plasma reduced the case fatality rate from 16.5% to 1.1% (122). Since the introduction of the Candid#1 vaccine, the incidence of AHF has dropped dramatically. This has resulted in fewer convalescent survivors for immune plasma production. Due to this recent development, the search for monoclonal antibodies and small molecule inhibitors against JUNV has intensified. Ribavirin, a nucleotide analog, was tested due to its broad-spectrum antiviral activity. While it does lower viremia in infected patients, it did not produce a significant increase in survival in patients 8 days or longer into infections (123). Many studies have characterized ribavirin analogs and other small molecule inhibitors, but as of current, none have entered clinical trials for AHF treatment (124–127). FDA-approved voltage gated calcium channel (VGCC) inhibitors were also shown to decrease JUNV entry and fusion into the cell (128). In addition, the characterization of newly synthesized p-chlorophenyl compound showed an inhibitory effect against JUNV, although it was lower than the currently available ribavirin (129). The generation of monoclonal antibodies to target JUNV infection is of significant interest to the field. Given the reduction in survivors and the success of immune plasma treatment, the continuation of antibody treatment is sought after. Currently, several monoclonal antibody candidates have been produced with promising results *in vitro* and *in vivo* (130, 131). Future clinical studies will determine whether they carry similar efficacy in human patients. As a final note, some antibodies produced in response to Candid#1 inoculation have demonstrated neutralizing activity against related MACV (132). Similar studies found little to no cross-neutralizing activity from Candid#1 elicited antibody pools suggesting it may be a rare occurrence (133). Further work would be required to determine if cross-neutralizing antibodies for JUNV and MACV can be produced and effectively utilized.

JUNV represents an excellent model pathogen for NW hemorrhagic fever viruses. The availability of Candid#1 allows for research to be completed at lower containment levels has produced valuable insight into JUNV pathogenesis. At the same time, significant differences between the vaccine strain and wild type viruses indicate that mutations introduced to the vaccine during development altered key mechanisms of the virus. By utilizing both wild type and Candid#1, we were able to determine protein incompatibilities between these strains that impact viral replication and infectious virion production. Our overall aim was to characterize factors of successful replication and growth in JUNV. We hypothesized that protein incompatibilities would lead to decreased growth and ultimately attenuation of the virus. These interactions, specifically between the Z and LP and the Z and GPC, resulted in decreased replication and growth kinetics *in vitro.* Furthermore, the Z/LP incompatibilities were shown to attenuate the virus in an *in vivo* guinea pig model. These novel results indicate an additional strategy for mammarenavirus attenuation outside of the previously characterized GPC attenuation.

Chapter 2 Materials and Methods

VIRAL CLONING AND VECTORS

The production of rJUNV was performed as previously described (134). BHK21 cells were transfected with plasmids harboring the L and S segments in an antigenomic orientation under the control of a murinePol-I promoter, and LP and NP ORFs under the control of a CMV-derived Pol-II promoter. The TCS was collected 4 days post transfection and purified using a 0.45 micron syringe filter to produce P0 stocks. Chimeric virus Pol I and Pol II plasmids were generated utilizing restriction enzyme and Gibson cloning methods. All pathogenic JUNVs were generated and utilized in the biosafety level 4 (BSL-4) facilities of the University of Texas Medical Branch (UTMB).

CELL LINES

A549, Vero, HEK 293T, and Vero E6 cells (ATCC) were propagated in Dublecco's modified Eagle's medium (DMEM) with 10% fetal bovine serum (FBS) and 1% penicillin/streptomycin (P/S). Baby hamster kidney (BHK-21) cells were propagated in modified Eagle's medium (MEM) with 10% FBS and 1% P/S. Cells were passaged approximately every 2-4 days or when confluency was reached.

VIRUS MINI-GENOME ASSAYS

Mini-genome assays were performed utilizing three or four plasmid systems in BHK-21 cells. Pol I promoter plasmids encoding a JUNV viral S segment (minigenome) with the NP and GPC ORFs replaced with Firefly Luciferase (fLuc) and green fluorescent protein (GFP) respectively were utilized. The S segment was generated in the antigenomic orientation resulting in the fLuc ORF encoded in the early gene orientation and GFP in the late. Pol II promoter plasmids encoding the ORF for LP, NP, and Z were also generated to result in overexpression of the respective proteins. One day prior to transfection, BHK-21 cells were seeded in 12-well plates. Once reaching 80% confluency, cells were transfected utilizing the Xtreme-Gene9 reagent system according to manufacturer's instruction. Two μg of total DNA, representing equal copy numbers of Pol I/S and Pol II NP/LP/Z were transfected. 36 hours post transfection (hpt), cell lysates were collected and fLuc activity was measured using the Promega Dual-Luciferase Reporter Assay according to manufacturer's instructions.

VIRUS PRODUCTION AND TITERING

Viral P1 stocks used in the studies were produced by infection of Vero E6 cells with P0 stocks and isolating the tissue culture supernatants (TCS) following 4 days. The TCS was then filtered through a 0.45 micron syringe filter and concentrated using an Amicon

Ultra-15 centrifugal filter. This centrifugation was performed at 3500 RPM for 30 min. For viral titration, Vero E6 cells were seeded into 12-well culture plates one day prior to infection. The following day, viral samples underwent a 10-fold dilution and subsequent addition to the cell monolayers. Plates were incubated for 1 hour at 37º C in an atmosphere of 5% CO_2. Following incubation, each well was overlaid with a solution of MEM with 2% FBS, 1% P/S, and 0.6% tragacanth gum. Plates were then incubated for 7 days at 37º C and 5% CO_2. Following incubation, each well was fixed with 10% formaldehyde, and stained with crystal violet. Plaques were then counted, and the corresponding titer determined.

VIRUS INFECTION *IN VITRO*

For all experimental infections, the indicated cell types were seeded the previous day and allowed to reach 80% confluency. Cells were then infected at an MOI of 0.01 with the indicated rJUNV. Cell lysates and/or supernatants were collected at the times indicated in each individual experiment.

VLP PRODUCTION AND ISOLATION

JUNV virus like particles (VLPs) were produced by transfection of HEK 293T cells with Z and/or GPC expression plasmids. Briefly, HEK 293T cells were seeded and allowed to reach 80% confluency before being transfected with Rom Z, Can Z, Rom GPC, and/or Can GPC Pol II-driven expression plasmids utilizing the Xtreme Gene9 transfection system according to manufacturer's instructions. Cell lysates and supernatants were collected at 36 hpt for analysis. Cell supernatants were centrifuged at 2500 RPM for 5 min to pellet cell debris. The supernatant was them filtered using a 0.45 micron syringe. The purified supernatant was subsequently layered onto a cushion of 20% sucrose in HBSS buffer. The samples were then ultra-centrifuged at 26,000 RPM for 3-4 hours in a Beckman SW28

rotor at 4º C. Following centrifugation, the supernatant was discarded and the pelleted VLPs were resuspended in 2X Laemmli SDS buffer for use in Western Blot. Cell lysates were washed with phosphate buffered saline (PBS) and collected in 2X Laemmli SDS buffer for sue in Western Blot.

WESTERN BLOT

Samples used in Western Blot analysis were collected in 2x Laemmli SDS buffer with 5% β-mercaptoethanol. Samples were then incubated at 95º C for 10 minutes. Gel electrophoresis was performed with 4-20% polyacrylamide SDS gels in a Tris/Glycine/SDS running buffer. Electrophoresis was performed for 40-60 minutes at 200V. The gels were then removed from the running buffer and transferred to a PVDF membrane utilizing the BioRad Trans-Blot Turbo machine according to manufacturer's instructions. Following transfer, the membranes were blocked with 5% milk in PBST for 1.5 hours at room temperature while shaking. Membranes were subsequently probed with primary antibody in 1% milk in PBST overnight at 4º C while shaking. The following day the membranes were washed 5X with PBST for 5 min at room temperature. Following the wash, the membranes were probed with secondary antibody in 1% milk in PBST for 2-3 hours at room temperature while shaking.

After incubation with the secondary antibody, the membranes were again washed 5X with PBST for 5 min at room temperature. Once all washes were complete, Thermo Scientific Pierce ECL 2 detection solution was added to the membrane, following manufacturer's instructions, and incubated for 5 min at room temperature. Chemiluminescent film was exposed to the membranes and developed to produce the final Western Blot image.

RNA ISOLATION AND CDNA PRODUCTION

Samples used for RNA isolation were collected in Trizol or Trizol-LS reagents. Cell monolayers were collected by adding 1 mL Trizol reagent per 10 cm^2 cell area. Liquid

samples were collected with a 4:1 ratio of Trizol-LS reagent to sample. Samples were kept in Trizol for 24 hours prior for inactivation. RNA was then collected from inactivated samples using the Zymo Direct-zol RNA Mini-prep kit according to manufacturer's instructions. RNA was eluted using RNAse/DNAse free water. Resulting RNA was either used in cDNA production or stored at -80 C.

RNA produced in the previous steps was used in the Invitrogen SuperScript III First Strand Synthesis System according to manufacturer's instructions. The cDNA was produced using random hexamer primers. Resulting cDNA was used immediately in PCR, qPCR, or stored at -20C.

QPCR

qPCR was performed utilizing the BioRad SsoAdvanced Universal SYBR Green Supermix according to manufacturer's instructions. Briefly, 4 uL of cDNA was added to 10 uL of the supermix, 250 nM of each primer, and 5.2 uL H_20. Standards for each locus were produced from known quantities of NP or GPC Pol II-driven expression plasmids to create a range of standards ranging from 10^2-10^9 gene copies. Samples were run on a BioRad CFX96 Real-Time System with a 2 min 95 C followed by 45 cycles of 10 sec 95 C and 1 min 55 C. The primers used for each locus are as follows: NP (TGTCATCAGAGAGGCAGTGG, CGTGAGAGTGTCTGCTACCA) GPC (ATCCTGCACAGAAGAAGCCT, TGGAACACCAGCTCATGTCT).

NORTHERN BLOT

RNA samples for use in Northern Blot were mixed with an RNA Sample buffer (RBS/Formamide/Formaldehyde) and incubated at 65º C for 10 min. Following incubation, they were run on a 1.2% agarose gel with RBS/Formaldehyde running buffer. Samples were electrophoresed at 110V for 2-3 hours. Following electrophoresis, the gel was washed 3X with deionized (DI) water and then submitted to an alkali treatment consisting of 50

mM NaOH for 20 min while shaking. After the alkali treatment the gel was washed again 3X in DI water and incubated in 100mM Tris-HCL pH 7.6 for 20 min while shaking. This incubation was followed again by 3X washes in DI water. Finally, the gel was incubated in 20X SSC for 10 min while shaking.

The gel was transferred using a Capillary Blotting system. First the wick was charged with 100% ethanol, rinsed with DI water, and primed with 20X SSC. The assembly was then created with Whatmann blotting paper, gel, a positively charged nylon membrane, and additional Whatmann blotting paper, all soaked in 20X SSC. A 10-15 cm stack of paper towels was then added on top and a weight placed above to keep pressure on the assembly. The transfer was allowed to proceed at room temperature for 24 hours.

After transfer, the membrane underwent crosslinking in the Stratalinker, a UV-crosslinking machine. The membrane was subsequently incubated for 1-2 hours at 68º C with a hybridization buffer (SSC/formamide/sodium lauroylsarcosine/SDS/blocking reagent). Following incubation, the buffer was discarded, and new buffer added with 2 µL RNA probe. The probes used were for NP and GPC ORFs. The NP probe was produced from the following primers and resulted in a 425 nt fragment: AAAGGCTGGAGCATCCATTC, CTAATACGACTCACTATAGCAGGGTCAGTGGCTGGTCCTTC. The GPC probe was produced from the following primers and resulted in a 476 nt fragment: CTAATACGACTCACTATAGCATGGTCGAGTGGACATTGG, TGTGTCCTTCTCAATGGTGGGTCTC. Both probes were produced using the Roche DIG RNA Labeling Kit, according to manufacturer's instructions and utilizing the T7 polymerase. The membrane was then incubated in the probe/hybridization buffer for 16-18 hours at 68º C.

Following probe hybridization, the membranes were washed and blocked using the Roche DIG Wash & Block Buffer Set, following manufacturer's instructions. Following washing and blocking, the membrane was incubated with 2-5 µL AP-a-DIG-Ab in blocking buffer for 30 min at room temperature. The membranes were then washed for 2X with 1X

Washing Buffer for 15 min at room temperature. The membranes were then briefly incubated in detection buffer and developed with the CDP-Star reagent. Chemiluminescent film was exposed to the membranes and developed to produce the final Northern Blot image.

ANIMAL USE AND INFECTION

8 week old female Hartley guinea pigs used in this study were purchased from The Charles River Laboratory. Animal studies were approved by the Institutional Animal Care and Use Committee (IACUC) at UTMB and performed in accordance with National Institutes of Health BSL-4 guidelines. Guinea pigs were inoculated with 10^3 PFU via the intraperitoneal (i.p.) route following anesthesia with an isoflurane precision variable-bypass vaporizer. Recording of death and disease symptoms was done using a standardized scale with the following definitions: development of discoordination, ataxia, encephalitis, seizures (ability to eat and drink), paralysis, hind limb or quadriplegic paralysis (no ability to eat and drink). Telemetric body temperature monitoring and body weight measurements were collected daily for the first 15 days of the study. Animals were euthanized after reaching a humane endpoint of 15% body weight or at the end of the study. For telemetry, guinea pigs were anesthetized and subcutaneously implanted with BMDS IPTT-300 transponders from Bio Medic Data Systems, Inc. via a trocar needle. Animals were euthanized following loss of 15% body weight from the start of the study.

BLOOD CLINICAL CHEMISTRY AND HEMATOLOGY

Blood collected from the animals was deposited into tubes containing EDTA. Standard hematologic analysis using a VetScan HM5 analyzer was performed on whole-blood

samples following manufacturer's instructions. Clinical chemical analysis was performed on serum utilizing a VetScan VS2 analyzer following manufacturer's instructions to obtain a comprehensive diagnostic profile.

PBMC Immunological Transcription Assay

Blood collected from animals at 9 dpi was used for the collection of PBMCs and lymphocytes. Blood was diluted 1:4 with PBS lacking Ca^{2+} and Mg^{2+}. The blood was then layered onto a Ficoll-paque Premium 1.084 cushion. The samples were then centrifuged at 340 x g for 30 min. The PBMC/lymphocyte layer was collected and washed 3 times with PBS lacking Ca^{2+} and Mg^{2+} at 300 x g for 5 min each. The resulting cell pellets were collected in Trizol-LS and used for an immunological transcription assay.

RNA was extracted through use of the Roche cellular RNA large volume kit in the MagNA Pure 96 instrument. cDNA was produced using the BioRad iScript system according to the manufacturer's instructions. The immunological PCR array was performed as previously described (135–137). Ct values were analyzed using delta delta CT.

Organ Titration and Histopathological Analysis

Following death or euthanasia, kidney, spleen, liver, lung and brain were collected from each animal. Half of each organ was placed in 10% buffered formalin for a minimum of 7 days while the other half was homogenized in 1 mL DMEM with 2% FBS. The homogenized samples were centrifuged at 10,000 RPM for 15 minutes and the resulting supernatant was collected. The supernatant was then used in plaque assay as described above to determine the viral load for each collected organ. Tissue placed in formalin was then paraffin embedded and sliced into 5 micron sections. These were then mounted and subjected to hematoxylin and eosin (H&E) staining and subsequent imaging.

PRNT

Plaque reduction neutralization tests (PRNTs) were performed on serum collected prior to euthanasia. 80 PFU of rRom was incubated for 1 hour at 37°C with 2 fold dilutions of the final serum. Following this initial incubation, VeroE6 cells were incubated with this virus/serum mixture for 1 hour at 37°C. Subsequently the monolayers were overlaid with MEM 2% FBS 1% P/S and 0.6% tragacanth gum. After 7 days the monolayers were fixed with 10% formalin and stained with crystal violet. Serum dilutions corresponding to a 50% plaque reduction were calculated.

STATISTICAL ANALYSIS

Statistical analysis was performed using GraphPad Prism 5 and 8 software. Samples with multiple replicates are shown as mean ±SD, with the exception of organ virus load which is shown as geometric mean ±geometric SD. Growth kinetics were analyzed via 2way ANOVA and the Bonferonni multiple comparisons test to determine significance compared to rRom. Analyte levels from clinical chemistry and hematology measurements and organ virus load were analyzed via 1way ANOVA and Dunnett's multiple comparison test to determine significance compared to rRom. Ct values from the PCR array were analyzed via the delta delta Ct procedure.

IFA

Cell monolayers were fixed with methanol on dry ice for 15 min. Following fixation, the cells were washed with PBS for 5 min, 5 times. Next the cells were incubated with 0.2% Triton X-100 in PBS for 5 min at 4º C. This was followed by another washing step with PBS for 5 min, 5 times. Cells were stained with anti JUNV NP antibody (AG12) conjugated with Alexa Fluor 568 diluted 1:1000 in 3% BSA in PBS. NP antibody incubation was performed at room temperature for 2 hours. Following primary incubation, the cells were

again washed with PBS for 5 min, 5 times. Nuclei were then stained with DAPI for 3 min at room temperature. A final wash was performed with 0.5% Triton X-100 in PBS for 5 min, 3 times, followed by PBS for 5 min, 2 times, and ddH_2O for 5 min, 1 time. The coverslips were then mounted onto microscopy slides utilizing ProLong Gold Antifade Mountant. Edges of the coverslips were sealed with clear nail polish prior to removal from the BSL-4. Images were taken utilizing the Olympus FV1000D Upright Microscope BX61 with the 60x/1.42 objective.

Chapter 3 The introduction of CanZ into wild type Rom results in attenuation

BACKGROUND AND PRELIMINARY DATA

The Candid#1 (Can) vaccine was developed by serial passage in mouse brain and fetal rhesus cell culture. The parental strain of Candid#1 was the original XJ strain, a pathogenic JUNV that is no longer available and for which no sequence was documented. The Romero (Rom) strain of JUNV is highly pathogenic in the guinea pigs and used as a model for JUNV pathogenesis. By comparing the genome sequences of Rom and Can, we can look for amino acid changes that may contribute to the attenuation and immunogenicity of Can. Since we do not know the sequence of the parental XJ strain, we cannot definitely determine which mutations were accrued during the passage history and which mutations represent natural differences between XJ and Rom. Because of this, it is necessary to individually characterize specific amino acid differences, to determine their effects on viral replication, attenuation, and immunogenicity.

Previous studies seeking to elucidate JUNV attenuation focused on mutations found in the viral GPC. Early studies have determined that Can GPC is the main genetic determinant of JUNV attenuation; resulting in 100% survival in experimental animals

when introduced into rRom (33). Additionally, it was shown that a transmembrane mutation in GP2 helped to confer and stabilize the attenuation observed. Later studies sought to build on this attenuation and immunogenic profile by characterizing GP1 mutations found in Can. JUNV GP1 contains several proposed N-linked glycosylation sites. Can contains a mutation ablating one glycosylation site that is conserved in Rom and earlier XJ passage 13 (XJ13) as well as other JUNVs. Can GPC mediated attenuation of JUNV correlates with ablation of a conserved glycosylation motif in GPC that results in altered GPC trafficking (27). The cells also demonstrated a higher unfolded protein response and ER stress when infected. This build-up of improperly folded GPC may result in increased antigen presentation and increased immunogenicity as seen in Can. *In vivo* studies would be required to determine whether this glycosylation ablation would produce the attenuation and immunogenicity seen in the Can vaccine.

Outside of GPC mutations, little has been studied about the effects of Can-like differences in the other three viral proteins on attenuation, immunogenicity, and viral replication. In addition, while it is known that the viral proteins interact with each other during the virus life cycle, it is unknown how incompatibilities between these proteins may affect the different stages of the viral life cycle. To determine how the introduction of Can ORFs would impact infectious virion production, chimeric rJUNV viruses were generated with Rom/Can segment exchanges as well as rRom with each individual Can ORF introduced. Growth kinetics were measured in Vero cells to determine if virus production would be impacted by the introduction of any Can proteins. Recombinant Romero (rRom), Candid#1 (rCan), Romero L segment/Can S segment (rRomL/CanS), Romero S segment/Candid L segment (rRomS/CanL), Romero/Candid LP (rRom/CanLP), Romero/CanNP (rRom/CanNP), and Romero/CandidGPC (rRom/CanGPC) all grew at similar levels. The only outlier was Romero/CanZ (rRom/CanZ), which exhibited a growth

rate approximately 2.5 logs lower than the other viruses. In addition, this virus produced small, pin-prick plaques in contrast to the larger plaques seen in rRom and rCan (Fig. 4).

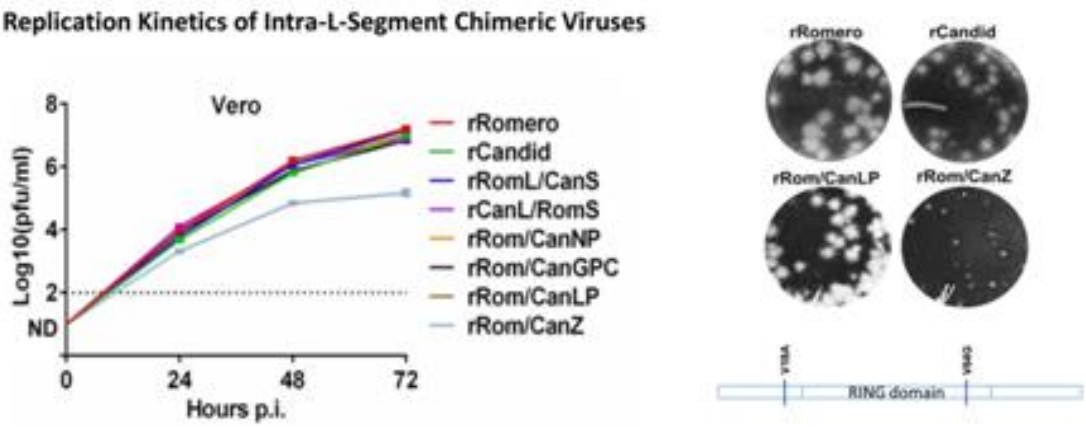

Figure 4. Growth kinetics and plaque phenotype of rJUNV. Vero cells were infected with each virus at an MOI of 1. Supernatants were collected following infection and at 0, 24, 48, and 72 hours post infection. Titers were determined by plaque assay on Vero E6 cells. Representative plaques were imaged to visualize plaque morphology.

These results showed that the introduction of a single Can ORF could drastically and significantly reduce the growth kinetics of rRom *in vitro*. Since rCan grows at similar levels, we hypothesize that compensatory amino acid differences found in other viral proteins rescues the high growth exhibited. When only the Z ORF is introduced, there is a likely incompatibility with Rom protein(s) that result in the decreased growth kinetics. When compared to Rom, Can Z only differs in two amino acids: a valine to alanine change at position 18 (V18A) and a valine to glycine change at position 64 (V64G).

The questions that arise from these results are as follows: 1. Which one or both of the two Can Z mutations is responsible for the incompatibility seen? 2. Does this incompatibility result in attenuation and does it impact immunogenicity *in vivo*? We hypothesize that both mutations contribute to this phenotype and that it will result in attenuated and immunogenic viruses in the guinea pig model.

RESULTS

The V64G mutation and not the V18A mutation is responsible for the reduced growth kinetics.

First, it was important to confirm the previous growth kinetic results. rRom, rCan, and rRom/CanZ viruses were used to infect VeroE6 and A549 cells (MOI 0.01). Growth kinetics were analyzed by collecting samples at 0, 24, 48, 72, and 96 hpi and determining the titer via plaque assay. The subsequent results confirmed the preliminary growth curves and demonstrated that rRom/CanZ grew at significantly lower rates than rRom and rCan in both VeroE6 and A549 cells (Fig. 5). These cell types represent IFN incompetent and competent cell respectively. In addition, the rRom/CanZ virus produced small, pinprick plaques. This was in contrast to the larger plaques shown in rRom and rCan.

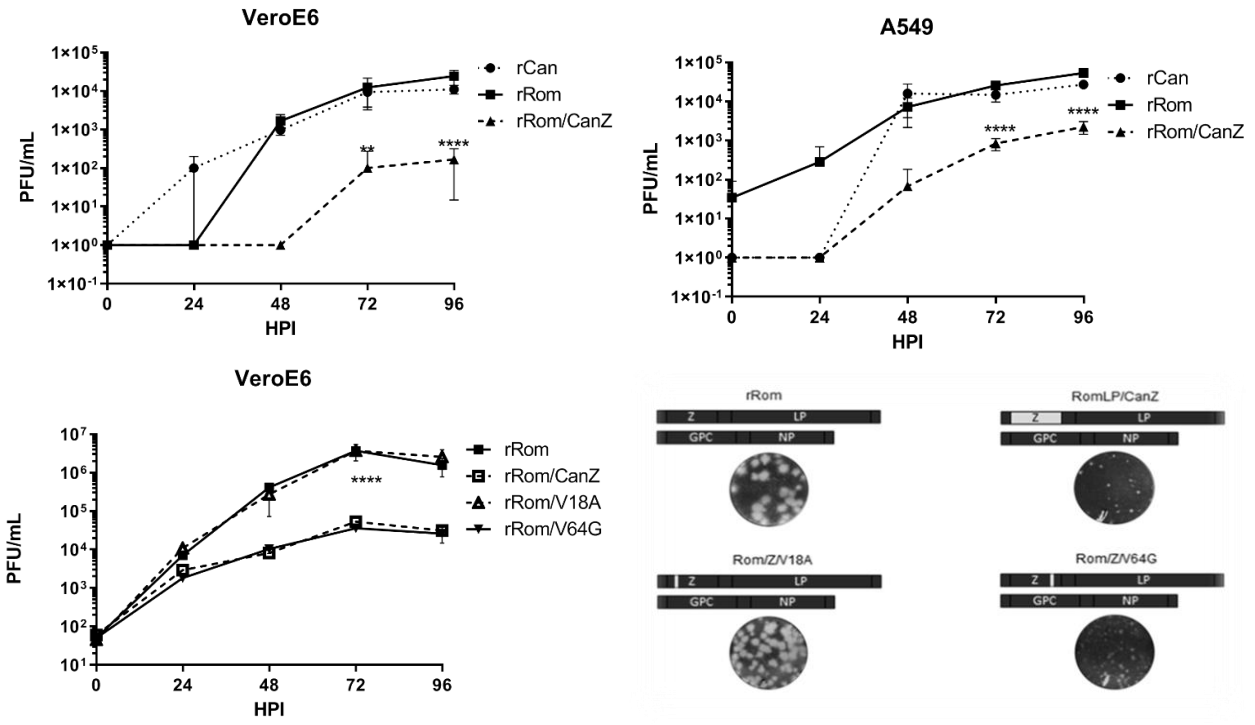

Figure 5. Growth kinetics and plaque phenotype of JUNV. VeroE6 or A549 cells were infected with each virus at an MOI of 0.01. Supernatants were collected following infection and at 0, 24, 48, 72, and 96 hours post infection. Titers were determined by plaque assay on Vero E6 cells. Error bars show the standard deviation from the mean. ** = $p < 0.01$, *** = $p < 0.001$ **** = $p < 0.0001$

Characterization of chimeric Rom/Can recombinant viruses showed that rRom with a Can Z (rRom/CanZ) exhibited a significant reduction in growth kinetics during a multi-step growth assay in both Vero E6 and A549 cells (Fig. 5). As a next step, we generated rRom containing each individual amino acid difference between Rom and Can Z proteins (rRom/V18A and rRom/V64G) and examined their growth kinetics in Vero cells following infection at MOI of 0.01 (Fig. 5). As with rRom/CanZ, we found that rRom/V64G but not rRom/V18A, exhibited reduced growth kinetics when compared to rRom. In addition, both rRom/CanZ and rRom/V64G exhibited a similar pin-point plaque phenotype, whereas plaques produced by rRom/V18A were similar to those produced by rRom.

The V64G and Can Z result in reduced RNA production *in vitro*

While it was demonstrated that rRom/CanZ and rRom/V64G reduced the production of progeny infectious virions, it was unknown whether these mutations affected viral replication. This represents a separation between replication (transcription and genome replication) from growth (assembly and budding). To determine this, rRom, rCan, rRom/CanZ, rRom/V18A, and rRom/V64G were used to infect A549 cells at MOI 0.01. Cell lysates were collected at 48 hpi and RNA was isolated for use in qRT-PCR and Northern Blot. There was not a significant difference in the copy number of RNA at the NP locus, but rRom/V64G, and rRom/CanZ tended to have lower levels than rRom. Samples produced in the same manner were used in Northern Blot analysis. Blots were probed with NP probes to produce a relative qualitative analysis. rRom/V64G showed the lowest RNA accumulation with rRom/V18A and rRom showing the highest. rCan and rRom/CanZ tended to exhibit similar levels of RNA accumulation (Fig. 6).

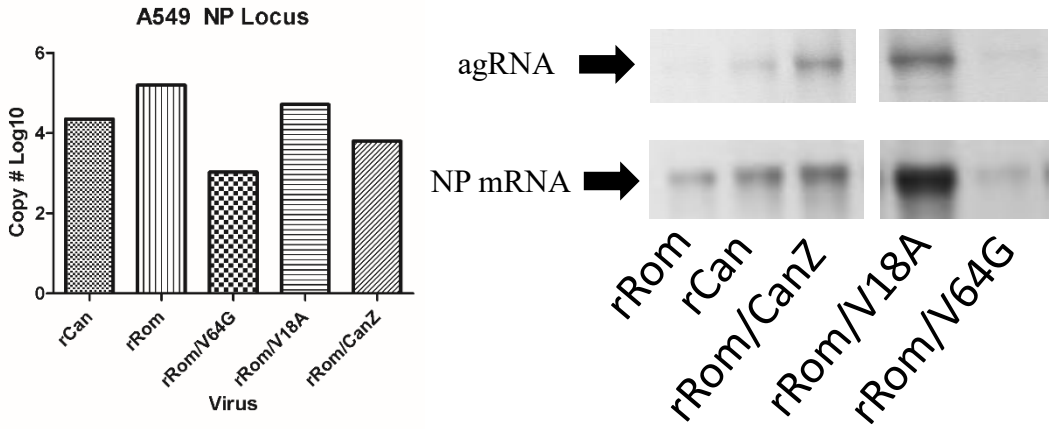

Figure 6. Accumulation of rJUNV RNA in infected cells. A549 cells were infected with each virus at an MOI of 0.01. Cell lysates were collected 48 hours post infection. Copy numbers were determined by qRT-PCR and comparison to a standard curve. Single replicate is shown. Northern Blot images all taken from the same gel.

rRom/CanZ spreads at a reduced rate compared to rRom

Given the low MOI's utilized in the RNA accumulation studies, the possibility remains that the low replication may in fact be a reflection of the low growth seen previously. To attempt to visualize this further, a time course infection was performed followed by immunofluourescent assay (IFA). VeroE6 cells were infected with either rRom or rRom/CanZ at MOI 0.01 and samples were collected every 12 hours and stained utilizing a conjugated anti JUNV NP antibody. Image fields were used to count the number of infected and uninfected cells as well as the peak NP intensity. The results indicated that rRom/CanZ spread at a reduced rate when compared to rRom. By 48 hpi, rRom NP was detectable in 87.2% of cells compared to the 12.1% in rRom/CanZ infection (Fig. 7). In

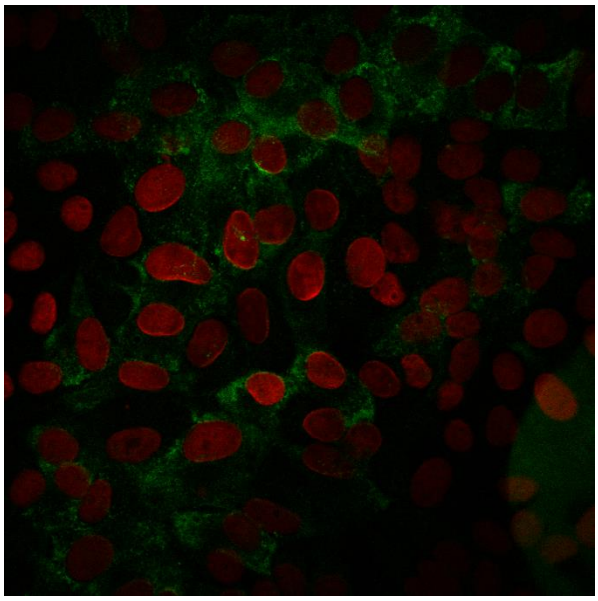

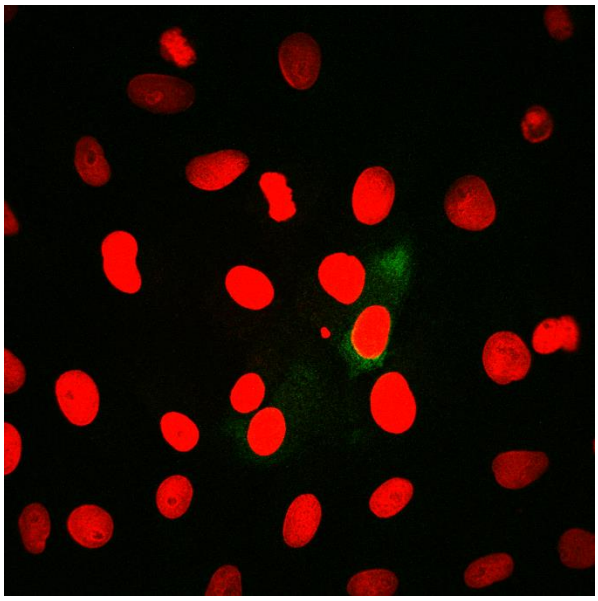

	Percentage Infected Cells		Peak Intensity (a.u.)	
Hours Post Infection	rRomero	rRomero/CanZ	rRomero	rRomero/CanZ
12	3.7	0	418	0
24	8.9	0	1128	0
36	9.0	1.4	1459	1183
48	87.2	12.1	2076	1783

Figure 7. Spread of rJUNV infection. VeroE6 cells were infected with each virus at an MOI of 0.01. rRom infection shown on left, rRom/CanZ infection shown on right. Cell monolayers were fixed at 12, 24, 36, and 48 hpi and stained with conjugated anti JUNV NP antibody. Images taken via confocal microscopy.

addition, the peak NP intensity in rRom infected cells was consistently higher at every time point when compared with rRom/CanZ. This shows that in addition to low spread, rRom/CanZ results in less overall NP production, as seen via IFA.

The rRom/CanZ and rRom/V64G are attenuated *in vivo*

In vitro characterization has demonstrated that rRom/CanZ and rRom/V64G have reduced growth kinetics whereas rRom/V64G showed notable reduction of viral NP mRNA accumulation in Northern Blot. We next examined whether rRom/CanZ and rRom/V64G were, compared to rRom, attenuated in the outbred Hartley guinea pig (HGP)

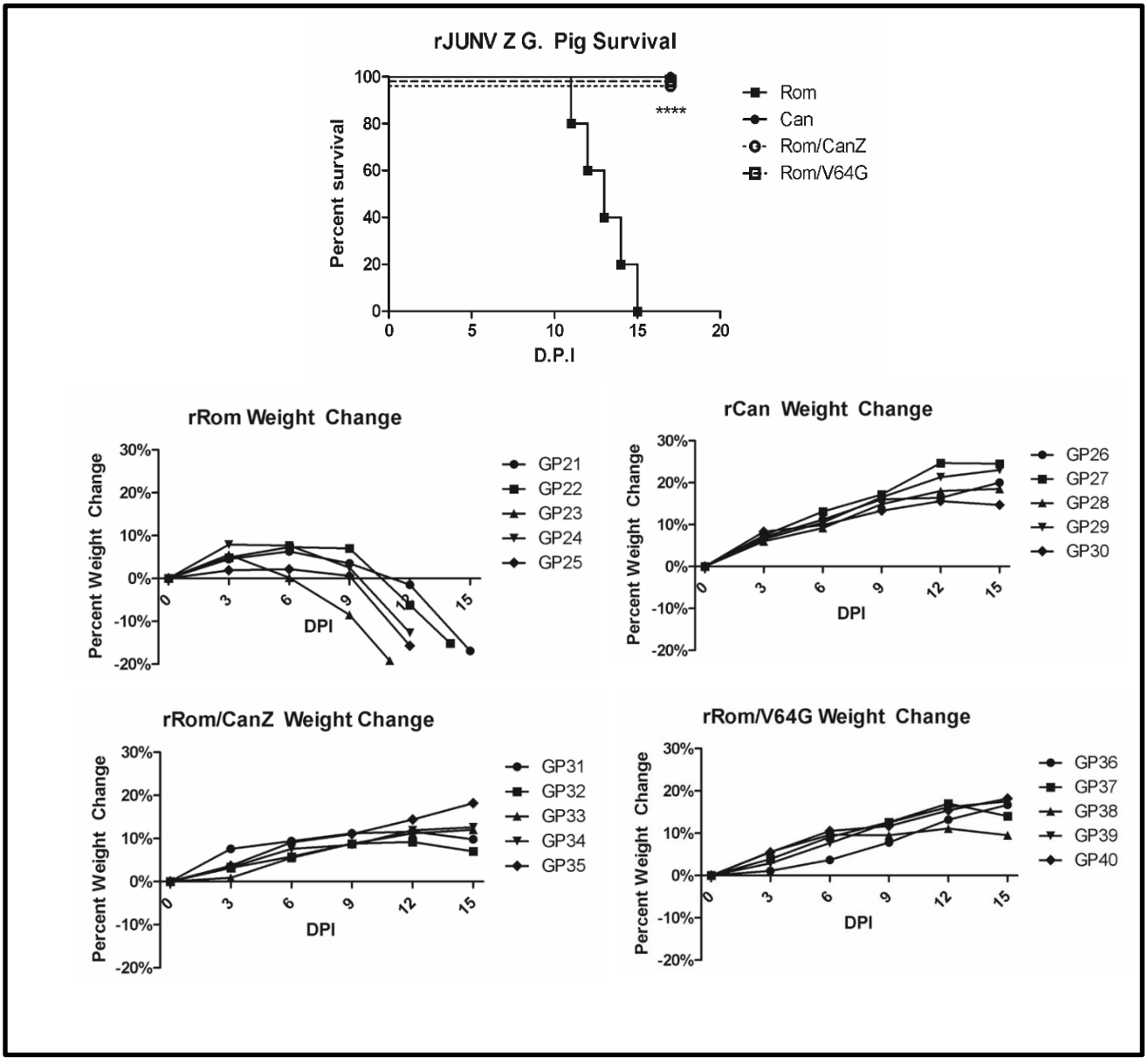

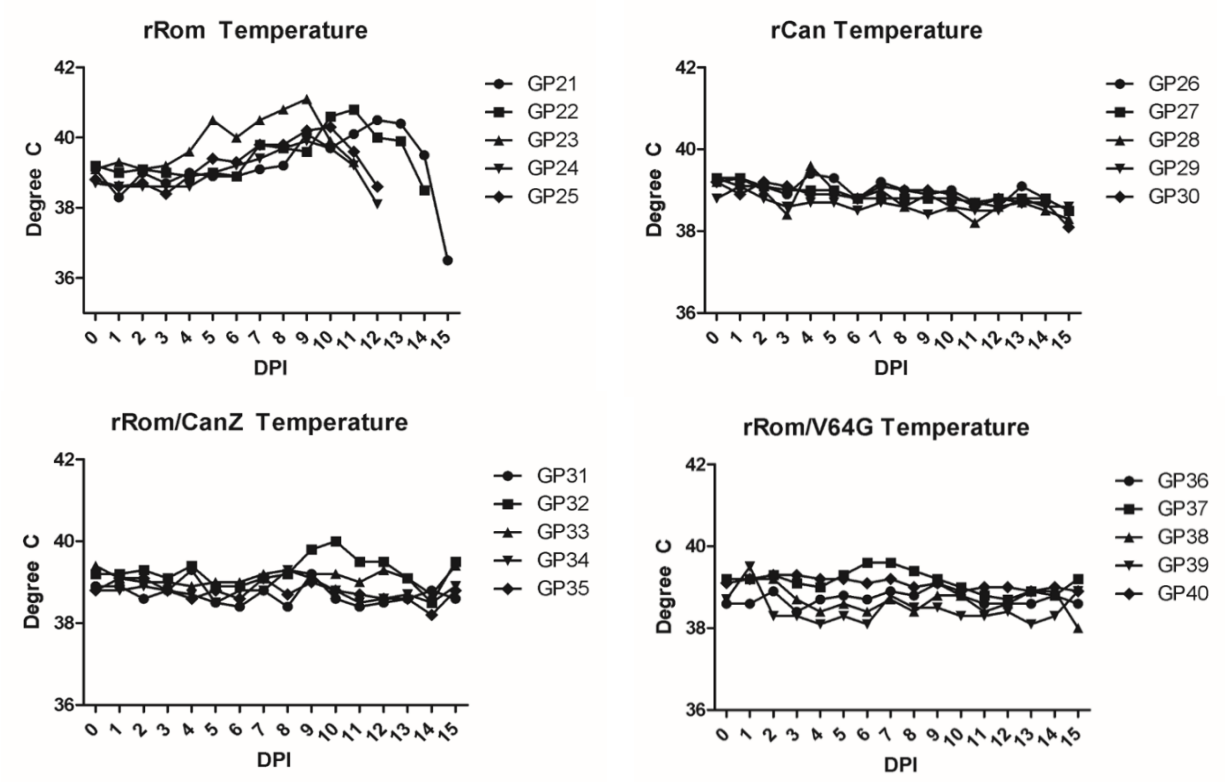

Figure 8. Survival, weight change, and temperature of Guinea Pigs infected with rJUNV. Animals were monitored daily for weight and clinical signs of disease. Panel A shows the survival of each group by day post infection. rCan, rRom/CanZ, and rRom/V64G infected animals all resulted in 100% survival, lines are separated for ease of viewing. Panels B-E demonstrate the percent weight change from start of study. Animals were euthanized after losing >15% body weight. Panels F-I demonstrates the daily body temperature of each animal through the course of the study. The red line indicates the clinical definition of fever at 39.5º C.

model of JUNV infections (33, 120). rRom infection results in complete lethality in this model. In addition, the Hartley guinea pig recapitulates many hallmarks of JUNV infection including leukopenia, thrombocytopenia, elevated liver enzymes, and hemorrhaging, all seen in AHF patients. Guinea pigs were infected with 10^3 PFU of rRom, rCan, rRom/CanZ, or rRom/V64G via the intraperitoneal (i.p.) route for a total of twenty animals. All animals were monitored for the appearance of clinical symptoms including weight loss and fever for 15 dpi. All HGPs infected with rCan, rRom/CanZ and rRom/V64G survived until the end of the study and did not develop noticeable clinical symptoms with the exception of one HGP inoculated with rRom/CanZ that exhibited transient fever (Fig. 8). In contrast, all

HGP inoculated with rRom exhibited weight loss and fever associated with progression of disease and succumbed to infection by 15 dpi. Daily animal weights were collected through the course of the study and shown as percent change from start of study. In addition, daily temperatures were collected and displayed (Fig. 8B-I).

Finally, at the necropsy of rRom-inoculated HGP, nasal bleeding, hemorrhage from the gastro-intestinal tract, small spleen, and petechial hemorrhage in the liver were observed. These examples of gross pathology were absent in all other inoculated HGPS.

The animals in the study were subjected to blood collections at 9 dpi and prior to euthanasia. Whole blood was used to collect hematology data, and serum samples were used to determine blood clinical chemistry data. rRom and rRom/V64G infected animals demonstrated white blood cell (WBC) and platelet (PLT) counts below normal levels at 9 dpi, although these were not significantly different from the other groups (Fig. 9). By the final time point, however, both rRom/CanZ and rRom/V64G infected animals had returned to approximately normal counts for both parameters. Interestingly, rCan infected

animals ended the study with WBC counts lower than normal, but above those of rRom animals. Consistent with the progression of hemorrhagic fever, rRom infected animals ended the study with nearly undetectable platelet levels.

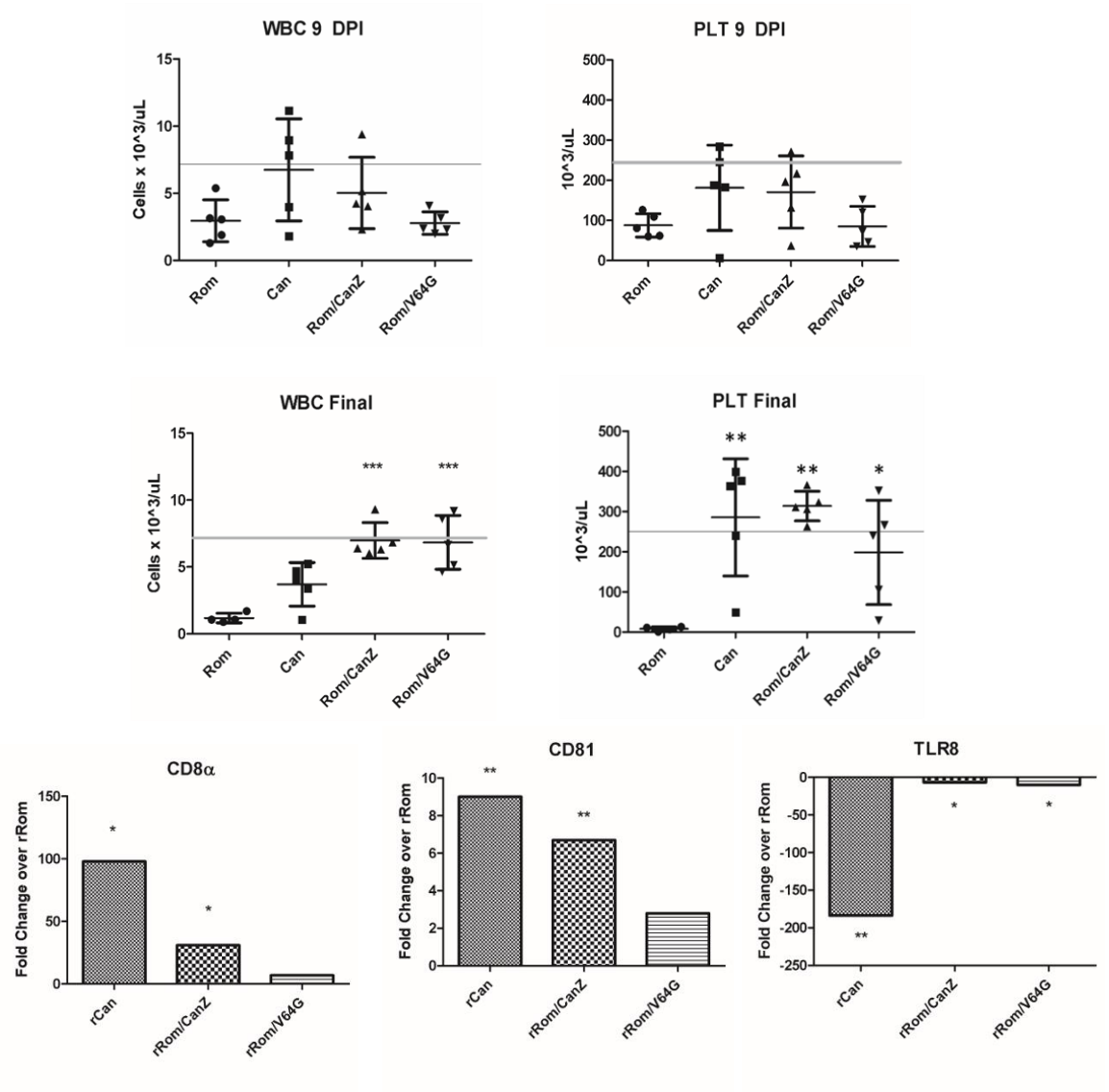

Figure 9. Hematological and immunological changes in Guinea Pigs infected with rJUNV. Blood was collected from all animals at 9 days post infection and at the end of the study. Final blood collection from rRom infected animals came on the day of euthanasia (11-15 dpi) while final collection from all other groups occurred 17 dpi. Error bars represent the standard deviation from the mean. The gray line indicates the lower bound of normal levels for healthy Hartley guinea pigs. PBMCs collected 9 dpi were used for RNA isolation and qRT-PCR analysis of CD8alpha, CD81, and TLR8. rCan, rRom/CanZ, and rRom/V64G samples were compared to rRom samples to determine fold changes. * = $p<0.05$, ** = $p < 0.01$, *** = $p < 0.001$

Peripheral blood mononuclear cells (PBMCs) were isolated from whole blood samples of HGP collected at 9 dpi. The RNA isolated from PBMCs was analyzed using an established immunological PCR array. Values were normalized to housekeeping genes and expressed as fold changes over rRom infected samples. In total, 96 targets were analyzed. rCan and rRom/CanZ infected samples demonstrated significantly higher RNA levels of CD8α ($CD8^+$ T cell marker) than rRom-infected samples. rRom/V64G infected samples did not exhibit a significant difference. Additionally, RNA levels of CD81 (antigen presenting cell marker) were significantly higher in rCan and rRom/CanZ infected samples. Finally, all groups showed a decreased RNA levels of TLR8 (ssRNA receptor), with rCan-infected samples showing the greatest reduction (Fig 9).

The PCR array also included a target for JUNV genomic RNA to determine the presence of JUNV in the sample. PBMC samples collected at 9 dpi exhibited detectable levels of JUNV RNA in 4 of 5 rRom infected HGP, whereas none of the samples from rCan, rRom/CanZ, and rRom/V64G infected animals contained detectable levels of JUNV RNA by 9 dpi. Results from all mRNA targets are shown in Supplementary Table 1.

Analysis of blood chemistry also yielded valuable information about the pathogenesis of each of these viruses. We compared 3 separate analytes: alanine transferase (ALT), an indicator of hepatic inflammation and damage; amylase (AMY), an indicator of pancreatic inflammation and damage and blood urea nitrogen (BUN) as indicator of renal disfunction. At 9 dpi most HGP were within the normal analyte ranges, with the exception of rRom-infected animals that exhibited slightly reduced AMY levels (Fig. 10). At the final blood collection, rRom-infected HGP exhibited elevated ALT and AMY levels that were above the ranges for healthy HGP. In addition, rCan and rRom/CanZ

were significantly lower than rRom infected levels, remaining within the healthy ranges. By the final collection, BUN levels were all still within the ranges for healthy HGP. rRom/CanZ and rRom/V64G infected samples exhibited significantly reduced BUN levels compared to rRom infected samples.

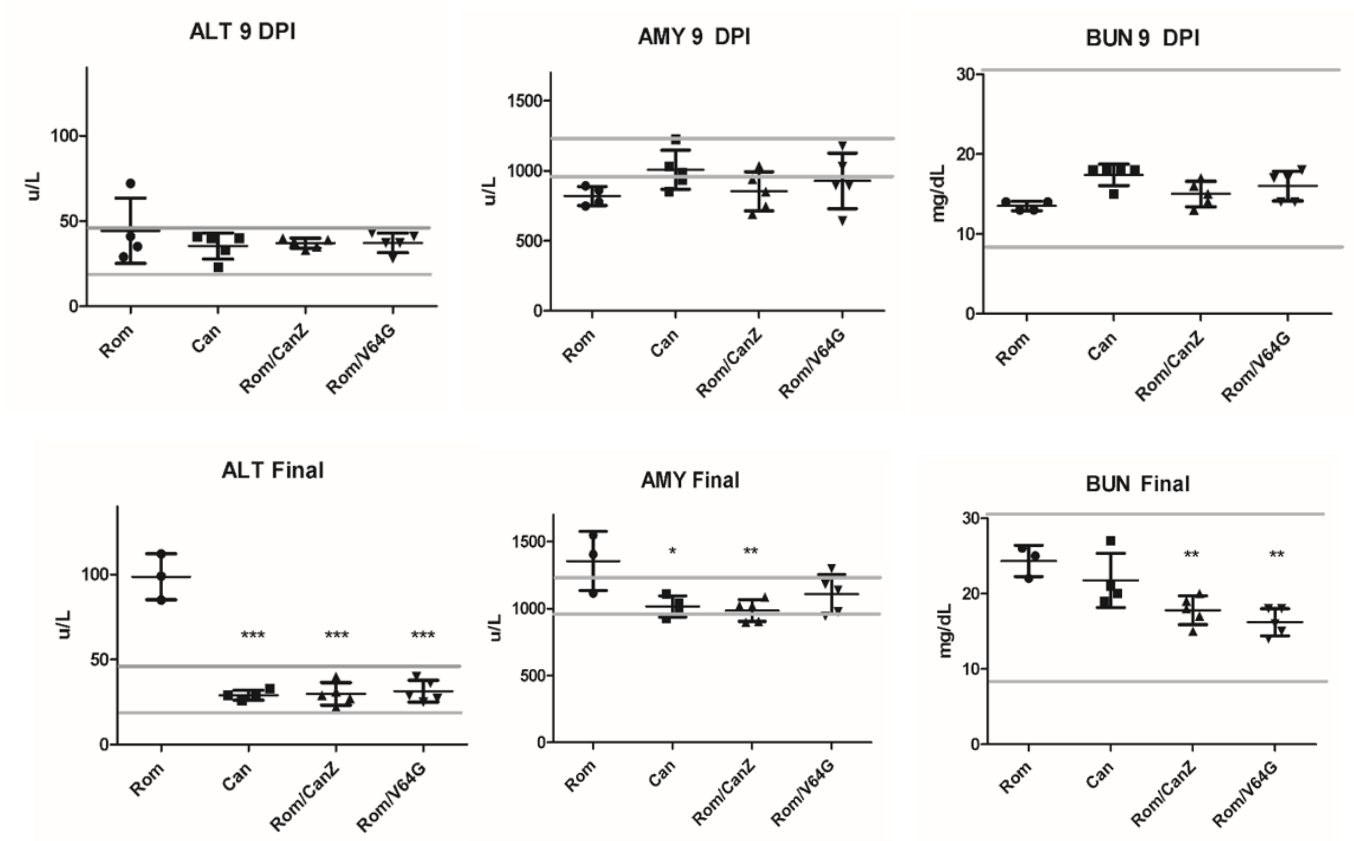

Figure 10. Clinical chemistry of Guinea Pigs infected with rJUNV. Serum was collected from all animals at 9 days post infection and at the end of the study. Final serum collection from rRom infected animals came on the day of euthanasia (11-15 dpi) while final collections from all other groups occurred 17 dpi. All groups were compared against rRom infected animals, and statistical significance is indicated by asterisk. The gray line indicates the upper and lower bound of normal levels for healthy Hartley guinea pigs. * = $p < 0.05$, ** = $p < 0.01$, *** = $p < 0.001$. Error bars represent standard deviation from the mean

One of the hallmarks of the Can vaccine is its limited organ dissemination within infected hosts (120). Accordingly, we examined whether rRom/CanZ and rRom/V64G infection

exhibited also restricted organ dissemination by determining viral loads in kidney, spleen, liver, lung, and brain of infected HGP. Only rRom infected HGP had detectable viral load in all 5 organs (Fig. 11).

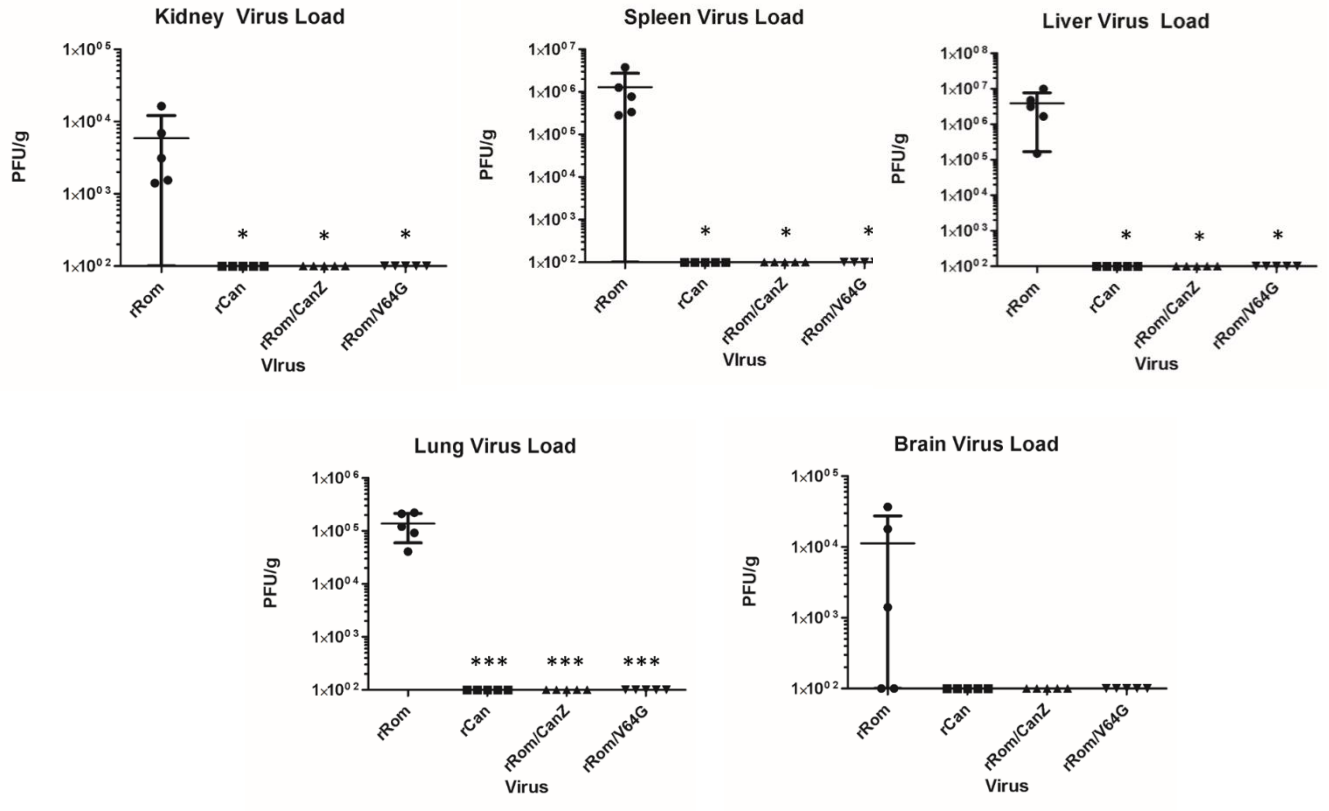

Figure 11. Viral loads in organs of Guinea Pigs infected with rJUNV. Following euthanasia or death, kidney, spleen, liver, lung, and brain samples were collected from all animals. Organs collected from rRom infected animals came on the day of euthanasia (11-15 dpi) while final collections from all other groups occurred 17 dpi. Samples are shown as geometric mean ±SD. All groups were compared against rRom animals and statistical significance is indicated by asterisk. The limit of detection was 100 PFU/g and forms the lowest point on the Y axis. * = $p < 0.05$, *** = $p < 0.001$

Serum from the final blood collections from infected HGP was utilized in PRNT assay with rRom. We could not collect enough serum to perform the assay for all animals. We tested serum samples from all 5 rRom, 2 rCan, 2 rRom/CanZ, and 3 rRom/V64G infected

HGP. We did not detect neutralizing activity in any rRom-infected serum sample, while all other samples had neutralizing titers ranging from 1:5-1:24.

Spleen homogenates from infected animals were utilized in qRT-PCR for the detection of JUNV NP locus RNA. In total 3 rRom, 3 rCan, 4 rRom/CanZ and 5 rRom/V64G infected spleens were tested. In addition, a LASV infected HGP spleen homogenate was used as a negative control. The results show that by the end of the study, all tested animals infected with rCan, rRom/CanZ and rRom/V64G showed no detectable JUNV NP locus RNA (Fig. 12.). All three samples infected with rRom exhibited a high copy number.

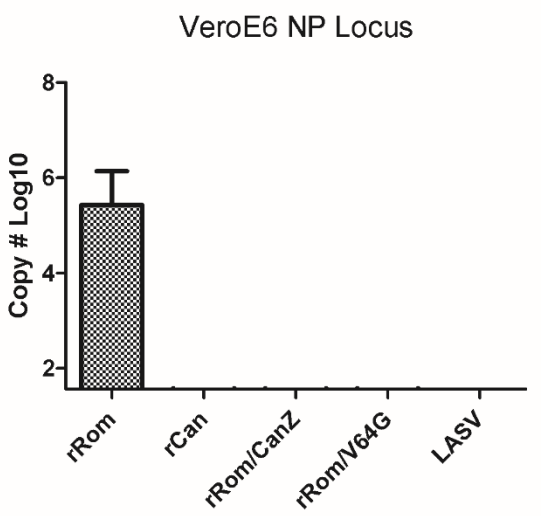

Figure 12. Viral NP RNA detection in HGP Spleen. Collected spleens were homogenized and utilized in qRT-PCR. Organs collected from rRom infected animals came on the day of euthanasia (11-15 dpi) while final collections from all other groups occurred 17 dpi. Sample size: 3 rRom, 3 rCan, 4 rRom/CanZ, 5 rRom/V64G, 1 LASV. Lower range of the Y-axis set to the negative control (LASV).

Histopathological assessment showed that rRom, but not rRom/CanZ or rRom/V64G, infected HGP exhibited significant spleen and liver damage. The rRom infected spleens demonstrated reduced lymphocytes in white pulp, increased congestion and likely necrosis in the red pulp. Neither rRom/CanZ nor rRom/V64G infected spleens exhibited any apparent pathology. The rRom infected livers exhibited fatty metamorphosis and

apoptotic nuclear fragmentation as seen in the sinusoid space. A single rRom/V64G infected liver exhibited fatty metamorphosis, but neither rRom/CanZ nor rRom/V64G infection resulted in apoptotic nuclear fragmentation. Brain damage was not detected in any of the examined infected HGP (Fig. 13).

A

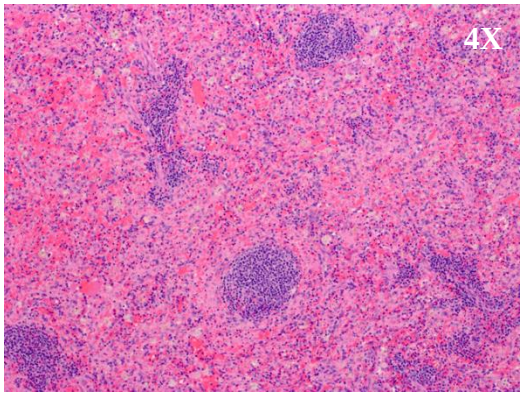

B

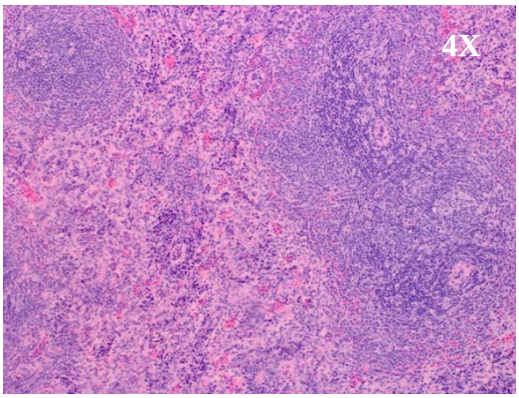

C

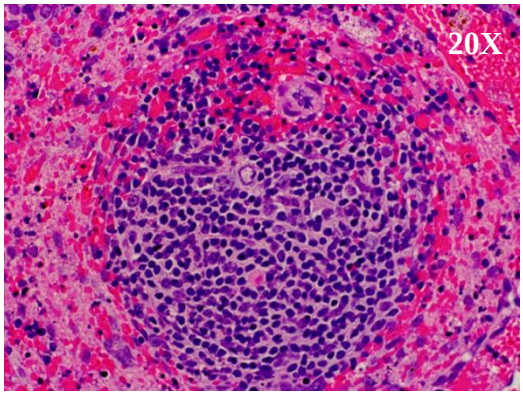

D

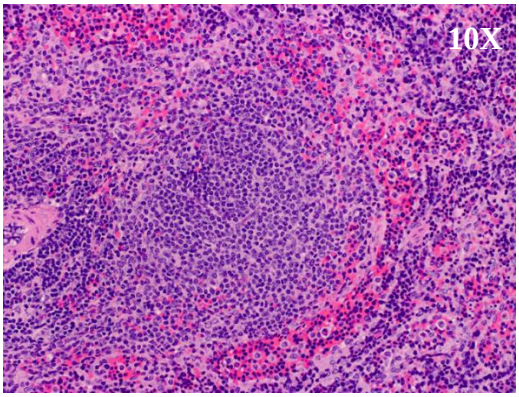

E

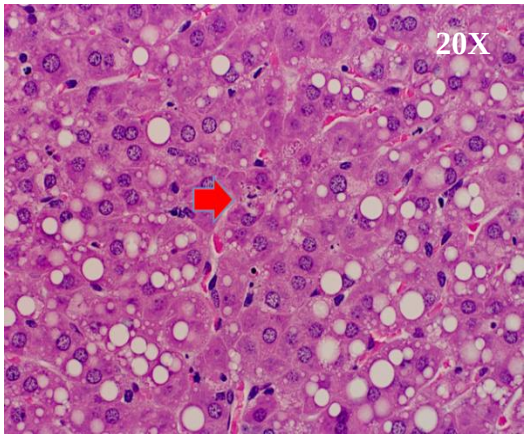

F

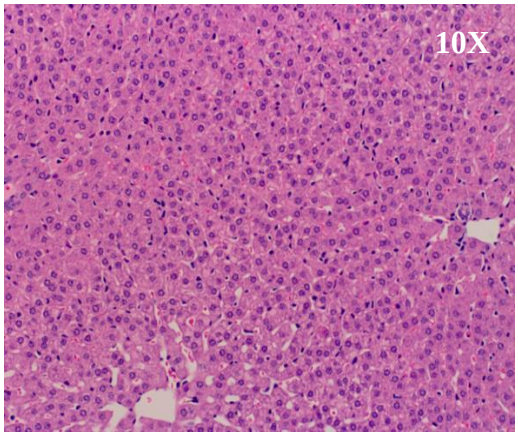

G

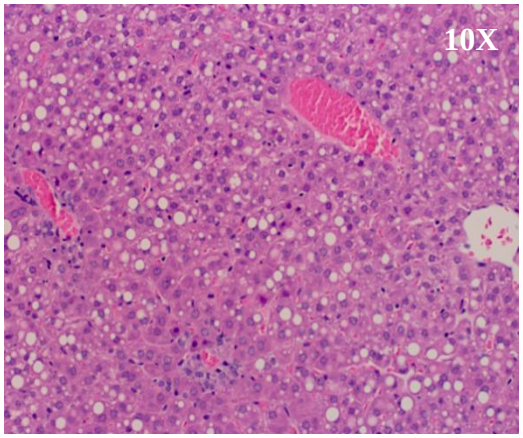

H

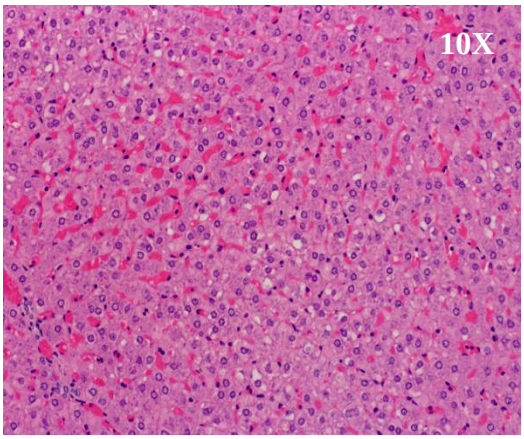

Figure 13 Histopathological changes of Guinea Pigs infected with rJUNV. Spleen and Liver samples from rRom, rRom/CanZ, and rRom/V64G infected animals were fixed, embedded, mounted, and stained by H&E. Representative fields were imaged for each group. Spleens are shown for rRom (A and C), rRom/CanZ (B), and rRom/V64G (D). Livers are shown for rRom (E and G), rRom/CanZ (F), and rRom/V64G (H). Magnifications are shown in the upper right of each panel. An arrow indicates nuclear fragmentation in the sinusoid.

Discussion

The development of vaccines and therapeutics for viral hemorrhagic fevers is a pressing concern for global public health. The *Mammarenavirus* genus contains many human pathogens including LASV, JUNV, MACV, GTOV, and SABV; each capable of causing hemorrhagic fever manifestations. Previous studies have shown that GPC is the main determinant of JUNV virulence as rRom/CanGPC exhibits an attenuated phenotype comparable to that of rCan (33). In addition, Can GPC mediated attenuation of JUNV correlates with ablation of a conserved glycosylation motif in GPC that results in altered GPC trafficking and increased cellular stress (27). However, there is a lack of knowledge about additional viral determinants of JUNV attenuation.

In the preceding work we have shown that a single mutation (V64G) in the RING domain of the virus matrix Z protein was sufficient to reduce viral replication and growth *in vitro* and attenuate the virus *in vivo.* The V18A mutation did not appear to affect growth *in vitro,* although it does appear to contribute to attenuation *in vivo.* Z interacts with LP, NP and GPC, but whether V18A and V64G mutations influence these interactions remains to be determined (36–38). The effect of the V64G mutation was readily apparent in cultured cells as decreased growth kinetics, whereas mutation V18A did not exhibit a noticeable phenotype in cultured cells. The single V64G mutant also demonstrated decreased RNA production as seen in qPCR and Northern Blot analysis. Viruses harboring both

(rRom/CanZ) mutations or the RING domain mutation (rRom/V64G) found in Can were shown to be attenuated *in vivo* and result in survival of all infected animals. At 9 dpi guinea pigs infected with rRom/V64G or rRom exhibited similar reductions in WBC, PLT counts and CD8α levels at 9 dpi, but WBC and PLT levels recovered in guinea pig infected with rRom/V64G. Guinea pigs infected with rCan or rRom/CanZ exhibited WBC and PLT counts and CD8α levels within the normal biological ranges. These findings are consistent with reports of decreased $CD8^+$ T cell levels in AHF patients (104). Our lethal rRom model in guinea pigs successfully recapitulates this key clinical feature seen in human disease. In addition, we are able to show that rCan infection does not result in this loss of leukocytes and CD8α mRNA transcription. Furthermore, the reduced white pulp and general spleen pathology seen in the rRom infected animals supports similar pathology seen in fatal human AHF cases (105). The rRom/CanZ virus exhibited a Can-like phenotype in early analyte measurements and mRNA transcripts, indicating that the combination of both V18A and V64G mutations results in a stronger attenuating phenotype than the one associated with the single V64G mutation. Attenuation conferred by both of these mutations is likely due to protein-protein incompatibility between the Can Z and some wild type Rom proteins since we do not see any growth impediments in full rCan virus. Since the RING domain interacts with NP and LP, the attenuation due to that mutation might be due to an incompatibility with one or both of those proteins. Since those two proteins are vital for viral replication, it stands to reason why an incompatibility involving NP or LP would result in the decreased replication seen *in vitro* and *in vivo*. The N terminal arm of Z interacts with the GPC, suggesting the possibility of an additional incompatibility with Rom GPC (35). An

incompatibility in this interaction may result in impaired virion formation and budding, leading to attenuation due to impaired production and spread of the virus in an animal host. It is likely that this effect may not be apparent in an *in vitro* system. All surviving animals cleared the virus, which prevented us to assess potential differences between rRom/CanZ and rRom/V64G in their ability to disseminate *in vivo*, using currently available samples. However, blood chemistry, hematology, and transcriptome results indicated that rRom/V64G infection resulted in clinical symptoms at early stages of infection, but no viral RNA was detected in PBMCs of rRom/V64G-infected guinea pigs. All available serum from surviving animals exhibited low PRNT levels, whereas rRom infected serum samples did not.

JUNV is the only HF-causing mammarenavirus for which there is a live attenuated vaccine, Can, with demonstrated safety and efficacy in humans. Therefore, understanding the attenuating mechanisms of Can might facilitate future vaccine development for related hemorrhagic fever-causing NW mammarenaviruses. The RING domain present in the matrix Z protein is highly conserved among mammarenaviruses, raising the possibility that counterpart mutations to the V64G attenuating mutation we have documented here for JUNV might attenuate the closely related MACV, GTOV, and SABV. The identification of these type of single mutations within the RING domain of Z in combination with known attenuating mutations within the virus GPC can significantly contribute to rationally designing live attenuated virus (LAV) candidates for highly pathogenic NW mammarenaviruses.

Chapter 4 The LP/Z incompatibility results in impaired rJUNV growth and replication

BACKGROUND AND PRELIMINARY DATA

The JUNV Z is a multifunctional protein that fulfills many roles during the virus life cycle. It acts as a matrix protein in the virion as well as interacts with all three additional viral proteins: LP, NP, and GPC. The N terminal domain of Z has been shown to be crucial for interaction with the glycoprotein (35), but not the LP or NP. The RING domain, on the other hand, has been shown to be critical for the LP and NP interactions (37–40). The early results from the preceding chapter indicate that compatibility between the RING domain of Z is crucial for wild type levels of growth and RNA production. Specifically, a single Can-like mutation in the RING domain (V64G) was able to result in an incompatibility with the wild type Rom proteins and produced the reduced growth and RNA production seen. In addition, this single mutation was able to confer attenuation on the recombinant virus in the lethal guinea pig model, although both Can-like Z mutations (V18A and V64G) resulted in a stronger attenuation profile.

Given the reduced replication, reduced growth, and attenuation associated with the V64G mutation, the natural question is what viral protein this mutation is incompatible with. Since the RING domain of Z is shown to interact with NP and LP, we hypothesized it would be one of those two proteins and not the glycoprotein. To determine where the incompatibility was occurring, preliminary experiments were conducted in which the V64G mutation was introduced into rRom in conjunction with the ORF of either Can LP, Can NP, or Can GPC. Since rCan shows replication and growth levels similar to wild type rRom, the introduction of a Can protein in conjunction with the Can V64G mutation should

return the chimeric virus to wild type growth levels. In addition, the homologous Can proteins should return the plaque phenotype from small to large.

The results indicated that the introduction of Can LP restored the P1 titers to wild type levels (Fig. 14). In addition, the plaques returned to a large phenotype. Introduction of the Can NP resulted in titers still a log below wild type and produced small plaque

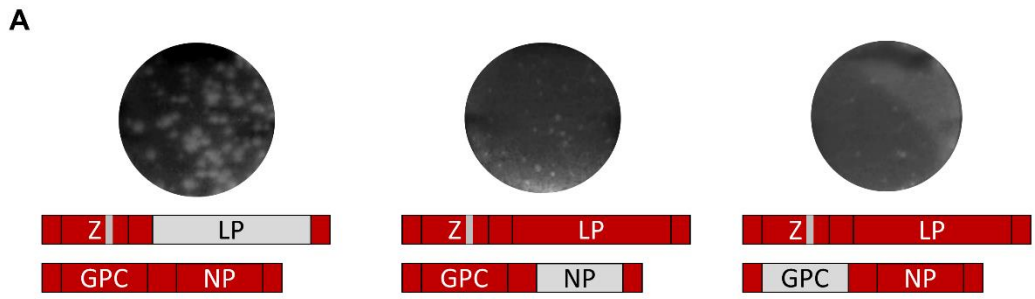

B

Passage 1 Titer at 4 dpi, Log10 PFU/mL		
Rom/Z-V64G + Can LP	Rom/Z-V64G + Can NP	Rom/Z-V64G + Can GPC
6.7	5.1	2

Figure 14. Initial characterization of rRom/V64G with either LP, NP, or GPC of rCan. rRom/V64G+CanLP, rRom/V64G+CanNP, and rRom/V64G+CanGPC were generated utilizing the plasmid system and blind passaged once. The resulting plaque morphologies and genomic representations are shown in A. The resulting viral titers are shown in B.

phenotypes. Interestingly, introduction of the Can GPC resulted in drastically reduced P1 titers, well below those seen in rRom/V64G alone. From this preliminary experiment, it can be seen that the Z/LP interaction in JUNV is critical for viral growth *in vitro*. Given only the P1 titers, it is unknown how the kinetics of these viral growths differ when compared to rRom and rCan.

While this experiment outlined the existence of a Z/LP incompatibility that can be rescued by the introduction of homologous proteins, it does not elucidate what regions of the LP are involved in this interaction. The JUNV LP protein is approximately 2210 amino acids in length, comprising 4 domains (17). The first domain (DI) exhibits endonuclease activity and has been implicated in cap-snatching from host mRNAs (18). The third domain (DIII) contains the conserved RNA-dependent RNA polymerase (RdRp) motifs of viral RNA polymerases (20, 21). These are the only two known enzymatic domains of the proteins. Domains two (DII) and four (DIV) do not have identified or characterized functions. Early characterization of the domains was used to physically separate the protein into DI, DII, and DIII/IV. These subunits were able to associate and perform the polymerase functions even when expressed separately, although DIII and DIV had to be kept together. Previous studies have indicated that the Z of Clade B mammarenaviruses can bind to both DI and DIII of the LP (38). By creating chimeric rJUNV proteins and viruses encoding permutations of Can and Rom DI, DII, and DIII/IV, we can determine which polymerase subunit is required for compatibility with the RING domain of Z.

The LP of Can differs from that of Rom by a total of 49 amino acids including all reported variations of Rom sequences. Taking into consideration that Can comes from a different parental strain than Rom, the sequences were normalized against all other published JUNV LP sequences. Amino acid changes that were varied across multiple published genomes were excluded, while those that were conserved among wild type JUNV strains but different in Can were kept as probable vaccine-specific changes. This resulted in 25 amino acid differences from Rom across all four domains (Table 2).

Table 2: Rom to Can LP AA coding differences (controlled)

LP Domain	AA change
Domain I	N10S, H76Y, N265K
Domain II	K366T, M415A, D462N, R463K, S679G, N740S, S924T, T928I, L936P
Domain III	K1059R, R1156K, C1344F, K1506R, Q1668K, V1700I
Domain IV	I1883V, K1884R, S1915G, R1979G, S1984G, N2005S, V2040A

A common way to determine the functionality of polymerases is through a mini-genome system. In this system, two Pol II-driven expression plasmids are used to produce the LP and NP proteins, in addition to a Pol-I driven expression of the modified S segment. The modified JUNV S minigenome segment has undergone manipulation to result in the NP and GPC ORFs being replaced with the firefly luciferase (fLuc) and green fluorescent protein (GFP) ORFs respectively in an antigenomic coding orientation. This orientation results in fLuc being produced as the late gene product following the accumulation of agRNA. With the LP and NP expressed, transcription and replication of the minigenome S segment can occur and produce the reporter genes listed above. These can then be measured to determine the relative activities of the experimental polymerases under a variety of conditions. In the case of arenavirus mini-genome systems, Pol II driven expression plasmids of the Z protein can also be introduced to measure the inhibiting effects of Z on the LP (Fig. 15).

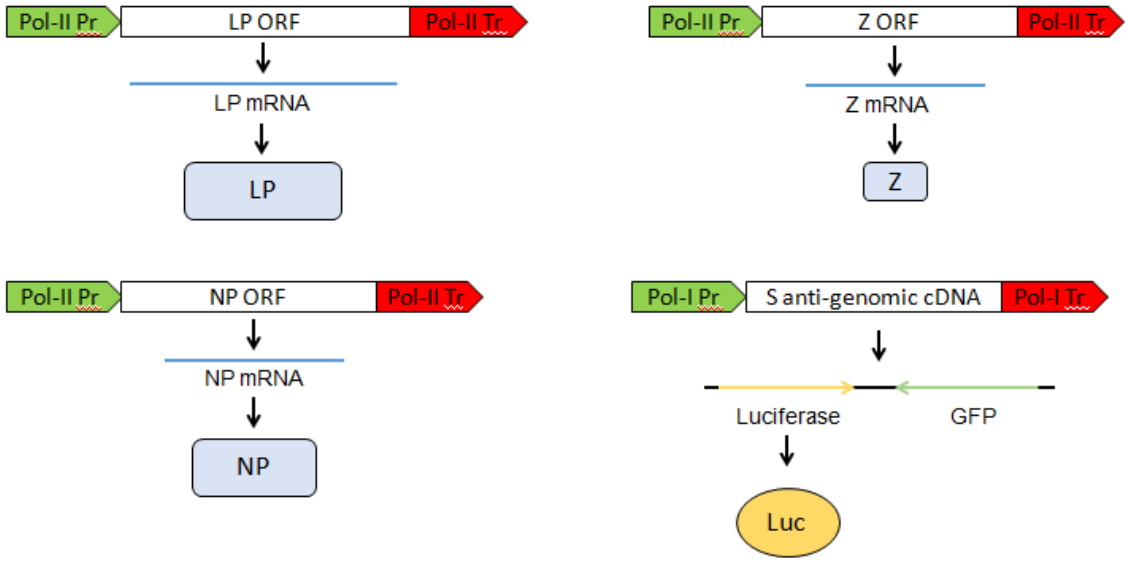

Figure 15. Arenavirus minigenome system. Minigenome assays are completed using the graphically represented plasmids. To determine the baseline activity of the LP, expression plasmids of the LP and NP are transfected in conjunction with the Pol-I promoted minigenome S segment. To determine the inhibitory effects of Z, a Z expression plasmid is also included. In this system, fLuc is produced as the late gene product.

RESULTS

The introduction of Can LP into rRom/V64G returns the growth kinetics to wild type levels.

While preliminary experiments demonstrated that the introduction of Can LP into rRom/V64G was able to return P1 titers to wild type levels, it did not demonstrate whether the growth kinetics of this virus would also return to wild type levels. To determine this, all chimeric rJUNV viruses used in the preliminary P1 study were examined via growth

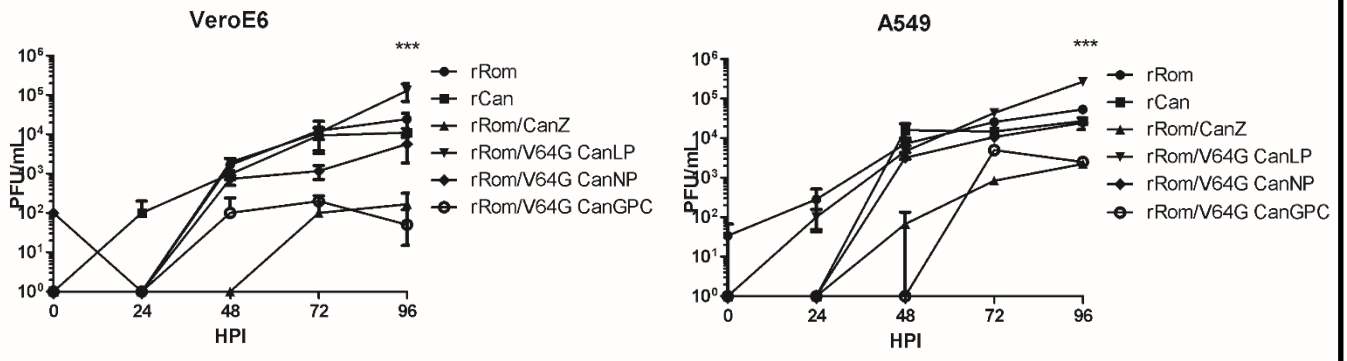

Figure 16. Growth kinetics of rRom/V64G with either LP, NP, or GPC of rCan. Growth kinetics for rRom, rCan, rRom/CanZ, rRom/V64G+CanLP, rRom/V64G+CanNP and rRom/V64G+CanGPC were measured in both VeroE6 and A549 cells. Infections were carried out in triplicate at MOI 0.01. *** = $p < 0.001$

kinetic assay. VeroE6 and A549 cells were infected with the indicated virus at MOI 0.01 and supernatant samples were collected following infection and at 24, 48, 72, and 96 hpi. Titers from each sample were determined via plaque assay. The results indicate that in both cell types rRom/CanZ and rRom/V64G+CanGPC produced infectious virions at several logs beneath wild type rRom and rCan (Fig.16). rRom/V64G+CanNP did not show drastic change in the growth kinetics when compared to the preliminary P1 experiment. rRom/V64G+CanLP not only restored titers to higher levels, but actually demonstrated growth significantly increased over rRom by the end of the experiment at 96 hpi.

Having confirmation that homologous Z/LP does in fact restore growth levels, it was important to determine what domains of the LP are responsible for the compatibility of these two proteins. To investigate this, chimeric LP ORFs were generated to represent all 6 permutations of Can and Rom DI, DII, and DIII/IV (Fig. 17). These were designated as SH001, SH002, SH003, SH004, SH005, and SH006.

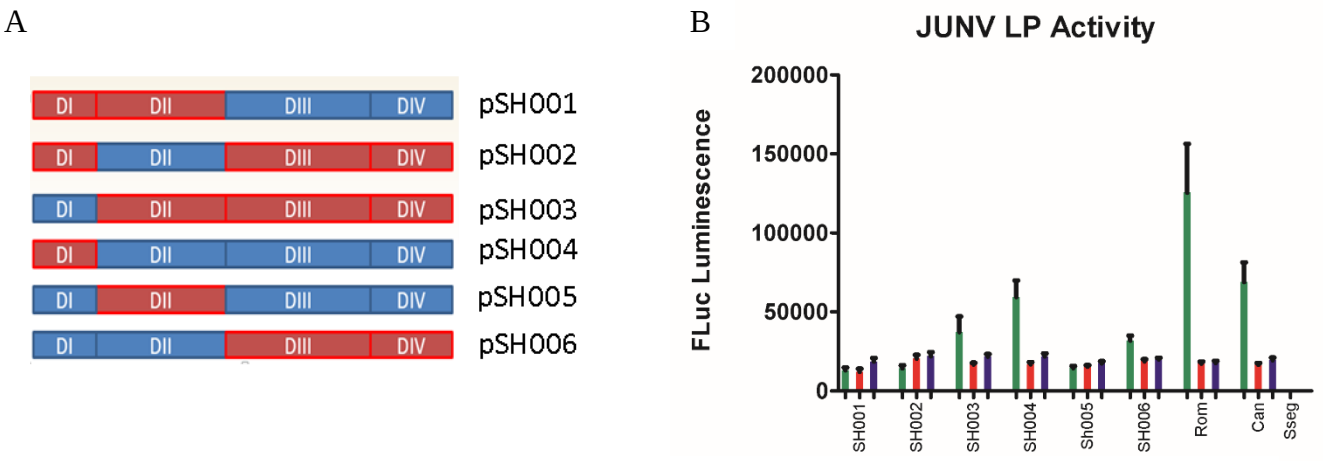

Figure 17. The rRom S-segment minigenome reporter activity with rRom NP, chimeric LP and Z of either rRom or rCan. Minigenome assays were performed for all six chimeric LP constructs in addition to Rom and Can LPs. All systems utilized a Rom NP and Rom minigenome S segment. Graphic representation of the constructs is shown in Panel A, with Red domains representing Rom and Blue domains representing Can. Panel B shows the measured fLuc levels in the absence of Z protein (green), in the presence of Rom Z (red), and in the presence of Can Z (blue).

Since these constructs represent chimeras from different strains of JUNV (Can and Rom), it was critical to determine if the polymerases were able to retain their polymerase activity. Each construct was utilized in a mini-genome system to determine the activity of the polymerase compared to Rom and Can LPs. In addition, each LP construct was also tested in the presence of Rom or Can Z proteins to determine if polymerase activity levels were subject to inhibition. It is possible that a chimeric virus may retain total polymerase function, but lose the ability to be repressed through interaction with Z. The results demonstrated that only SH003, SH004, and SH006 demonstrated polymerase activity that was able to be inhibited by the introduction of a Z protein. SH001, SH002, and SH005 showed consistently low levels of activity, even in the presence of the Z protein, indicating that those permutations may result in proteins with decreased polymerase activity.

All six LP constructs were used to be produced as Pol I driven genomic plasmids in preparation for the production of recombinant viruses. All of the successfully recovered recombinant viruses were generated with a Rom S segment (NP and GPC). The L segments were generated with the indicated LP construct and either the Rom or Can Z. Of the six constructs, only SH003, SH004, and SH006 were able to produce rJUNV, indicating that the other three constructs were not viable. The SH003, SH004, and SH006 constructs in conjunction with the Can Z ORF were designated SH016, SH017, and SH019. SH003 and SH004 with the Rom Z ORF were as designated SH022 and SH023. SH006 with a Rom Z ORF was not able to be recovered as a recombinant virus.

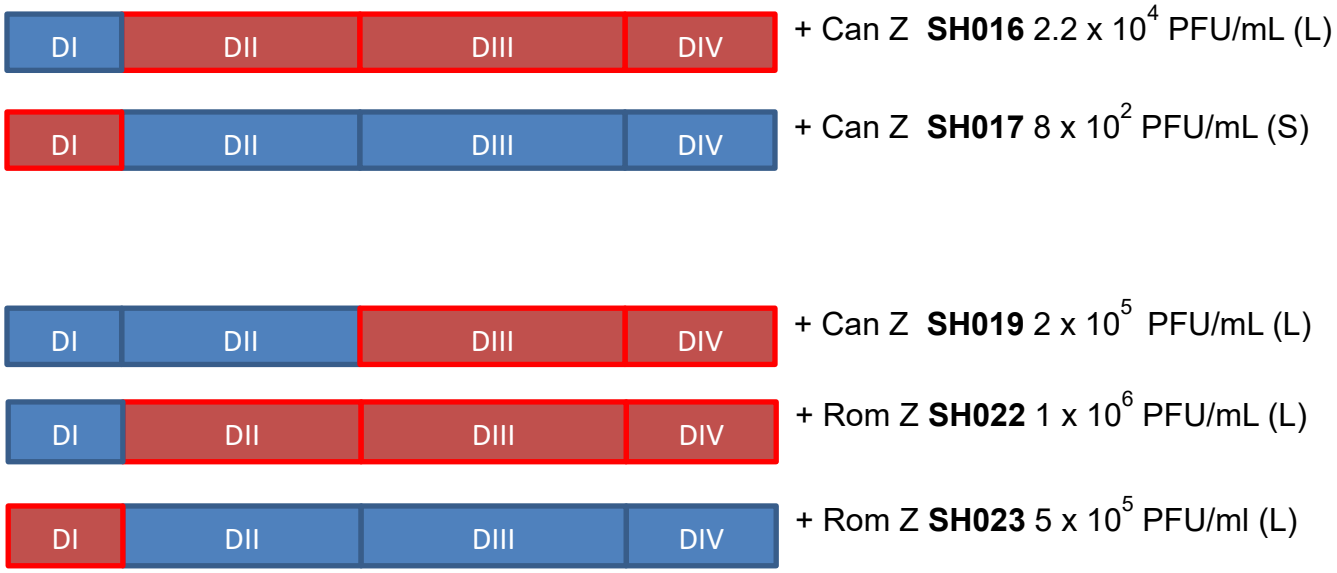

Figure 18. Production of rJUNV harboring chimeric LP. rJUNV was produced utilizing the Pol-I/II recombinant virus system. All viruses were produced utilizing a Rom S segment. Each virus is shown with a graphical representation of the LP, a description of the Z, and the P1 titer. Plaque morphology is indicated as either small (S) or large (L).

SH019, SH022, and SH023 all showed high P1 titers and a large plaque phenotype (Fig. 18). SH016 demonstrated a large plaque phenotype but had a P1 titer approximately 1 log

lower than the other viruses. Finally, SH017 exhibited drastically reduced titers and the small plaque phenotype originally seen in the Z/LP incompatibility of rRom/CanZ.

The initial results indicated that compatibility between Can Z and the DI of LP is responsible for the reduced growth kinetics initially seen. However, growth kinetics are required to confirm what is seen in the P1 titers. To determine this, all chimeric viruses except for SH017 were used to infect VeroE6 and A549 cells at MOI 0.01. SH017 had a titer that was too low for use in any subsequent experiments. rRom, rCan, and rRom/CanZ were also included to provide reference points to the previous phenotypes described.

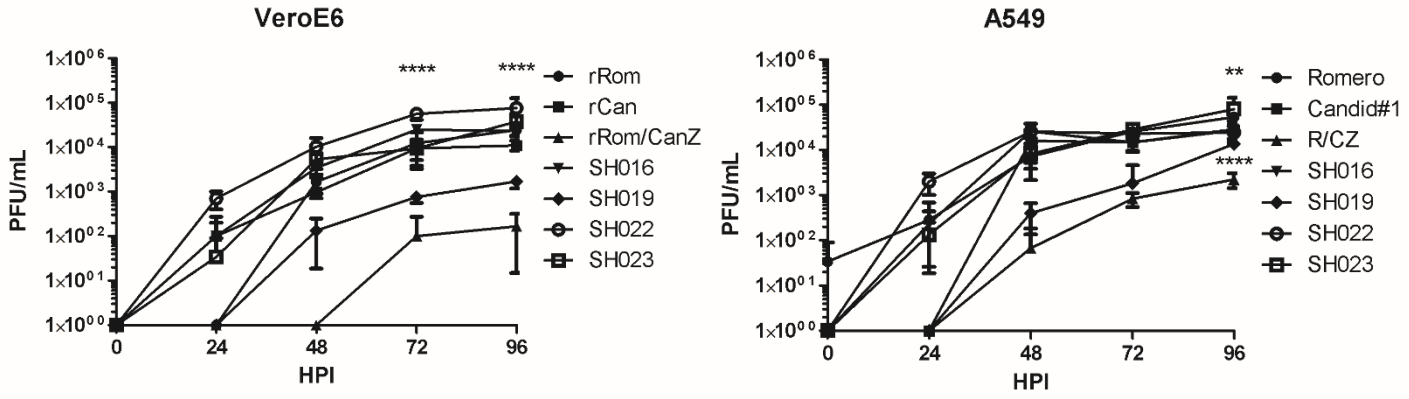

Figure 19. Growth kinetics of chimeric LP rJUNV. rJUNV was used to infect VeroE6 and A549 cells at MOI 0.01. SH022 demonstrated significantly higher growth in VeroE6 while SH019 and rRom/CanZ exhibited significantly lower growth compared to rRom. Infections were carried out in triplicate at MOI 0.01 ** = $p < 0.01$, **** = $p < 0.0001$

The growth kinetics indicate that both SH019 and rRom/CanZ grow at lower levels and rates compared to wild type rRom (Fig. 19). In addition, it demonstrates that SH022 exhibited significantly higher growth than rRom in VeroE6 cells. These results indicate that any combination involving a Rom Z produces normal or higher than normal growth levels, while rRom/CanZ and SH019 (both with a Can Z) resulted in decreased growth.

Interestingly, SH016 appears to enjoy normal growth while SH019 is reduced. This is a direct inversion from the results seen in the P1 titers previously. The replicated nature of the growth kinetics lends more credence to their results and demonstrate the importance of confirming P1 titer information with growth kinetic measurements.

One possible hypothesis for the reduced growth seen in some, but not all, viruses containing Can Z is that Can Z is released from the cell more readily than Rom Z. If Can Z is unable to interact with the LP or NP, it may move to the cell surface and engage in self budding and subsequent release from the cell. This could potentially result in decreased infectious virion production and an increase in non-viable particle production, or virus like particles (VLPs). To determine whether Can Z was able to be released from the cell at higher rates than Rom Z, a simple experiment was conducted. It is known that Z is the minimal budding factor for the virus, meaning it is able to form VLPs on its own and leave the cell. To determine if Can Z inherently leaves the cell at faster rates than Rom Z, expression plasmids of each protein were transfected into cells. After 36 hours, the cell monolayers and supernatants were collected, and VLPs were purified from the supernatant. Relative Z levels were then determined via Western blot to examine the relative abundance of intracellular and VLP Z levels. In addition, since Z interacts with GPC at the cell surface in preparation, it is possible that the presence or absence of Can or Rom GPC may affect the budding rates of Z. Briefly, it is possible that a productive interaction with GPC is required for Z to remain in the cell until proper budding is achieved. To address this as well, conditions were carried out in which Rom or Can GPC were also expressed at the same time as Z.

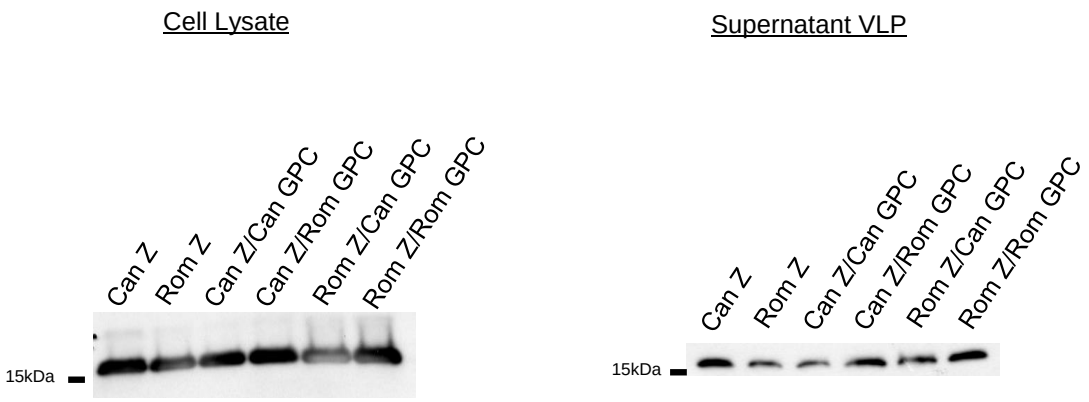

Figure 20. JUNV Z accumulation in VLPs. Cell lysates and supernatants were collected 36 hours following transfection with the indicated expression plasmids. Samples were probed with an anti-JUNV Z antibody to determine relative abundance.

The results show that intracellularly, Z levels are fairly constant across all condition (Fig. 20). This was expected in an overexpression environment created by the expression plasmids. The supernatants, however, show minor trends. There is a minor trend of increased Can Z over Rom Z, and in addition, it appears that Can Z can be slightly better retained in the cell when Can GPC is also present. However, these results are qualitative and do not provide conclusive proof of Can Z exiting the cell at higher rates than Rom Z. Because of that, we cannot conclude that Can Z is leaving the cell at an increased rate and it is unlikely that increased Can Z budding rates is responsible for the decreased growth phenotypes we observe in growth kinetics.

Since the growth of SH019 appeared to be impaired, it was important to determine whether this was an issue in virion production (budding, late stages) or viral replication (early stages). To determine this, each virus was used to infect VeroE6 and A549 cells at MOI 0.01. RNA was collected at 48 hpi and used for qRT-PCR at the NP locus. The locus chosen will measure both NP mRNA as well as antigenomic RNA, showing an aggregate of both transcription and genome replication.

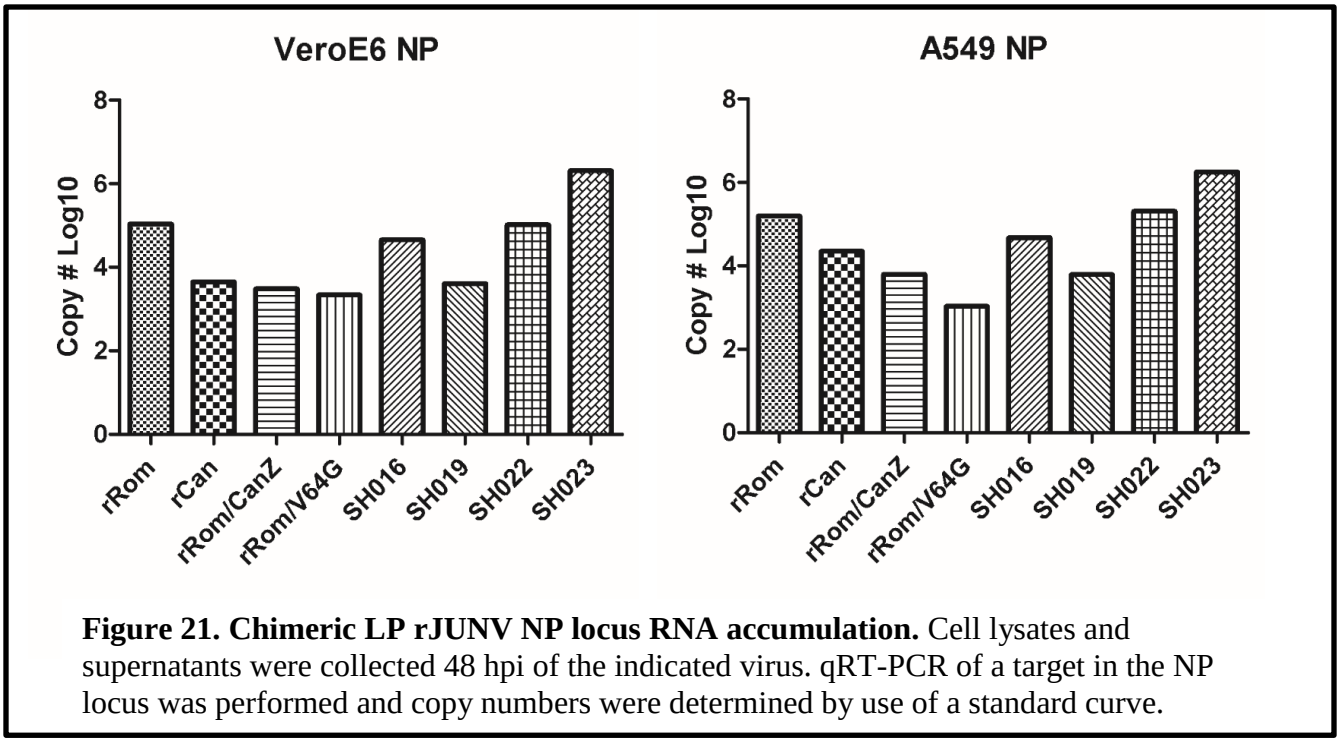

Figure 21. Chimeric LP rJUNV NP locus RNA accumulation. Cell lysates and supernatants were collected 48 hpi of the indicated virus. qRT-PCR of a target in the NP locus was performed and copy numbers were determined by use of a standard curve.

The results confirm what we had seen earlier in the growth kinetics involving chimeric LP rJUNV. rRom/CanZ, rRom/V64G, and SH019, which all seem to produce about 1:10 the amount of NP locus RNA compared to wild type rRom in VeroE6 cells (Fig. 21). Interestingly, rCan also seems to produce low levels in VeroE6 that are slightly elevated in A549. Throughout all growth and replication experiments, rJUNV appears to grow more efficiently in A549 when compared to VeroE6 cells. SH016 and SH022 both appear to produce NP RNA at rRom levels in both cell types. SH023, meanwhile exhibited consistently high levels of RNA production in both cell types. This production was approximately 1 log higher than rRom, and subsequently about 2 logs higher than rRom/CanZ, rRom/V64G, and SH019.

DISCUSSION

Previous experiments had indicated that an incompatibility likely existed between the Can Z and a wild type Rom protein that resulted in decreased growth *in vitro* and

attenuation *in vivo*. Additionally, this incompatibility was determined to be localized to the RING domain of Z, implicating LP and/or NP as the likely incompatible partner. Preliminary experiments elucidated that the introduction of a Can LP in conjunction with the Can-like Z V64G mutation resulted in a restoration of higher titers and large plaques seen in wild type Rom. Growth kinetic experiments were able to confirm the results of the P1 preliminary experiment. rRom/V64G with Can LP not only restored growth to rRom-like levels but even exceeded the replication of rRom. Interestingly, rRom/V64G with Can GPC resulted in drastically reduced P1 titers and low growth kinetics. Future work will be required to determine what effects the Z/GPC incompatibility has on virus growth and replication.

To understand what domains of the LP are implicated in the incompatibility with Can Z, chimeric LP ORFs were generated and cloned into Pol II-promoter expression plasmids. These expression plasmids were utilized in a minigenome system to determine their activity both uninhibited and inhibited with Can or Rom Z. The results demonstrated that only three of the constructs (SH003, SH004, and SH006) showed an activity able to be repressed by introduction of Z. All of the polymerases showed activity below that of Rom and Can. It is not surprising that Rom and Can have optimized their polymerase domains to work in concert with each other, and that moving these domains between strains can de-optimize the system. In this assay, it was shown that Can Z and Rom Z inhibit every polymerase to the same degree. This suggests that the incompatibility seen likely does not involve an ablation of ability to inhibit the LP. However, the minigenome system relies on an overexpression of Z, likely unseen in natural infection. If there was a subtle change in the ability of Z to inhibit LP, it would not be seen in the overexpressed minigenome system. Nevertheless, the three active polymerases did justify a transition to a recombinant virus system harboring these chimeric LPs.

The generation of all six LPs with a Rom S into rRom was only successful for the same three constructs that showed elevated polymerase activity. These three were

successfully recovered with the Can Z, and two of the three were successfully recovered with the Rom Z. The first and most striking observation was that the SH017 virus resulted in extremely low P1 titers and a small plaque phenotype. This virus had an LP consisting of Rom DI, Can DII-IV, and a Can Z. This result indicates that the Can Z mismatch may be in conjunction with DI of the polymerase. When DI is Rom and the Z is Can, as it is in this virus, the titers and plaques seem to follow the phenotype seen in rRom/CanZ. An incompatibility at this location might implicate alterations to the endonuclease function of DI as part of the phenotype. However, this virus had such a low titer that it could not be utilized in subsequent characterization. Attempts to passage the virus and amplify it were consistently unsuccessful. This means that growth kinetics were never obtained, and it was never able to be comprehensively characterized in terms of RNA production.

The remaining four, recovered rJUNV chimeric constructs (SH016, SH019, SH022, and SH023) were all able to be further characterized. Growth kinetic assays revealed that SH019 demonstrated the most impaired growth, similar to rRom/V64G. Unlike SH017, SH019 has a Can DI that is homologous with the included Can Z. In this construct, the DIII and DIV is from Rom, suggesting a possible second region of incompatibility with Can Z. Given that Z is predicted to bind at both DI and DIII, it is not surprising that incompatibilities at both domains could impact replication and growth. In this case, it would appear that the Z/DI interaction is more important for replication than the Z/DIII interaction, given that SH019 showed impaired, but still measurable growth whereas SH017 could barely be propagated at all.

Another major revelation from these growth kinetic assays is that it appears that only Can Z can generate incompatibility and not Rom Z. This is confirmation of earlier studies showing that a Rom L segment and Can S segment did not impact infectious virion production even though in this scenario the LP and Z were still homologous. In our studies, SH022 and SH023 only differed from SH016 and SH017 respectively by the introduction of Rom Z instead of Can Z. SH022 and SH023 showed normal or above normal growth

rates whereas their counterparts with Can Z (SH016 and SH017) were both impaired at P1 titers. SH016 however did show normal kinetics in the growth time course. This one way incompatibility (CanZ/RomLP but not RomZ/CanLP) is novel and provides an excellent tool for studying JUNV protein-protein interactions. By understanding the mechanisms by which LP and Z interact, and how this relates to replication and growth will advance the field of mammarenavirus biology.

One possible reason for decreased virion production with Can Z containing viruses would be that Can Z may simply leave the cell more efficiently than Rom Z. This would result in more Can Z VLPs and fewer infectious virions. The experiment to study this was simple and didn't seek to draw intricate conclusions. Instead, it was simply to determine whether there was a drastic difference in Z accumulation found in VLPs with either Can or Rom Z expression plasmids. The results did not show stark relative differences, only a trend that Can Z may result in more protein outside of the cell. From these results, we hypothesize that Can Z leaving the cell is likely not the driving factor for the differences we observed in the viral growth kinetics. Recent reports have shown that mutations in Z can result in Z being degraded in the cell (42). Our overexpression system did not include this mutation in Can Z, and therefore we did not see the same reduction at lease in western blot. Therefore, we cannot exclude the possibility that mutations found in the Can Z could cause it to be degraded at a faster rate than Rom Z and result in the decreased virus production that has been observed. Since intracellular levels of both Can and Rom Z appeared equal, additional experiments would be necessary to determine whether degradation is occurring but is being masked by the overexpression system. This is an unlikely scenario, but still a possibility that cannot be ruled out.

To confirm the phenotypes seen in growth kinetics, RNA production at the NP locus was measured via qRT-PCR. These results showed that in VeroE6, rRom/CanZ, rRom/V64G, and SH019 all showed similar, low levels of RNA. This confirms what was seen earlier. Surprisingly, rCan showed similarly low levels, putting that result at odds with

the high growth observed. This may be due to the fact that low MOI infections do not capture the immediate RNA production that would be seen in a high MOI infection. The correspondence of low RNA production with low growth of rRom/CanZ, rRom/V64G, and SH019 supports the hypothesis that these changes are due to an incompatibility between Z and LP, and not simply due to the absence of Can Z in the cell. By having both replication and virion production impacted, the extent of this incompatibility is increased. SH023 exhibited a very surprising phenotype in terms of RNA production. While it grows at similar rates to rRom, it produces about 1 log more RNA in both cell types. This virus has an LP comprised of Rom DI and Can DII-IV with Rom Z. These results may suggest that the Z/DI homology is important for successful growth and replication, and also that the addition of Can DIII may increase the activity of the polymerase. Since Can was passaged 44 times in mouse brains and later in cell culture, the selective pressure was likely toward increased polymerase activity and not so much on virion production. SH023 may represent an overly optimized LP containing the stability of Rom and the activity of a Can DIII. Future studies would be needed to determine if these interactions with DI and DIII are critical for the virus life cycle. In addition, each of these domains contain several amino acid differences from Can. By inserting individual mutations, the exact locations of incompatibility could be elucidated.

While the reduced growth and replication *in vitro* of these viruses is very instructive, it does not reveal information about how these chimeric LP constructs affect pathogenicity. Future guinea pig studies will be necessary to determine whether any of these constructs, specifically SH017 and SH019 are attenuated *in vivo*. Given the results of Chapter 3, we would hypothesize that since these viruses show similar *in vitro* phenotypes as rRom/CanZ and rRom/V64G, they would also share the same attenuation profile. In addition, it would be very instructive to study the pathogenicity of SH023. If the high RNA production resulted in higher pathology, it would represent a previously unknown method of increasing pathogenicity through the LP. If, however, the virus was equal to or less

pathogenic than rRom, it may be more immunogenic. An overactive polymerase may produce more RNA and proteins, that can act as both antigens for the innate and adaptive immune system.

The incompatibility between Z and LP presents a novel attenuating mechanism for JUNV. By determining what regions of LP are responsible for this incompatibility, we can design future NW mammarenavirus vaccines with this same incompatibility. In addition, if the permutations found in SH023 were in fact more immunogenic, it would further advance designed vaccine development by not only identifying attenuating interactions but also immunogenic interactions. In this way the development of vaccines for MACV, GTOV, SABV, and other emerging mammarenaviruses could be refined and accelerated.

Chapter 5 Conclusions

Junin virus is a highly pathogenic member of the family *Arenaviridae*. JUNV is a member of the NW group of mammarenaviruses, sharing Clade B of the group with numerous other human pathogens including MACV, GTOV, and SABV(6). These latter viruses are the causative agent of Bolivian hemorrhagic fever (BHF), Venezuelan hemorrhagic fever (VHF), and Brazilian hemorrhagic fever (BzHf). JUNV itself is the causative agent of Argentine hemorrhagic fever (AHF) in humans. This disease is characterized by febrile and hemorrhagic manifestations that can result in a 15-20% case fatality rates during outbreaks (91). Fortunately, a live-attenuated vaccine strain of JUNV was developed in the 1980's through collaboration between Argentina and the United States of America. This vaccine, when distributed, resulted in a dramatic decrease in the incidence of AHF in endemic Argentina. The vaccine was produced through serial passage of the parental JUNV XJ strain to produce an attenuated phenotype (113). The resulting strain, Candid#1, has only recently been studied in-depth to determine the factors involved in JUNV replication, growth, and attenuation. Chief among these results, it was

demonstrated that the glycoprotein of Can alone was sufficient to attenuate wild type JUNV (33). Additional research focused on the NP, LP, and Z proteins of the virus indicated the roles that each of these play in replication, immune evasion, and virion formation. All of this allowed for a better understanding of JUNV, and arenaviral replication and growth strategies *in vitro* and *in vivo*. The presence of Can also allowed for further research into JUNV at a decreased bio-safety level. This was critical since all work with wild type strains of JUNV require high containment (BSL-4) facilities. In addition, the availability of a pathogenic and non-pathogenic JUNV strain allowed for further understanding of attenuating factors.

Preliminary experiments shown in this report sought to determine the effects of Can ORFs on wild type JUNV growth through the production of chimeric rJUNV. These viruses contained various combinations of Can and wild type Rom ORFs. The most striking observation in growth kinetic experiments was that the introduction of the Can Z ORF into the Rom virus resulted in a significant decrease in growth kinetics. In addition, this chimeric virus exhibited an altered plaque morphology that demonstrated as small, pin-prick plaques. Since these effects are not seen in rCan growth or plaque experiments, it was hypothesized that this reduction was the result of incompatibility between the Can Z and some other wild type Rom protein. The Can Z only contains two aa differences when compared with the Rom Z: V18A and V64G. Position 18 lies within the N-terminal arm of Z while position 64 lies within the RING domain. To determine which of these mutations was responsible for the observed phenotype, each was introduced into wild type rRom and the subsequent growth kinetics were measured. The results showed that the V64G mutation and not the V18A mutation was responsible for the low titer, small plaque phenotype observed in rRom/CanZ virus infection. Viruses harboring the V18A mutation alone did not exhibit any significant changes in growth kinetics. Since the original hypothesis was that the Can Z was resulting in an incompatibility with a wild type Rom protein, the elucidation of the V64G mutation as the responsible party further narrowed down the likely

interaction partners. While the Z protein has been shown to interact with all three other viral proteins, certain regions have been shown to be important in each interaction. For example, it has been shown that the RING domain of Z is crucial for interaction with LP and NP but not GPC (35, 37, 38). Since the V64G mutation is located within the RING domain, we hypothesize that this incompatibility is likely between the Z protein and either the LP or NP.

Prior to determining the incompatibility, however, it was important to understand whether the Can Z incompatibility would result in an altered phenotype *in vivo*. It had previously been shown to decrease replication and growth *in vitro*, but it was unknown how this incompatibility would affect the virus' ability to replicate, disseminate, and cause disease in an animal model. The ultimate goal of all basic science research is to turn the results in the lab into translational results. If a given mutation affects virus growth *in vitro*, but has not affect during systemic infection, it is of little use beyond simple information. We therefore studied this question by using the rRom, rCan, rRom/CanZ and rRom/V64G viruses to infect the established, Hartley guinea pig model of JUNV pathogenesis (33). These same previous studies had shown that the GPC ORF alone was able to confer attenuation *in vivo*. Our results, however, indicate a new role for Z in the attenuation of JUNV. All animals infected with the rRom/CanZ and rRom/V64G viruses survived. In addition, none of the animals experienced weight loss or significant temperature increases during the duration of the study. In contrast, animals infected with the wild type rRom virus all succumbed to infection between 11-15 dpi and exhibited elevated body temperatures and dramatic weight loss. Almost all of the organs collected from rRom infected animals demonstrated a detected viral load while no virus was detectable in rCan, rRom/CanZ, and rRom/V64G infected animals. This was further demonstrated by the absence of JUNV RNA in PBMCs collected 9 dpi in rCan, rRom/CanZ, and rRom/V64G infected animals, but present in rRom infected samples. These results indicate that rRom/CanZ and rRom/V64G were both attenuated *in vivo* and that the host was likely able to clear the

infection by 9 dpi. This is a novel finding that establishes the Z protein as a target for attenuating mechanisms within the virus. Additionally, this attenuation was able to be conferred by only a single mutation.

Early in infection, however, there are differences to be seen between rRom/CanZ and rRom/V64G pathogenesis. Hematology and clinical chemistry results indicate that rRom/V64G produces a rRom-like reduction in platelets and white blood cells early in infection. rRom/CanZ, however, retains the normal levels reported in rCan infection. Both experimental viruses resulted in no detectable tissue damage, analyte level anomalies, or reduced immune markers, showing that any early pathology was resolved by the end of the study. This indicates that while rRom/V64G is fully attenuated, it may retain more virulence than rRom/CanZ, especially early in infection. This would implicate the second Can Z mutation, V18A, as an additional attenuating factor. How this mutation would affect replication, growth, and pathogenesis remains unknown.

With the understanding that the Can Z, specifically the V64G mutation, can result in decreased *in vitro* kinetics and ultimately be attenuated *in vivo*, it became important to understand what incompatibility was responsible for the observed phenotype. To address this question, preliminary experiments were conducted in which the V64G mutation was introduced into rRom in addition to the ORF of either Can LP, NP, or GPC. The plaque morphology and growth kinetics of the resulting viruses were evaluated. Since rCan does not produce the low titer, small plaque phenotype seen in rRom/CanZ, the introduction of the homologous Can ORF with V64G should reverse the wild type phenotype concerning replication and plaque morphology. The results indicated that when Can LP was introduced, the virus was able to once again produce large plaques and high titers. This demonstrates that the incompatibility of Can Z is likely with the Rom LP protein. The Z and LP are known to interact extensively through the viral life cycle. High concentrations of Z are able to inhibit the polymerase by binding to the LP and locking it to the RNA template. In addition, the binding of Z to both NP and LP assists in the translocation of the

replicative complex from the cytosol to the plasma membrane in preparation for budding. And, incompatibility of Z with LP could therefore affect replication, assembly, and/or budding of the virus. Previous studies have shown that Z is able to bind the LP at domains I and III of the protein. This corresponds to the endonuclease and polymerase domains respectively. Currently, Z is not thought to bind in the non-enzymatic regions of the LP, DII and DIV. However, whether both sites (DI and DIII) are bound *in vivo* and whether they are bound at equal rates is unknown. It is possible that the virus may favor one site over the other or use one site exclusively over the other. Additionally, given our preliminary data, it is unknown whether incompatibility with one or both binding sites results in the reduced growth phenotype observed.

In order to determine what regions of the LP were important for the observed incompatibility, chimeric LP ORFs were generated that represented all permutations of Rom and Can DI, DII, DIII/DIV. Six total constructs were generated with DIII and DIV not being separated. By producing each of these proteins, it was hoped to determine Z/LP combinations that replicated and grew at rRom levels and rRom/CanZ levels respectively. After generation, each construct was tested in a mini-genome system to determine whether it was still functional. The possibility remained that Rom and Can domains would not be compatible. All six of the polymerase constructs demonstrated activity. Three of the six constructs demonstrated activity high enough to be measurably decreased following the introduction of Z. The remaining three constructs had low, baseline levels of activity in either the presence or absence of Z. Each LP was encoded into an agRNA expressing plasmid and utilized in the production of recombinant viruses. All recombinant viruses were produced with a Rom S segment and the indicated chimeric L segments. Only three of the chimeric LPs were able to be successfully recovered as recombinant viruses. These were the same three constructs that showed high polymerase activity in the mini-genome system. These three polymerase constructs were all used to produced rJUNV with a Can Z ORF (SH016, SH017, SH019). In addition, two of the three constructs were used to

produce rJUNV with a Rom Z ORF (SH022, SH023). Attempts to generate rJUNV with the other constructs did not result in the production of infectious virus.

Viral titers for the first passage (P1) of each chimeric virus was determine via plaque assay. The initial results indicated that SH017 exhibited extremely low P1 titers and the small plaque phenotype indicative of the LP/Z incompatibility. All other viruses appeared to have comparable titers, with SH016 being slightly lower than the others. Since SH017 only contained a single Rom LP domain (DI), it would appear that incompatibility between the Rom DI and Can Z is resulting in the low titers and small plaques seen. Unfortunately, since the titers of SH017 were exceedingly low, no further characterization of the virus was possible. Subsequent attempts to amplify and passage the virus were unsuccessful.

The four remaining viruses were all characterized *in vitro*. Surprisingly, SH019 demonstrated reduced growth kinetics when measured over a time course. This was at odds with the original, high P1 titer, but repeated measures of the experiment confirmed the low growth. Unlike SH017, SH019 retains a homologous Can DI and Can Z. This construct, however, has a Rom DIII/IV, indicating that both the DI/Z and DIII/Z or possibly DIV/Z interaction may be crucial for proper viral replication. This would not be surprising since the Z protein is shown to be able to interact with both DI and DIII. SH022 and SH023 confirmed that the phenomenon is only seen with Can Z proteins, and not with Rom Z proteins. Both of these viruses demonstrated consistently high growth and replication rates. Their growth rates were either equal to or above that seen in rRom. qRT-PCR analysis of all four viruses showed that SH019 exhibited the low RNA levels seen in rRom/CanZ and rRom/V64G. This correlated with the low growth kinetics seen previously. In further confirmation of the growth kinetics, SH022 and SH023 both had RNA levels higher than rRom, suggesting that these viruses may replicate more efficiently than rRom *in vitro*. Sadly, SH017 could not be analyzed for growth kinetics or RNA accumulation, meaning we were unable to determine how SH017 compared to SH019. Future studies to amplify

and characterize SH017 will be pursued to understand how that combination of LP/Z affects viral growth and replication levels.

The crowning characterization for all of these viruses will be to determine their activity and pathogenicity *in vivo*. Particularly, it will be important to determine whether SH017 and SH019 are attenuated *in vivo*, in correlation with their impaired growth and titers *in vitro*. As we have previously shown, the Can Z (or just V64G mutation) in the Rom backbone is sufficient to attenuate JUNV in the guinea pig model when in conjunction with a Rom-like LP. If SH017 and SH019 were also attenuated, this would demonstrate that the incompatibility of Can Z with either DI or DIII of the LP is responsible for the attenuating effects. If only one construct exhibited attenuation, it would suggest that one of the Z/LP interactions has an impact on attenuation. Further study would then be justified to determine which mutations in these two domains are responsible for the incompatibility with the V64G mutation. After controlling for normal variation between published JUNV sequences, Can LP differs from Rom LP by three aa in DI and six aa in DIII. Once all of this had been determined, it would shed extremely valuable insight into the mechanisms of arenavirus replication and pathogenicity. In addition, it would allow for the targeted development of related NW mammarenavirus vaccines through the modulation of the LP and Z proteins on the L segment.

Additionally, we believe it will be of the utmost importance to analyze the pathogenicity of SH023. This virus has consistently shown to have higher growth and RNA accumulation than rRom. This means that this construct may represent an over-optimized replication complex that works more efficiently than rRom, at least *in vitro*. The chance remains that in the presence of an immune response, this virus is unable to maintain the high levels of replication. On one hand, faster and greater replication may cause the virus to grow, spread, and cause more disease in the host. On the other hand, faster replication may result in faster activation of the immune system and subsequent clearance of the virus in the host. Even if the virus is not attenuated, there is a chance it would still be more

immunogenic due to the mechanism described above. If that were true, use of this chimeric polymerase in conjunction with another attenuating mechanism (such as Can GPC) could result in a virus with the same safety and attenuation profile as Can but even more immunogenic, representing an improvement to the vaccine overall. All of these hypotheses would eventually need to be analyzed in future animal studies, to further determine the mechanisms of the LP/Z interaction on pathogenicity. Each of these studies and results would be exceptionally novel and represent significant expansions of our current understanding of JUNV.

One of the hallmarks of the Z protein is the RING domain, previous described above to be crucial for protein-protein interaction during the virus life cycle. RING domains in related proteins have been shown to demonstrate ubiquitin E3 ligase activity. Briefly, this ligase works in concert with other ubiquitin ligase proteins to covalently attach ubiquitin groups onto target proteins. To date, no studies have sought to determine whether Z exhibits E3 ligase activity or what proteins would be the ligase target. Given the effects of V64G on viral replication, it would be informative to study the E3 ligase activity of Rom and Can Z to determine whether they are different. In addition, if Z exhibits ligase activity it could result in auto-ubiquitination that may be important for the function of Z during the viral life cycle. All of these questions and research directions would need to be addressed in future studies made relevant by the results demonstrated here outlining an attenuating mechanism for JUNV Z protein.

All of the described experiments, results, and conclusions add valuable insight into JUNV replication, growth, attenuation, and protein-protein interactions. We have shown that a single mutation in the Z protein of Rom is sufficient to attenuate the virus *in vivo*. Attenuation utilizing the Z protein has never been attempted or demonstrated before in the field of mammarenavirus pathogenicity, marking a novel approach to vaccine development. Our results indicate that a likely incompatibility with the Rom LP results in

the attenuation seen previously. While animal studies utilizing LP/Z combinations would be required to confirm these preliminary findings, the introduction of a homologous Can LP is sufficient to restore growth and replication *in vitro*. Through the use of chimeric LP constructs, we hypothesize that the incompatibility involves both the DI and DIII regions of the polymerase. This corresponds to the endonuclease and polymerase domains respectively. Further characterization would determine the mechanisms behind this incompatibility.

All of these results will advance the field vaccine development by isolating attenuating strategies in JUNV. While the Candid#1 vaccine is safe and effective, these additional strategies can then be used to design vaccines for MACV, GTOV, and SABV, related NW mammarenaviruses. In addition, it allows vaccine developers to maintain a toolbox of attenuating strategies to use in the event of an emerging, pathogenic mammarenavirus. In this way, morbidity and mortality from current and future mammarenavirus epidemics can be reduced and minimized. The effect on global public health and economic increase is incalculable, and worthy of all resources invested in its establishment. Through these and other advances in arenavirus biology and vaccine development, we can seek to further serve the world at large by improving the quality of care and quality of life for millions of individuals.

Target	rCan vs rRom Fold Change	rRom/CanZ vs. rRom Fold Change	rRom/V64G vs. rRom Fold Change
TLR-2	1.2	5.8	1.3
TLR-3	-11.2	-4.1	1.9
TLR-4	-47.9	-13.5	-10.8
TLR-6	-1.5	1.7	3.5
TLR-7	10.6	3.0	13.4
TLR-8	-183.7	-6.8	-10.1
TLR-9	-3.7	-2.8	2.4
TLR-10	1.2	8.1	1.2
CD4	2.3	1.9	1.1
CD8alpha	97.8	30.8	6.8
CD62L	-2.4	-2.7	1.9
CD107a	-1.6	-1.2	-2.0
CD107b	1.1	-1.2	1.6
CD134	1.2	1.2	1.6
CD152	15.1	3.9	
CD223	8.0	7.3	9.1
CD126-1	-1.3	-1.4	-2.9
CD130	-1.0	-2.9	-1.5
CD19-2	5.0	10.2	1.6
CD22	30.4	19.3	11.5
CD79a	2.8	3.0	-1.3
CD79b	2.2	2.6	-1.6
CD20(2)	2.8	2.3	2.2
CD94	2.4		
CD23	2.9	-1.8	3.8
CD25	2.3	1.4	9.0
CD39	3.3	5.7	
CD69	3.7	10.6	1.2
CD72	1.0	2.5	-2.2
CD92	1.4	-1.4	-1.5
CD93(2)	3.1	1.2	2.8
CD115	3.5	4.8	-1.4
CD2	12.3	10.3	1.1
IFN gamma	3.5	2.0	5.6
IFNAR1	2.8	-6.2	1.2
IFNGR1(2)	-21.2	-4.3	-11.1
GM-CSF		1.7	
LTA	1.5	9.9	3.0
lysozyme	-4.5	-1.7	-2.1
KLRG1	17.7	27.5	
beta2 u-globin	1.5	1.5	-19.9
MHC-II	-1.2	4.0	1.3
CIITA	24.5	27.0	3.8
RANTES	35.8	22.9	2.4
MCP-1	-5.0	-9.9	10.9
Fc gamma1/2 receptor	-1.9	1.0	-1.2
NFkB1	-1.1	1.1	-1.4
IL-15(3)	1.5	-1.1	2.0
CXCL10	-758.1	-5.8	-16.1
CXCL11	5.1		
GNCP-1b	-70.9	-40.0	-45.7
IL-1b	15.7	1.5	5.8
TNFSF4	-1.0		
CCR6-1	-1.3	3.0	-3.0
CD36(2)	-1.1	3.2	1.6
CD180	7.2	27.7	7.5
CD28	1.3	-2.4	-2.4
CD40	11.3	3.5	1.9
CD44	-1.0	-2.0	-2.8
CD81	9.0	6.7	2.8
SOD1	1.5	1.1	1.0
IFNAR2	-1.4	-2.2	-5.1
CD96	10.8	1.1	8.7
IL-12p40	12.8	58.1	14.6
IL-4 receptor	-1.4	-1.7	-6.1
IL-16	6.3	1.1	8.5
IL-23 receptor		2.0	
IL-27	-11.5	-2.6	1.1
IL-27 receptor a	12.2	4.3	1.7
CD14	-2.5	-2.2	-4.6
IL-7 receptor	-2.3	-1.2	-1.4
IL-18	-1.0	-3.8	-5.0
IL-21	4.5		
CCR3 receptor	1.4	1.4	2.8
IL-8	-1.2	1.9	1.0
SOD2	-1.2	-1.1	-1.0
TGFbeta	-1.5	-1.4	-3.8
TNFalpha	1.6	-2.2	1.5
CXCL12	-3.2	-2.4	1.5
CCR4 receptor	2.1	1.7	
CXCR1	-4.6	-3.2	-4.5
CXCR3	14.3	1.7	6.5
CXCR2 IL-8 receptor beta	-1.8	-2.1	-4.5
IL-5 receptor beta chain	-17.0	-4.6	-24.6

Supplementary Table 1. PBMCs were collected from animals 9 dpi and utilized in PCR array for the following targets. Results are shown as fold change relative to rRom infected animals. Empty cells represent no amplification for the given target.

Bibliography

1. Lumsden LL. 1958. St. Louis encephalitis in 1933; observations on epidemiological features. Public Health Rep Wash DC 1896 73:340–353.

2. Armstrong C, Lillie RD. 1934. Experimental Lymphocytic Choriomeningitis of Monkeys and Mice Produced by a Virus Encountered in Studies of the 1933 St. Louis Encephalitis Epidemic. Public Health Rep 1896-1970 49:1019–1027.

3. Parodi AS, Greenway DJ, Rugiero HR, Frigerio M, De La Barrera JM, Mettler N, Garzon F, Boxaca M, Guerrero L, Nota N. 1958. [Concerning the epidemic outbreak in Junin]. El Dia Medico 30:2300–2301.

4. Buckley SM, Casals J. 1970. Lassa Fever, a New Virus Disease of Man from West Africa. Am J Trop Med Hyg 19:680–691.

5. Blasdell KR, Duong V, Eloit M, Chretien F, Ly S, Hul V, Deubel V, Morand S, Buchy P. 2016. Evidence of human infection by a new mammarenavirus endemic to Southeastern Asia. eLife 5.

6. Arenaviridae - Negative Sense RNA Viruses - Negative Sense RNA Viruses (2011). Int Comm Taxon Viruses ICTV.

7. Briese T, Paweska JT, McMullan LK, Hutchison SK, Street C, Palacios G, Khristova ML, Weyer J, Swanepoel R, Egholm M, Nichol ST, Lipkin WI. 2009. Genetic detection and characterization of Lujo virus, a new hemorrhagic fever-associated arenavirus from southern Africa. PLoS Pathog 5:e1000455.

8. Bowen MD, Rollin PE, Ksiazek TG, Hustad HL, Bausch DG, Demby AH, Bajani MD, Peters CJ, Nichol ST. 2000. Genetic diversity among Lassa virus strains. J Virol 74:6992–7004.

9. Jahrling PB, Hesse RA, Rhoderick JB, Elwell MA, Moe JB. 1981. Pathogenesis of a pichinde virus strain adapted to produce lethal infections in guinea pigs. Infect Immun 32:872–880.

10. Archer AM, Rico-Hesse R. 2002. High genetic divergence and recombination in Arenaviruses from the Americas. Virology 304:274–281.

11. Fulhorst CF, Charrel RN, Weaver SC, Ksiazek TG, Bradley RD, Milazzo ML, Tesh RB, Bowen MD. 2001. Geographic distribution and genetic diversity of Whitewater Arroyo virus in the southwestern United States. Emerg Infect Dis 7:403–407.

12. Charrel RN, Feldmann H, Fulhorst CF, Khelifa R, de Chesse R, de Lamballerie X. 2002. Phylogeny of New World arenaviruses based on the complete coding sequences of the small genomic segment identified an evolutionary lineage produced by intrasegmental recombination. Biochem Biophys Res Commun 296:1118–1124.

13. Charrel RN, de Lamballerie X, Fulhorst CF. 2001. The Whitewater Arroyo virus: natural evidence for genetic recombination among Tacaribe serocomplex viruses (family Arenaviridae). Virology 283:161–166.

14. Hepojoki J, Hepojoki S, Smura T, Szirovicza L, Dervas E, Prähauser B, Nufer L, Schraner EM, Vapalahti O, Kipar A, Hetzel U. 2018. Characterization of Haartman Institute snake virus-1 (HISV-1) and HISV-like viruses-The representatives of genus Hartmanivirus, family Arenaviridae. PLoS Pathog 14:e1007415.

15. Shi M, Lin X-D, Chen X, Tian J-H, Chen L-J, Li K, Wang W, Eden J-S, Shen J-J, Liu L, Holmes EC, Zhang Y-Z. 2018. The evolutionary history of vertebrate RNA viruses. Nature 556:197–202.

16. Buchmeier MJ. 2007. Arenaviridae: the viruses and their replicationField Virology, 4th ed. Lippincott-Raven.

17. Brunotte L, Lelke M, Hass M, Kleinsteuber K, Becker-Ziaja B, Günther S. 2011. Domain structure of Lassa virus L protein. J Virol 85:324–333.

18. Morin B, Coutard B, Lelke M, Ferron F, Kerber R, Jamal S, Frangeul A, Baronti C, Charrel R, de Lamballerie X, Vonrhein C, Lescar J, Bricogne G, Günther S, Canard B. 2010. The N-terminal domain of the arenavirus L protein is an RNA endonuclease essential in mRNA transcription. PLoS Pathog 6:e1001038.

19. Vogel D, Rosenthal M, Gogrefe N, Reindl S, Günther S. 2019. Biochemical characterization of the Lassa virus L protein. J Biol Chem.

20. Vieth S, Torda AE, Asper M, Schmitz H, Günther S. 2004. Sequence analysis of L RNA of Lassa virus. Virology 318:153–168.

21. Hass M, Lelke M, Busch C, Becker-Ziaja B, Günther S. 2008. Mutational Evidence for a Structural Model of the Lassa Virus RNA Polymerase Domain and Identification of Two Residues, Gly1394 and Asp1395, That Are Critical for Transcription but Not Replication of the Genome. J Virol 82:10207–10217.

22. Sánchez AB, de la Torre JC. 2005. Genetic and biochemical evidence for an oligomeric structure of the functional L polymerase of the prototypic arenavirus lymphocytic choriomeningitis virus. J Virol 79:7262–7268.

23. Qi X, Lan S, Wang W, Schelde LM, Dong H, Wallat GD, Ly H, Liang Y, Dong C. 2010. Cap binding and immune evasion revealed by Lassa nucleoprotein structure. Nature 468:779–783.

24. Mateer E, Paessler S, Huang C. 2019. Confocal Imaging of Double-Stranded RNA and Pattern Recognition Receptors in Negative-Sense RNA Virus Infection. J Vis Exp JoVE.

25. Huang C, Kolokoltsova OA, Mateer EJ, Koma T, Paessler S. 2017. Highly Pathogenic New World Arenavirus Infection Activates the Pattern Recognition Receptor Protein Kinase R without Attenuating Virus Replication in Human Cells. J Virol 91.

26. Pythoud C, Rodrigo WWSI, Pasqual G, Rothenberger S, Martínez-Sobrido L, Torre JC de la, Kunz S. 2012. Arenavirus Nucleoprotein Targets Interferon Regulatory Factor-Activating Kinase IKKε. J Virol 86:7728–7738.

27. Manning JT, Seregin AV, Yun NE, Koma T, Huang C, Barral J, de la Torre JC, Paessler S. 2017. Absence of an N-Linked Glycosylation Motif in the Glycoprotein of the Live-Attenuated Argentine Hemorrhagic Fever Vaccine, Candid #1, Results in Its Improper Processing, and Reduced Surface Expression. Front Cell Infect Microbiol 7:20.

28. Eichler R, Lenz O, Strecker T, Garten W. 2003. Signal peptide of Lassa virus glycoprotein GP-C exhibits an unusual length. FEBS Lett 538:203–206.

29. York J, Romanowski V, Lu M, Nunberg JH. 2004. The Signal Peptide of the Junín Arenavirus Envelope Glycoprotein Is Myristoylated and Forms an Essential Subunit of the Mature G1-G2 Complex. J Virol 78:10783–10792.

30. Agnihothram SS, York J, Nunberg JH. 2006. Role of the Stable Signal Peptide and Cytoplasmic Domain of G2 in Regulating Intracellular Transport of the Junín Virus Envelope Glycoprotein Complex. J Virol 80:5189–5198.

31. Lenz O, ter Meulen J, Klenk HD, Seidah NG, Garten W. 2001. The Lassa virus glycoprotein precursor GP-C is proteolytically processed by subtilase SKI-1/S1P. Proc Natl Acad Sci U S A 98:12701–12705.

32. Rojek JM, Lee AM, Nguyen N, Spiropoulou CF, Kunz S. 2008. Site 1 protease is required for proteolytic processing of the glycoproteins of the South American hemorrhagic fever viruses Junin, Machupo, and Guanarito. J Virol 82:6045–6051.

33. Seregin AV, Yun NE, Miller M, Aronson J, Smith JK, Walker AG, Smith JN, Huang C, Manning JT, de la Torre JC, Paessler S. 2015. The Glycoprotein Precursor Gene of Junin Virus Determines the Virulence of the Romero Strain and the Attenuation of the Candid #1 Strain in a Representative Animal Model of Argentine Hemorrhagic Fever. J Virol 89:5949–5956.

34. Perez M, Greenwald DL, de la Torre JC. 2004. Myristoylation of the RING finger Z protein is essential for arenavirus budding. J Virol 78:11443–11448.

35. Capul AA, Perez M, Burke E, Kunz S, Buchmeier MJ, de la Torre JC. 2007. Arenavirus Z-glycoprotein association requires Z myristoylation but not functional RING or late domains. J Virol 81:9451–9460.

36. Capul AA, de la Torre JC, Buchmeier MJ. 2011. Conserved residues in Lassa fever virus Z protein modulate viral infectivity at the level of the ribonucleoprotein. J Virol 85:3172–3178.

37. Loureiro ME, Wilda M, Levingston Macleod JM, D'Antuono A, Foscaldi S, Marino Buslje C, Lopez N. 2011. Molecular determinants of arenavirus Z protein homo-oligomerization and L polymerase binding. J Virol 85:12304–12314.

38. Wilda M, Lopez N, Casabona JC, Franze-Fernandez MT. 2008. Mapping of the tacaribe arenavirus Z-protein binding sites on the L protein identified both amino

acids within the putative polymerase domain and a region at the N terminus of L that are critically involved in binding. J Virol 82:11454–11460.

39. Salvato MS. 1993. Molecular Biology of the Prototype Arenavirus, Lymphocytic Choriomeningitis Virus, p. 133–156. *In* Salvato, MS (ed.), The Arenaviridae. Springer US, Boston, MA.

40. Salvato MS, Schweighofer KJ, Burns J, Shimomaye EM. 1992. Biochemical and immunological evidence that the 11 kDa zinc-binding protein of lymphocytic choriomeningitis virus is a structural component of the virus. Virus Res 22:185–198.

41. Kranzusch PJ, Whelan SPJ. 2011. Arenavirus Z protein controls viral RNA synthesis by locking a polymerase–promoter complex. Proc Natl Acad Sci 108:19743–19748.

42. Iwasaki M, de la Torre JC. 2018. A Highly Conserved Leucine in Mammarenavirus Matrix Z Protein Is Required for Z Interaction with the Virus L Polymerase and Z Stability in Cells Harboring an Active Viral Ribonucleoprotein. J Virol 92.

43. Ziegler CM, Eisenhauer P, Manuelyan I, Weir ME, Bruce EA, Ballif BA, Botten J. 2018. Host-Driven Phosphorylation Appears to Regulate the Budding Activity of the Lassa Virus Matrix Protein. Pathog Basel Switz 7.

44. Perez M, Craven RC, de la Torre JC. 2003. The small RING finger protein Z drives arenavirus budding: implications for antiviral strategies. Proc Natl Acad Sci U S A 100:12978–12983.

45. Urata S, de la Torre JC. 2011. Arenavirus budding. Adv Virol 2011:180326.

46. Ziegler CM, Eisenhauer P, Bruce EA, Weir ME, King BR, Klaus JP, Krementsov DN, Shirley DJ, Ballif BA, Botten J. 2016. The Lymphocytic Choriomeningitis Virus Matrix Protein PPXY Late Domain Drives the Production of Defective Interfering Particles. PLoS Pathog 12:e1005501.

47. Cao W, Henry MD, Borrow P, Yamada H, Elder JH, Ravkov EV, Nichol ST, Compans RW, Campbell KP, Oldstone MB. 1998. Identification of alpha-dystroglycan as a receptor for lymphocytic choriomeningitis virus and Lassa fever virus. Science 282:2079–2081.

48. Radoshitzky SR, Abraham J, Spiropoulou CF, Kuhn JH, Nguyen D, Li W, Nagel J, Schmidt PJ, Nunberg JH, Andrews NC, Farzan M, Choe H. 2007. Transferrin receptor 1 is a cellular receptor for New World haemorrhagic fever arenaviruses. Nature 446:92–96.

49. Helguera G, Jemielity S, Abraham J, Cordo SM, Martinez MG, Rodríguez JA, Bregni C, Wang JJ, Farzan M, Penichet ML, Candurra NA, Choe H. 2012. An antibody recognizing the apical domain of human transferrin receptor 1 efficiently inhibits the entry of all new world hemorrhagic Fever arenaviruses. J Virol 86:4024–4028.

50. Herrador A, Fedeli C, Radulovic E, Campbell KP, Moreno H, Gerold G, Kunz S. 2019. Dynamic Dystroglycan Complexes Mediate Cell Entry of Lassa Virus. mBio 10.

51. Shimojima M, Kawaoka Y. 2012. Cell surface molecules involved in infection mediated by lymphocytic choriomeningitis virus glycoprotein. J Vet Med Sci 74:1363–1366.

52. Shimojima M, Ströher U, Ebihara H, Feldmann H, Kawaoka Y. 2012. Identification of cell surface molecules involved in dystroglycan-independent Lassa virus cell entry. J Virol 86:2067–2078.

53. Fedeli C, Torriani G, Galan-Navarro C, Moraz M-L, Moreno H, Gerold G, Kunz S. 2018. Axl Can Serve as Entry Factor for Lassa Virus Depending on the Functional Glycosylation of Dystroglycan. J Virol 92.

54. Cohen-Dvashi H, Kilimnik I, Diskin R. 2018. Structural basis for receptor recognition by Lujo virus. Nat Microbiol 3:1153–1160.

55. Spiropoulou CF, Kunz S, Rollin PE, Campbell KP, Oldstone MBA. 2002. New World arenavirus clade C, but not clade A and B viruses, utilizes alpha-dystroglycan as its major receptor. J Virol 76:5140–5146.

56. Montemiglio LC, Testi C, Ceci P, Falvo E, Pitea M, Savino C, Arcovito A, Peruzzi G, Baiocco P, Mancia F, Boffi A, des Georges A, Vallone B. 2019. Cryo-EM structure of the human ferritin-transferrin receptor 1 complex. Nat Commun 10:1121.

57. Jemielity S, Wang JJ, Chan YK, Ahmed AA, Li W, Monahan S, Bu X, Farzan M, Freeman GJ, Umetsu DT, Dekruyff RH, Choe H. 2013. TIM-family proteins promote infection of multiple enveloped viruses through virion-associated phosphatidylserine. PLoS Pathog 9:e1003232.

58. Rojek JM, Sanchez AB, Nguyen NT, de la Torre J-C, Kunz S. 2008. Different mechanisms of cell entry by human-pathogenic Old World and New World arenaviruses. J Virol 82:7677–7687.

59. Pasqual G, Rojek JM, Masin M, Chatton J-Y, Kunz S. 2011. Old world arenaviruses enter the host cell via the multivesicular body and depend on the endosomal sorting complex required for transport. PLoS Pathog 7:e1002232.

60. Oppliger J, Torriani G, Herrador A, Kunz S. 2016. Lassa Virus Cell Entry via Dystroglycan Involves an Unusual Pathway of Macropinocytosis. J Virol 90:6412–6429.

61. Eschli B, Quirin K, Wepf A, Weber J, Zinkernagel R, Hengartner H. 2006. Identification of an N-terminal trimeric coiled-coil core within arenavirus glycoprotein 2 permits assignment to class I viral fusion proteins. J Virol 80:5897–5907.

62. Shulman A, Katz M, Cohen-Dvashi H, Greenblatt HM, Levy Y, Diskin R. 2019. Variations in Core Packing of GP2 from Old World Mammarenaviruses in their Post-Fusion Conformations Affect Membrane-Fusion Efficiencies. J Mol Biol 431:2095–2111.

63. Cohen-Dvashi H, Israeli H, Shani O, Katz A, Diskin R. 2016. Role of LAMP1 Binding and pH Sensing by the Spike Complex of Lassa Virus. J Virol 90:10329–10338.

64. Raaben M, Jae LT, Herbert AS, Kuehne AI, Stubbs SH, Chou Y-Y, Blomen VA, Kirchhausen T, Dye JM, Brummelkamp TR, Whelan SP. 2017. NRP2 and CD63 Are Host Factors for Lujo Virus Cell Entry. Cell Host Microbe 22:688-696.e5.

65. Pyle JD, Whelan SPJ. 2019. RNA ligands activate the Machupo virus polymerase and guide promoter usage. Proc Natl Acad Sci U S A 116:10518–10524.

66. Harrison SC. 2015. Viral membrane fusion. Virology 479–480:498–507.

67. Martínez-Sobrido L, Zúñiga EI, Rosario D, García-Sastre A, de la Torre JC. 2006. Inhibition of the Type I Interferon Response by the Nucleoprotein of the Prototypic Arenavirus Lymphocytic Choriomeningitis Virus. J Virol 80:9192–9199.

68. Martínez-Sobrido L, Giannakas P, Cubitt B, García-Sastre A, de la Torre JC. 2007. Differential Inhibition of Type I Interferon Induction by Arenavirus Nucleoproteins. J Virol 81:12696–12703.

69. Hiscott J. 2007. Triggering the Innate Antiviral Response through IRF-3 Activation. J Biol Chem 282:15325–15329.

70. Rodrigo WWSI, Ortiz-Riaño E, Pythoud C, Kunz S, de la Torre JC, Martínez-Sobrido L. 2012. Arenavirus Nucleoproteins Prevent Activation of Nuclear Factor Kappa B. J Virol 86:8185–8197.

71. King BR, Hershkowitz D, Eisenhauer PL, Weir ME, Ziegler CM, Russo J, Bruce EA, Ballif BA, Botten J. 2017. A Map of the Arenavirus Nucleoprotein-Host Protein

Interactome Reveals that Junín Virus Selectively Impairs the Antiviral Activity of Double-Stranded RNA-Activated Protein Kinase (PKR). J Virol 91.

72. Fan L, Briese T, Lipkin WI. 2010. Z proteins of New World arenaviruses bind RIG-I and interfere with type I interferon induction. J Virol 84:1785–1791.

73. Baillet N, Krieger S, Journeaux A, Caro V, Tangy F, Vidalain P-O, Baize S. 2019. Autophagy Promotes Infectious Particle Production of Mopeia and Lassa Viruses. Viruses 11.

74. Roldán JS, Candurra NA, Colombo MI, Delgui LR. 2019. Junín Virus Promotes Autophagy to Facilitate Viral Life Cycle. J Virol.

75. Perez Vidakovics MLA, Ure AE, Arrías PN, Romanowski V, Gómez RM. 2019. Junín virus induces autophagy in human A549 cells. PloS One 14:e0218730.

76. Lukashevich IS, Clegg JC, Sidibe K. 1993. Lassa virus activity in Guinea: distribution of human antiviral antibody defined using enzyme-linked immunosorbent assay with recombinant antigen. J Med Virol 40:210–217.

77. Frame JD. 1989. Clinical features of Lassa fever in Liberia. Rev Infect Dis 11 Suppl 4:S783-789.

78. Bausch DG, Demby AH, Coulibaly M, Kanu J, Goba A, Bah A, Condé N, Wurtzel HL, Cavallaro KF, Lloyd E, Baldet FB, Cissé SD, Fofona D, Savané IK, Tolno RT, Mahy B, Wagoner KD, Ksiazek TG, Peters CJ, Rollin PE. 2001. Lassa fever in

Guinea: I. Epidemiology of human disease and clinical observations. Vector Borne Zoonotic Dis Larchmt N 1:269–281.

79. Frame JD, Yalley-Ogunro JE, Hanson AP. 1984. Endemic Lassa fever in Liberia. V. Distribution of Lassa virus activity in Liberia: hospital staff surveys. Trans R Soc Trop Med Hyg 78:761–763.

80. Monson MH, Cole AK, Frame JD, Serwint JR, Alexander S, Jahrling PB. 1987. Pediatric Lassa fever: a review of 33 Liberian cases. Am J Trop Med Hyg 36:408–415.

81. Monath TP, Maher M, Casals J, Kissling RE, Cacciapuoti A. 1974. Lassa fever in the Eastern Province of Sierra Leone, 1970-1972. II. Clinical observations and virological studies on selected hospital cases. Am J Trop Med Hyg 23:1140–1149.

82. Monath TP, Mertens PE, Patton R, Moser CR, Baum JJ, Pinneo L, Gary GW, Kissling RE. 1973. A hospital epidemic of Lassa fever in Zorzor, Liberia, March-April 1972. Am J Trop Med Hyg 22:773–779.

83. Manning JT, Forrester N, Paessler S. 2015. Lassa virus isolates from Mali and the Ivory Coast represent an emerging fifth lineage. Front Microbiol 6:1037.

84. McGregor I, Georges AJ, Gonzalez JP, Abdul-Wahid S, Saluzzo JF, Meunier DMY, McCormick JB. 1985. Antibodies to Lassa and lassa-like viruses in man and mammals in the Central African Republic. Trans R Soc Trop Med Hyg 79:78–79.

85. 2019. Lassa Fever | CDC.

86. Demby AH, Inapogui A, Kargbo K, Koninga J, Kourouma K, Kanu J, Coulibaly M, Wagoner KD, Ksiazek TG, Peters CJ, Rollin PE, Bausch DG. 2001. Lassa fever in Guinea: II. Distribution and prevalence of Lassa virus infection in small mammals. Vector Borne Zoonotic Dis Larchmt N 1:283–297.

87. Ter Meulen J, Lukashevich I, Sidibe K, Inapogui A, Marx M, Dorlemann A, Yansane ML, Koulemou K, Chang-Claude J, Schmitz H. 1996. Hunting of peridomestic rodents and consumption of their meat as possible risk factors for rodent-to-human transmission of Lassa virus in the Republic of Guinea. Am J Trop Med Hyg 55:661–666.

88. Sewlall NH, Richards G, Duse A, Swanepoel R, Paweska J, Blumberg L, Dinh TH, Bausch D. 2014. Clinical Features and Patient Management of Lujo Hemorrhagic Fever. PLoS Negl Trop Dis 8.

89. Paweska JT, Sewlall NH, Ksiazek TG, Blumberg LH, Hale MJ, Lipkin WI, Weyer J, Nichol ST, Rollin PE, McMullan LK, Paddock CD, Briese T, Mnyaluza J, Dinh T-H, Mukonka V, Ching P, Duse A, Richards G, de Jong G, Cohen C, Ikalafeng B, Mugero C, Asomugha C, Malotle MM, Nteo DM, Misiani E, Swanepoel R, Zaki SR, Outbreak Control and Investigation Teams. 2009. Nosocomial outbreak of novel arenavirus infection, southern Africa. Emerg Infect Dis 15:1598–1602.

90. 2019. Lymphocytic Choriomeningitis (LCM) | CDC.

91. Enria D. 2004. Arenavirus Infections, p. 1191–1212. *In* Tropical Infectious Diseases: Principles, Pathogens, and Practice. Saunders.

92. Patterson M, Grant A, Paessler S. 2014. Epidemiology and pathogenesis of Bolivian hemorrhagic fever. Curr Opin Virol 5:82–90.

93. de Manzione N, Salas RA, Paredes H, Godoy O, Rojas L, Araoz F, Fulhorst CF, Ksiazek TG, Mills JN, Ellis BA, Peters CJ, Tesh RB. 1998. Venezuelan hemorrhagic fever: clinical and epidemiological studies of 165 cases. Clin Infect Dis Off Publ Infect Dis Soc Am 26:308–313.

94. Sayler KA, Barbet AF, Chamberlain C, Clapp WL, Alleman R, Loeb JC, Lednicky JA. 2014. Isolation of Tacaribe virus, a Caribbean arenavirus, from host-seeking Amblyomma americanum ticks in Florida. PloS One 9:e115769.

95. Salazar-Bravo J, Ruedas LA, Yates TL. 2002. Mammalian reservoirs of arenaviruses. Curr Top Microbiol Immunol 262:25–63.

96. Piacenza MF, Calderón GE, Enría D, Provensal MC, Polop JJ. 2018. [Spatial difference in the incidence of Argentine Hemorrhagic Fever and composition and abundance of rodents in the assemblage]. Rev Chil Infectologia Organo Of Soc Chil Infectologia 35:386–394.

97. Frame JD, Baldwin JM, Gocke DJ, Troup JM. 1970. Lassa fever, a new virus disease of man from West Africa. I. Clinical description and pathological findings. Am J Trop Med Hyg 19:670–676.

98. McCormick JB, King IJ, Webb PA, Johnson KM, O'Sullivan R, Smith ES, Trippel S, Tong TC. 1987. A case-control study of the clinical diagnosis and course of Lassa fever. J Infect Dis 155:445–455.

99. Yun NE, Walker DH. 2012. Pathogenesis of Lassa Fever. Viruses 4:2031–2048.

100. Okokhere PO, Ibekwe TS, Akpede GO. 2009. Sensorineural hearing loss in Lassa fever: two case reports. J Med Case Reports 3:36.

101. Liao BS, Byl FM, Adour KK. 1992. Audiometric comparison of Lassa fever hearing loss and idiopathic sudden hearing loss: evidence for viral cause. Otolaryngol--Head Neck Surg Off J Am Acad Otolaryngol-Head Neck Surg 106:226–229.

102. Cummins D, McCormick JB, Bennett D, Samba JA, Farrar B, Machin SJ, Fisher-Hoch SP. 1990. Acute sensorineural deafness in Lassa fever. JAMA 264:2093–2096.

103. Grant A, Seregin A, Huang C, Kolokoltsova O, Brasier A, Peters C, Paessler S. 2012. Junín Virus Pathogenesis and Virus Replication. Viruses 4:2317–2339.

104. Vallejos DA, Ambrosio AM, Feuillade MR, Maiztegui JI. 1989. Lymphocyte subsets alteration in patients with argentine hemorrhagic fever. J Med Virol 27:160–163.

105. González PH, Cossio PM, Arana R, Maiztegui JI, Laguens RP. 1980. Lymphatic tissue in Argentine hemorrhagic fever. Pathologic features. Arch Pathol Lab Med 104:250–254.

106. Ayala-Peña VB, Armiento MN, Fernández Bell Fano PM, Santillán GE, Scolaro LA. 2019. Infection of Rat Osteoblasts with Junin Virus Promotes the Expression of

Bone Morphogenetic Protein 6, an Osteogenic Differentiation Inducer. Intervirology 1–8.

107. Cuevas CD, Ross SR. 2014. Toll-like receptor 2-mediated innate immune responses against Junín virus in mice lead to antiviral adaptive immune responses during systemic infection and do not affect viral replication in the brain. J Virol 88:7703–7714.

108. Cuevas CD, Lavanya M, Wang E, Ross SR. 2011. Junin virus infects mouse cells and induces innate immune responses. J Virol 85:11058–11068.

109. Sarute N, Ibrahim N, Medegan Fagla B, Lavanya M, Cuevas C, Stavrou S, Otkiran-Clare G, Tyynismaa H, Henao-Mejia J, Ross SR. 2019. TRIM2, a novel member of the antiviral family, limits New World arenavirus entry. PLoS Biol 17:e3000137.

110. Macal M, Lewis GM, Kunz S, Flavell R, Harker JA, Zúñiga EI. 2012. Plasmacytoid dendritic cells are productively infected and activated through TLR-7 early after arenavirus infection. Cell Host Microbe 11:617–630.

111. Buechler MB, Gessay GM, Srivastava S, Campbell DJ, Hamerman JA. 2015. Hematopoietic and nonhematopoietic cells promote Type I interferon- and TLR7-dependent monocytosis during low-dose LCMV infection. Eur J Immunol 45:3064–3072.

112. Lee LN, Burke S, Montoya M, Borrow P. 2009. Multiple mechanisms contribute to impairment of type 1 interferon production during chronic lymphocytic

choriomeningitis virus infection of mice. J Immunol Baltim Md 1950 182:7178–7189.

113. Barrera Oro JG, McKee KT. 1991. Toward a vaccine against Argentine hemorrhagic fever. Bull Pan Am Health Organ 25:118–126.

114. Enria DA, Ambrosio AM, Briggiler AM, Feuillade MR, Crivelli E, Study Group on Argentine Hemorrhagic Fever Vaccine. 2010. [Candid#1 vaccine against Argentine hemorrhagic fever produced in Argentina. Immunogenicity and safety]. Medicina (Mex) 70:215–222.

115. WHO | List of Blueprint priority diseases. WHO.

116. Hallam HJ, Hallam S, Rodriguez SE, Barrett ADT, Beasley DWC, Chua A, Ksiazek TG, Milligan GN, Sathiyamoorthy V, Reece LM. 2018. Baseline mapping of Lassa fever virology, epidemiology and vaccine research and development. NPJ Vaccines 3:11.

117. Gonzalez-Quintial R, Baccala R. 2018. Murine Models for Viral Hemorrhagic Fever. Methods Mol Biol Clifton NJ 1604:257–267.

118. Hall WC, Geisbert TW, Huggins JW, Jahrling PB. 1996. Experimental infection of guinea pigs with Venezuelan hemorrhagic fever virus (Guanarito): a model of human disease. Am J Trop Med Hyg 55:81–88.

119. Bell TM, Bunton TE, Shaia CI, Raymond JW, Honnold SP, Donnelly GC, Shamblin JD, Wilkinson ER, Cashman KA. 2016. Pathogenesis of Bolivian Hemorrhagic Fever in Guinea Pigs. Vet Pathol 53:190–199.

120. Yun NE, Linde NS, Dziuba N, Zacks MA, Smith JN, Smith JK, Aronson JF, Chumakova OV, Lander HM, Peters CJ, Paessler S. 2008. Pathogenesis of XJ and Romero Strains of Junin Virus in Two Strains of Guinea Pigs. Am J Trop Med Hyg 79:275–282.

121. Peters CJ, Jahrling PB, Liu CT, Kenyon RH, McKee KT, Barrera Oro JG. 1987. Experimental studies of arenaviral hemorrhagic fevers. Curr Top Microbiol Immunol 134:5–68.

122. Maiztegui JI, Fernandez NJ, de Damilano AJ. 1979. Efficacy of immune plasma in treatment of Argentine haemorrhagic fever and association between treatment and a late neurological syndrome. Lancet Lond Engl 2:1216–1217.

123. Enria DA, Briggiler AM, Levis S, Vallejos D, Maiztegui JI, Canonico PG. 1987. Tolerance and antiviral effect of ribavirin in patients with argentine hemorrhagic fever. Antiviral Res 7:353–359.

124. Sepúlveda CS, García CC, Damonte EB. 2018. Antiviral activity of A771726, the active metabolite of leflunomide, against Junín virus. J Med Virol 90:819–827.

125. Contin M, Sepúlveda C, Fascio M, Stortz CA, Damonte EB, D'Accorso NB. 2019. Modified ribavirin analogues as antiviral agents against Junín virus. Bioorg Med Chem Lett 29:556–559.

126. Gowen BB, Westover JB, Sefing EJ, Van Wettere AJ, Bailey KW, Wandersee L, Komeno T, Furuta Y. 2017. Enhanced protection against experimental Junin virus infection through the use of a modified favipiravir loading dose strategy. Antiviral Res 145:131–135.

127. Torriani G, Trofimenko E, Mayor J, Fedeli C, Moreno H, Michel S, Heulot M, Chevalier N, Zimmer G, Shrestha N, Plattet P, Engler O, Rothenberger S, Widmann C, Kunz S. 2019. Identification of clotrimazole-derivatives as specific inhibitors of Arenavirus fusion. J Virol.

128. Lavanya M, Cuevas CD, Thomas M, Cherry S, Ross SR. 2013. siRNA screen for genes that affect Junín virus entry uncovers voltage-gated calcium channels as a therapeutic target. Sci Transl Med 5:204ra131.

129. Fascio ML, Sepúlveda CS, Damonte EB, D'Accorso NB. 2019. Synthesis and antiviral activity of some imidazo[1,2-b][1,3,4]thiadiazole carbohydrate derivatives. Carbohydr Res 480:61–66.

130. Zeitlin L, Geisbert JB, Deer DJ, Fenton KA, Bohorov O, Bohorova N, Goodman C, Kim D, Hiatt A, Pauly MH, Velasco J, Whaley KJ, Altmann F, Gruber C, Steinkellner H, Honko AN, Kuehne AI, Aman MJ, Sahandi S, Enterlein S, Zhan X, Enria D, Geisbert TW. 2016. Monoclonal antibody therapy for Junin virus infection. Proc Natl Acad Sci U S A 113:4458–4463.

131. Pan X, Wu Y, Wang W, Zhang L, Xiao G. 2018. Novel neutralizing monoclonal antibodies against Junin virus. Antiviral Res 156:21–28.

132. Clark LE, Mahmutovic S, Raymond DD, Dilanyan T, Koma T, Manning JT, Shankar S, Levis SC, Briggiler AM, Enria DA, Wucherpfennig KW, Paessler S, Abraham J. 2018. Vaccine-elicited receptor-binding site antibodies neutralize two New World hemorrhagic fever arenaviruses. Nat Commun 9:1884.

133. Leske A, Waßmann I, Schnepel K, Shifflett K, Holzerland J, Bostedt L, Bohn P, Mettenleiter TC, Briggiler AM, Brignone J, Enria D, Cordo SM, Hoenen T, Groseth A. 2019. Assessing cross-reactivity of Junín virus-directed neutralizing antibodies. Antiviral Res 163:106–116.

134. Emonet SF, Seregin AV, Yun NE, Poussard AL, Walker AG, de la Torre JC, Paessler S. 2011. Rescue from Cloned cDNAs and In Vivo Characterization of Recombinant Pathogenic Romero and Live-Attenuated Candid #1 Strains of Junin Virus, the Causative Agent of Argentine Hemorrhagic Fever Disease. J Virol 85:1473–1483.

135. Wali S, Gupta R, Veselenak RL, Li Y, Yu J-J, Murthy AK, Cap AP, Guentzel MN, Chambers JP, Zhong G, Rank RG, Pyles RB, Arulanandam BP. 2014. Use of a Guinea pig-specific transcriptome array for evaluation of protective immunity against genital chlamydial infection following intranasal vaccination in Guinea pigs. PloS One 9:e114261.

136. Veselenak RL, Milligan GN, Miller AL, Pyles RB, Bourne N. 2018. Transcriptional Analysis of the Guinea Pig Mucosal Immune Response to Intravaginal Infection with Herpes Simplex Virus Type 2. Virology 518:349–357.

137. Veselenak RL, Miller AL, Milligan GN, Bourne N, Pyles RB. 2015. Development and Utilization of a Custom PCR Array Workflow: Analysis of Gene Expression in Mycoplasma genitalium and Guinea Pig (Cavia porcellus). Mol Biotechnol 57:172–183.